Theoretical Studies of the Chemotaxis of Biological Cells

Vom Fachbereich Physik
der Universität Duisburg - Essen
(Campus Duisburg)

zur Erlangung des akademischen Grades eines
Doktors der Naturwissenschaften
genehmigte Dissertation von

Bidisha Nandy

aus

Kolkata, India

Referent: Prof. Dr. Artur Baumgärtner
Korreferent: Prof. Dr. Dietrich Wolf
Tag der mündlichen Prüfung: 17. März, 2008

Abstract

Living organisms contain thousands of interacting complex networks of macromolecules, and there are very few tools to understand them. The present thesis is an attempt to elucidate some aspects of two interacting networks which are responsible for the coordinated chemotactic locomotion of a cell. One of the networks, the directional sensing network, is responsible for the reception of external molecular signals to which the cell is exposed. This network also transforms the external signal into an internal one ('response'), which is amplified and used by the the second network, the polarization network, to tune and to guide the cellular motor which propells the cell using its polymerizing cytoskeleton.

A stochastic model, a type of cellular automata model, has been developed and employed in order to address various questions. For example, how an external signal with a weak spatial gradient can be translated by molecules into a strongly amplified and localized response, and how this response regulates the local activity and the spatial distribution of the actin cytoskeleton which controls the velocity and the direction of the cell's movements. By using a stochastic model, which includes explicit particles, the investigations provide a link to known approaches in theoretical physics, as there are, e.g., cooperative phenomena in many-body problems and space-time correlations in nonlinear dynamics. Since the present study is the first attempt employing a stochastic model, as compared to previous kinetic and deterministic models for chemotaxis, the achieved results contain new and important information.

It is shown, among others, that the amplification of the response exhibits a transition as function of the gradient of the signal. The spatial localization of the response, represented by the distribution of activated PIP molecules along the cell membrane, depends on the gradient and the maximum of the signal. Using the 'Local Exciter and Global Inhibitor' (LEGI) model, proposed recently by other researchers for the directional sensing network, it is shown how the spacial-temporal distributions of the two types of inhibitor and exciter molecules are correlated to the amplification of the response in terms of activated PIP molecules. The major advantage of the present approach, however, is the combination of a particle-based LEGI network with a particle-based polarization network, where the latter includes explicitly linear and branching polymerization of actin filaments. Taking the two regulatory networks, including their signaling molecules and the actin molecules together, a minimal cell model has been developed, where the cell membrane is represented by a two-dimensional flexible ring polymer. During Monte Carlo simulations of this model, the chemotactic motion of the cell could be monitored. The analysis of the trajectories shows that the magnitude of the drift velocity can be tuned by the combination of the signal gradient, the signal maximum and the signal-mediated polymerization of the filaments. This explains the experimentally known high sensitivity of chemotactic cell to weak external signal gradients.

Contents

1 Introduction

The phenomenon of cell locomotion plays a conspicuously pertinent role in many biological phenomena. Starting from embryogenesis and inflammation, to wound healing and during the growth of axons [1], - the causality arising out of cell motility appears somewhat omnipresent. However, the irony is, although the molecular components participating in the regulation of cell motility are known to a large extend, the exact schemes of their cooperativity and their formation of a signaling network are not always well-understood, hitherto [2]. - Admission of this fact coupled with the realization regarding importance of cell motility in the entire realm cell biology, forms the central motivation for the present work.

On a more precise note, 'motility' is a biological term which refers to the ability to move spontaneously. It can apply to either single-celled or multicellular organisms. Cell motility is required for diverse physiological processes including the formation of vascular and neuronal networks, muscle contraction, immune responses and the establishment of cell architecture and polarity. Cell migration underlies many human diseases including metastatic cancers, congenital brain defects and certain immune disorders [1, 2].

Cell motility is widely believed to be one of the crowning achievements of evolution [3]. Primitive cells were probably immobile. With the evolution of multicellular organisms, primitive organs were formed by migrations of single cells and groups of cells from distant parts of the embryo [3]. In adult organisms, movements of single cells in search of foreign organisms are integral to the host's defenses against infection. Higher organisms like mammals and birds and fish have the ability to locomote and most significantly they walk, fly or swim. In fact cell locomotion or motility can be used as one of the criteria to define life.

The cell movement can by and large be divided in two groups. One class of the movements take place through liquids and based on anthropocentric analogy is called 'swimming'. The swimming cells like sperm cells and bacteria propel themselves with the aid of a flagellar motor. The second class of movements take place through the rigid surface and is named as 'crawling'. The crawling of amoeboid cell takes part in a large variety of processes. In case of inflammatory diseases (these include asthma, arthritis, atherosclerosis, Alzheimer's disease and allergies) immune cell migration has been observed to be critically important for the delivery of protective immune responses to tissues. In wound healing, skin cells move into the wound and build a new skin material. During the embryogenesis of higher animals, nerve cells construct a network of nervous connection from the periphery to the brain , which wire the entire organism.

Different experiments have suggested (and hinted) that all crawlling cells contain ba-

sically same molecular components which are responsible for the mechanisms describe above [2]. Moreover, all the cells develop similar structures; for example, into the direction of locomotion they form lamellar protrusions. By fluorescence and electron microscopy studies it has been found further that the protruded parts of the cell contain dense network of filaments [2]. The coordinated acts of assembly and the dis-assembly of the filaments ultimately controls the cell locomotion. Close observation of these filaments reveals a very interesting fact. All single filament has polar structure and contains functionally two different ends. One end of the filament, elongates much faster than does the opposite and the other end preferentially shrink. These unequal growth rates leads to a forward motion of filaments and it is known as treadmilling. Experimental observation reveals alongside that, the process of filament polymerization plays a crucial role in various forms of cell motility [4, 5, 6, 7, 8]. Growth of new filaments from the side of existing filaments is known as branching. This branching leads to increase filament concentration quite significantly. Hence this branching process leads to an autocatalytic polymerization. These two features form the starting points for synthesis of our present model of cell locomotion.

It is known from experiment that cell locomotion is a collective response of directional sensing and polarization response [9]. The term 'directional sensing' refers to the ability of a cell to detect an asymmetric extracellular signal and to generate an internal amplified response; whereas 'polarization' stands for the asymmetric change in cell morphology and shape. Directional sensing and polarization are the two bio-physical causes which ensure that bodily cells, bacteria and other single-cell or multicellular organisms direct their movements according to certain chemicals in their environment. This is important for bacteria to find food (for example, glucose) by swimming towards the highest concentration of food molecules, or to flee from poisons (for example, phenol). - This set of movements are broadly referred to as 'chemotaxis'. Chemotaxis is called positive if movement is in the direction of a higher concentration of the chemical in question, and negative if the direction is opposite.

Although migration of cells was detected from the early days of the development of microscopy (Leeuwenhoek), erudite description of chemotaxis was first made by T.W. Engelmann (1881) and W.F. Pfeffer (1884) in bacteria and H.S. Jennings (1906) in ciliates. Nobel prize winner E. Metchnikoff also contributed to the study of the field with investigations of the process as an initial step of phagocytosis. The significance of chemotaxis in biology and clinical pathology was widely accepted in the 1930s. The most fundamental definitions belonging to the phenomenon were also drafted by this time. However, arguably the most important aspects in quality control of chemotaxis assays were described by H. Harris in the 1950s. In the 1960s and 1970s, the revolution of modern cell biology and biochemistry provided a series of novel techniques which became available to investigate the migratory responder cells and subcellular fractions responsible for chemotactic activity. The pioneering works of J. Adler represented a significant turning point in understanding the whole process of intracellular signal transduction of bacteria [10].

Recent researches on the same field have become much more categorical and they suggest clearly that inside the cell a complex regulatory protein network is responsible for cell locomotion. Generally, cell responds and moves toward the extracellular signal. But sometimes even without presence of any extracellular signal cell can polarize [11]. Thus there can be reasons to believe that a cell has an inherent ability to polarize by using some internal feedback network. However to explain the gradient sensing ability several model has been proposed by researchers. Perhaps the best model for this description is the 'Local Exciter and Global Inhibitor' (LEGI) activity model [9, 12]. According to this LEGI model two different particles with their different nature of activity and different time constants play the central role of gradient sensing. Taking a cue from this assertion, to extend the scope of it and to understand the underlying detailed causality behind the entire phenomenon, the main purpose of the present work was formulated in the way of building, for the first time, a stochastic model of the regulatory network responsible for the directional sensing and to couple the amplified response generated by directional sensing with the filament for cell polarization.

While it is easy to intuitively assume that the locomotion of biological cells is based on signal-mediated polymerization of their cytoskeletons, it has been shown recently [13, 14] using computer simulations and theoretical considerations, that the persistency of the random motion and the chemotaxis of a cell is essentially due to the autocatalytic polymerization kinetics of the cytoskeletal actin network. Further, how the entire process, consisting of the mechanisms behind substrate coupling and energy supply (during motion) together with polymerization processes, leads to the general concept of cell motility - is also elucidated. The effectiveness of these studies point unmistakably to the reliability and strength of computational procedures while studying the system. A significant part of the present work therefore banks on various computational schemes to decipher the depths of cell motility. Furthermore, since an acute need to computationally model the detailed scheme of biochemical network of relevant cellular proteins (which regulate the polymerization of the cytoskeleton in some way or other, like - Arp2/3, cofilin, gelsolin, profilin, capZ) was perceived, special attention was provided to include these considerations into the present model. Since the aforementioned proteins play a decisive role in changing the rate constants of polymerization and therefore have the potential to change the geometry of the cytoskeletal network (which will henceforth determine velocity and direction of cell locomotion among others [15, 16, 17, 18, 19, 20], inclusion of them into the present study has made sure that this essentially computational study becomes biologically relevant.

The work is organized as follows. In chapter 2, the basic facts regarding cell locomotion and common biological terminology are introduced. In this chapter the experimental findings about the amoeboid cell locomotion has been collected. Since it is known to us that the actin cytoskeleton plays a significant role in the determination of cell morphology and motility, studies related to it have been given a noteworthy importance here. In chapter 3 a description is given about the method used for computer simulation. In chapter 4, a model of amoeboid locomotion is presented based on treadmilling

and branching mechanism. In this model the dynamics of the steady state assembly of filament has been observed in the framework of stochastic processes. In chapter 5, it is described how homogeneous uniform external signals are coupled to membrane receptors, and a directional sensing mechanism is introduced. By using proteins regulatory network the adaptation and amplification has been studied for different parameter sets. In chapter 6, the studies of the directional sensing for chemotactic signals are presented. Homogeneous and inhomogeneous both gradient sources have been studied. In chapter 7, I describe how the polarization network and the directional sensing network are coupled in order to study the cell's chemotactic motion.

2 Biological Background of Cell Motility

2.1 Introduction:

Directed purposeful movement is one of the basic characteristics that we most closely relate with living organisms and essentially all known forms of life in this planet. Directed cell movement requires the cell to be able to convert its stores of chemical energy into mechanical energy. The present chapter will attempt to provide an introduction about the background of cell motility and detailed phenomenon of amoeboid cell locomotion observed by different biological experiments and discussed on several recent reviews and research articles [21, 4, 22, 23, 24].

2.2 Biological importance of cell motility:

Cell motility, like most of the known biological processes entail a great deal of multi-faceted significance. Although it is not possible here to submit a comprehensive account of all the biological implications of cell motility; an array of salient aspects due to the same is provided below.
1) It is known that most cancers are not life threatening until they metastasize and spread throughout the body. Metastasis occurs when previously sessile cells in a tumor acquire the ability to move and invade nearby tissues and circulate in the bloodstream or lymphatic system. A treatment that blocked the ability of tumor cells to acquire motility would largely prevent metastasis.
The elaborate wiring of the human nervous system is generated during fetal development by the motile behavior of nerve cells, which send projections crawling along molecularly defined path to connect peripheral body parts to the central nervous system. After spinal chord injuries, these connections are broken. But medical treatment that reverse paralysis.
2) Defect in cell motility during fetal development are responsible for many common birth defect , including cleft palate and spin bifida.
3) Other kinds of cell motility are responsible for a variety of conditions, ranging from male infertility to hereditary deafness to a susceptible to lung infections seen in people with cystic fibrosis.
4) Cell motility also underlies wound healing and the immune response.

Thus studies into the problem in cell motility and related internal components, quite understandably, form topics of enormous scientific and social interest owing to their therapeutic importance in living bodies [2]. Cell has highly efficient machinery to generate mechanical forces (in piconewton to nanonewton range) that functions over distances of nanometers to micrometers in an aqueous environment. When our understanding regarding the mechanics of cell movement will be as close as possible to reality, we would be able to adapt the cell movement machinery for design purpose which may help to alert us to the presence of pathogens or guide delivery of drugs.

2.3 Types of cell movements:

Movement of whole cells can be roughly divided into two functional categories: swimming or movement through liquid water and crawling, or movement across a rigid surface.
In bacteria flagellum there is a long filament constructed by the non covalent polymerization of hundreds of identical protein subunits, called flagellin. The speed of flagellar swimming, typically range from about 10 to 100 micrometers per second. Some bacteria such as vibrio cholerae (responsible for cholera) have a single flagellum at one pole and swim rapidly. Others, including the common laboratory organism Escherichia coli, have multiple flagella distributed around their surfaces that gather together in a bundle during swimming and can fly apart in a regulated direction. Rotary flagella have never been found in eukaryotes. Most swimming eukaryotic cells, ranging from human sperm to paramecia use flexible oar. When the cell surface projections used as oars are short and numerous, as on a paracium, they are called cilia; on the other hand, when they are long and few as on sperm, they are called flagella. Though bacterial flagella and eukaryotic flagella share the same name, although they are distinct structures.
Movement of cells across rigid surfaces can be achieved by an even greater variety of mechanisms than cell swimming. The best characterized amongst numerous schemes is amoeboid motility (known otherwise as crawling motility). It is a general process shared by eukaryotic cell ranging from soil amoebae to human white blood cells. In case of amoeboid motility, cell attaches itself to a rigid substrate and extends a projection of leading edge which then attaches to the substrate. There are three types of projections; (1) long thin projections are called filopodia, (2) flat vail shaped projections, lamellipodia and (3) thick knobby projections, pseudopodia. All these three types of projections are filled with network of actin filaments. About actin filaments a detail discussion will be presented in the next section. After protrusion and attachment the crawling cell contracts to move the cell body forward by retracting the rear part of the cell [25]; a cartoon of different steps of cell locomotion is representing by fig. 2.2. The speed of amoeboid movement can range from one micrometer per hour to more than one micrometer per second; it depends upon cell type and type of stimulation. Many forms of amoeboid cell motility can be observed in various kinds of cells. Their motion is closely connected with the tasks performed by the respective cells. An overview of crawling cells

and their purpose of motion is given in table 2.1.

Cell	*Function*
Keratocytes	Wound healing
Fibroblasts	Remodelling of the skin
Leukocytes	Defense against infection
Dictyostelium Discoideum	Formation of a slime mould
Neural growth cones	Development of the embryo
Listeria monocytogenes	Infection of uninfected cell

Table 2.1: Various crawling cells and some of their motives for locomotion.

Here an introduction of different crawling cells is given as an example of different crawling motion. Detailed discussion on different locomoting cell has done last part of the current chapter.
A very simple locomotion is observed in keratocyte. The keratocyte is one of the fastest moving cells with a simple shape and geometry. The fragment derived from it is lack of nucleus but still can locomote and is very simpler motile system to study. The fibroblast, neutrofils and Dictyostelium discoideum usually move with same mechanism. The motion of the neural growth cones of nerve cells is similar to that of keratocytes. The Listeria monocytogenes uses the locomotive machinery of an infected host cell to propel itself inside it and spread to neighboring, non infected cells.
The most important protein for all motile mechanisms is actin protein. About actin protein in details is described in section 2.5. Fig. 2.1 is representing different dynamic actin organizational structure through accessory actin binding proteins. There are other cells that do not utilize actin to locomote, as example Ascaris spermatocytes. The present work is focused on actin related mechanisms.
Body of any eukaryotic cell consists of two parts; one is nucleus, which contains the genetic information about the cell; while the second is the cytoplasm. The cytoplasm can have two different states: 1) Sol: where it is liquid 2) Gel: where it is in a semisolid state. These two cytoplasmic states undergo a continuous regular transformation from one to another and is extremely significant in its role in cell movement. A brief algorithmic sketch of this complex and continuous transformation is provided below.
State 1) The cytoplasm at the center of the cell is termed the endoplasm and is intially in the sol state.
State 2) Endoplasm flows towards an end (say, the front) of the cell.
State 3) When the endoplasm reaches the leading edge of the cell, it turns back into a gel state, called the ectoplasm. Ectoplasm which forms the cortex - just beneath the surface of the cell membrane.
State 4) As the region moves to the rear of the cell, the cytoplasm returns to the sol state (State 1) and moves once again to the front of the cell.

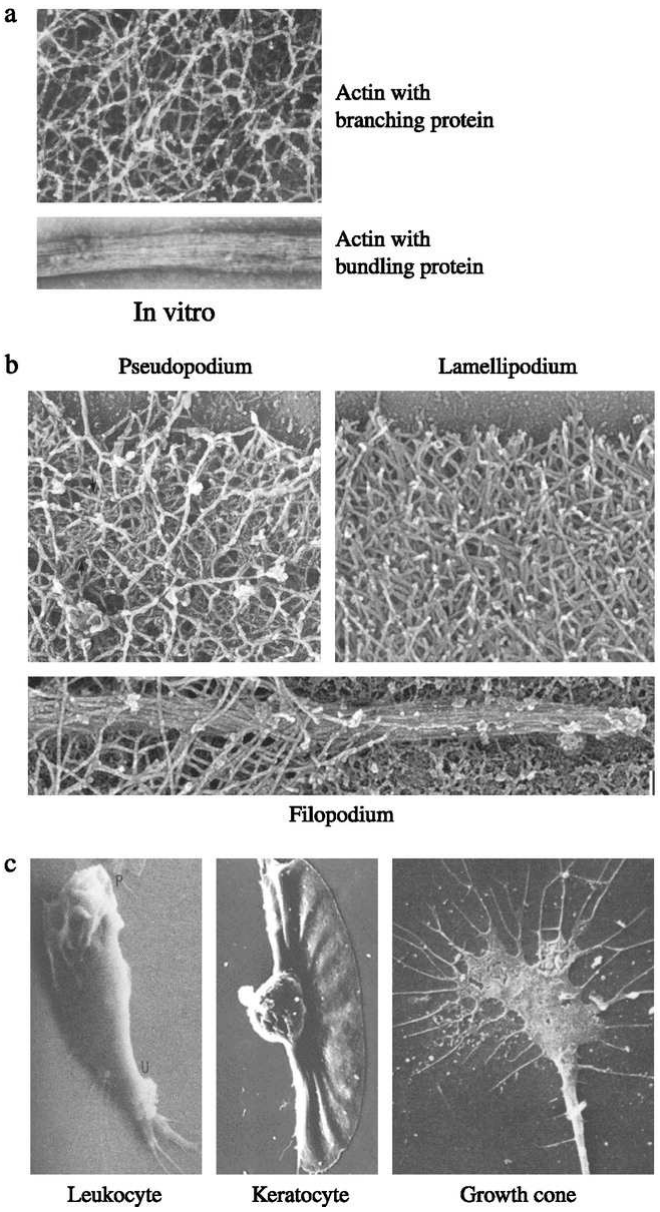

Figure 2.1: Various organizational structures produced by actin [25].

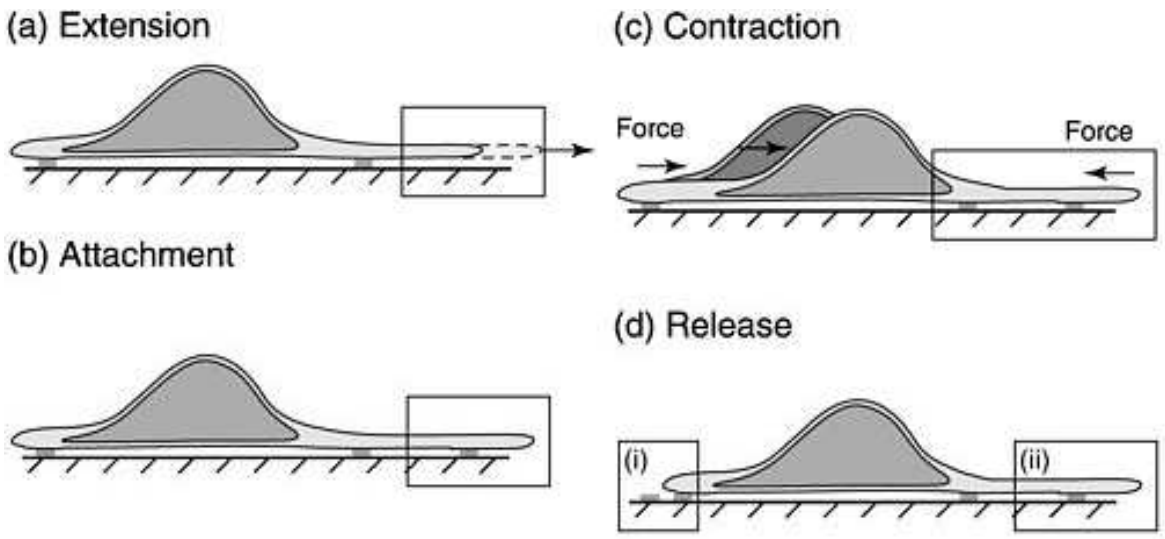

Figure 2.2: Cartoon of the four steps of cell locomotion and their possible microscopic origin.

In this way the cytoplasm is constantly cycling between the gel and the sol state while cell is moving.

2.4 The cytoskeleton:

It is a cytoplasmic system of fibers and is critical to cell motility. The cytoskeleton plays a structural role by supporting the cell membrane and by forming tracks along which organelles and other elements move in cytosol. The cytoskeleton has three major functions : 1) Maintaining of cell shape and organelle positioning. 2) Localization of macromolecules (such as mRNAs) and biochemical reactions. 3) Cell motility (there are many different types of cell motility). It is suggested that without the cytoskeleton, the cell would have no shape. In the electron microscope image the cytoskeleton appear as a random array of fibers. This array consists of three types of cytosolic fibers which is described bellow. Fig. 2.3 is representing a cartoon of cell body including the membrane and cytoskeleton.

2.4.1 Microtubules:

The first cytosolic fiber is microtubule which is tubular protein polymer of uniform diameter and variable length. The microtubule wall is made up to 13 protofilaments. Microtubules assemble from nucleating structures in the cell and are in equilibrium with a pool of tubulin subunites. Microtubules are composed of heterodimers of alpha tubulin and beta-tubulin. The two ends of microtubules are different. One end of the

polymer is more dynamic (called plus end) than the other (minus end). Two classes of biological motors (dynamit and kinesine) interact with microtubules to generate force for cell motility.

2.4.2 Intermediate Filaments:

Intermediate filaments are protein polymers of uniform diameter (10 nm) and variable length. The proteins structure varies with different tissue types. Intermediate filaments have no known association with cell motility. Intermediate filament assembly and disassembly is controlled by phosphoprylation and occurs along the length of the filament. Intermediate filament have a tissue specific protein composition, which has diagnostic value in the pathology lab for typing tumors.

2.4.3 Microfilaments:

The main and most important cytoskeletal component related to cell motility is the actin filament. All eukaryotic species contain actin. This cytoskeletal protein is abundant protein in many eukaryotic cells, often consisting 5 % or more of the total cell protein. Actin filaments appear in electro micrographs as threads about 8 nm wide. They consist of a tight helix of uniformly oriented actin molecules which is known as globular actin, or G-actin. Like a microtubule, an actin filament is a polar structure, with two structurally different ends. One is relatively inert and slow growing minus end and other is a faster growing end, the plus end. The minus end is also referred to as pointed end in some literatures, as the plus end is called the barbed end.
The term barbed and pointed are due to the optical appearance of myosin s-1 stained actin filaments in electron micrographs [26, 27]. The pointed end looks like a spike, where as the barbed end seems more frayed. G-actins are added to the filaments(F-actin) at both ends and this phenomena is termed as polymerization. The reverse process is also possible, which is called depolymerization of filament by monomer substraction. A large number of proteins are involved in the processes of (de-)polymerization, and they are called actin binding proteins. Some of them are mentioned later in section 2.7.
The table 2.2 is presented to give an idea about the dimension of actin filament. When actin filaments grow, in vivo monomer addition occurs mainly at the leading edge of the cell [23]. In next section the mechanism of actin filament is discussed in detail.

2.5 Actin filaments:

It is evident from the discussion hitherto that actin is perhaps the single most important molecule when describing cell locomotion. But comprehensive knowledge of the intricate mechanism behind actin functioning still eludes mankind, especially when it comes to describe the exact processes which associate movement of the cell. Many actin binding

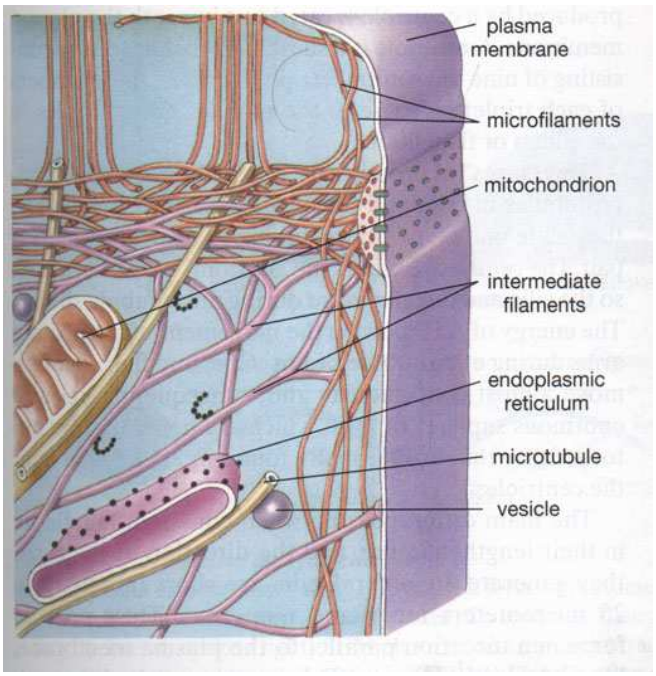

Figure 2.3: Illustration of cell body with the membrane [28].

Size of a G-actin monomer	$5.5nm \times 5.5nm \times 3.5nm$
Typical length of actin filaments	$22\mu m$ invitro this corresponds to about 10000 monomers
Width of actin filaments	about $7-9nm$, as they are a double stranded chains
Persistence length of actin filaments	$1.8\mu m$
Density of G-actin monomers	about $100\mu M$ in vivo this corresponds to a particle density of roughly $10^{-5}/nm^3 = 10^{-2}/(10nm)^3$

Table 2.2: Some properties of actin monomers and filaments.

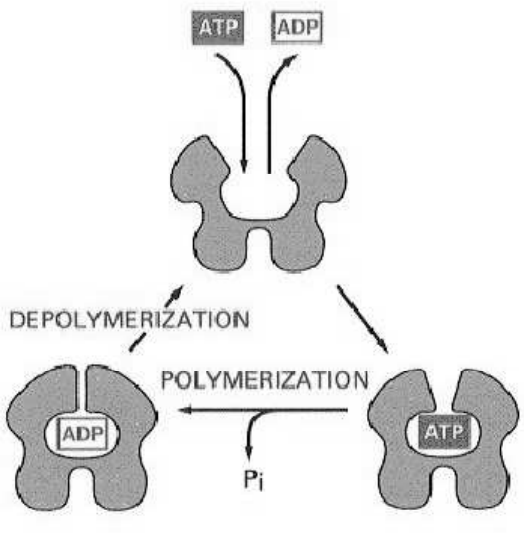

Figure 2.4: ATP and ADP trapped actin monomer.

proteins have been identified over the years [29] and a more explicit scheme of mechanism is in the process of being established, however the emergence of functioning scheme from molecular to cellular scale is not entirely understood hitherto. As an alternative to purely biological means to derive knowledge, the onus for the present work was assigned to computational procedures to study the entire system, especially by concentrating on the actins. Further, it was recognized that focussing on a unique feature of actins might prove to be more incisive.

This 'unique feature' mentioned above, is a characteristic in the property space of actin. Shortly after polymerization, the terminal phosphate of the ATP bound to actin molecule hydrolyzed, leaving the resulting ADP trapped in the polymer. The actin molecule is clam shaped and binds ATP in the crevice between its two halves: like a clam shell, it can open and close. When actin takes part in polymerization the cell is clamped shut by interactions between amino acids on both lips of the shell and the back side of the next subunit in the polymer. fig 2.4 is representing the cartoon of actin monomer.

We can express the dynamic properties of polymerization at the ends of polymers by following

$$F_n + \ M \longleftrightarrow \ F_{n+1} \tag{2.1}$$

Here F_n denotes a filament of length n and M denotes a monomer. By omitting the effect of nucleation and filament severing we can write a simple equation of motion for the density [M] of monomers [30, 31, 32]

$$F + \ M \underset{k^-}{\overset{k^+}{\rightleftharpoons}} \ F \ : \qquad \frac{d[\ M]}{dt} = -k^+[\ M] + k^- \ . \tag{2.2}$$

The equation implies, that the polymerization reaction is independent of the length of the filament and same as the depolymerization.
The polymerization of actin filaments proceeds in three sequential phases. The first phase is defined as lag period where G-actin aggregates into short unstable oligomers. Once the oligomer reaches a certain length it can act as a stable seed or nucleus, which in second phase rapidly elongates into filament by the addition of actin monomers to both of its ends. As F-actin filaments grow, the concentration of G-actin monomer decreases until it is in equilibrium with the filament. This third phase is steady state. Once the steady phase is reached, the equilibrium concentration of the pool of unassembled actin is called critical concentration.

$$K_e = \frac{k^-}{k^+} \tag{2.3}$$

At equilibrium

$$\left.\frac{d[\ M]}{dt}\right|_{[\ M]=[\ M]_c} = 0\ .$$

$$[M]_c = Ke \tag{2.4}$$

Here $[M]_c$ is called the critical constant. If the actual concentration $[M] > [M]_c$ then monomers are added to the polymers and if $[M] < [M]_c$, polymers shrink. The plus end of actin filaments polymerizes at up to ten times the rate of minus end. The critical concentration for actin polymerization is about 0.2 micromolar. This concentration is very much lower than the concentration of unpolymerized in a cell.
Shortly after polymerization, the terminal phosphate of the ATP bound to actin molecule is hydrolyzed, leaving the resulting ADP trapped in the polymer. ATP provides energy chemically by hydrolyzing one phosphate ion, i.e. by going through the chemical reaction.

$$\mathrm{ATP} \longrightarrow \mathrm{ADP} + \mathrm{Pi} + \mathrm{energy}\ ,$$

About 7 kcal/mole ATP are released and ADP, adenosine diphosphate is formed. ATP binding to actin assist the process of polymerization and this is the reason why pure actin is not found and we only find most actins as associated with either ATP or ADP. In the absence of energy supply mostly ADP-actin is found. The role of ATP hydrolysis in actin polymerization is not to form the filament, instead it serves to weaken the bonds in the polymer and thereby promote depolymerization. When actin molecules are released by disassembly of a filament, there is a relatively long delay before they can be reused in filament assembly. In principle, this property of actin allowes the cell to maintain a high cytosolic concentration of unpolymerized actin molecules in the form of ADP actin. In table 2.3 the values of the association and dissociation reaction constants are given for the two ends of actin filaments.

It is obvious that the rate constant for ADP-actin and ATP-actin are quite different for the two ends of actin filament.

		ADP-actin	ATP-actin
	barbed end		
$k^+/(^{-1}s^{-1})$:	association	$4.0^{[33]}$, $3.8^{[34]}$	$10^{[33]}$, $11.6^{[34]}$
$k^-/(s^{-1})$:	dissociation	$7.2^{[34]}$	$0.8^{[33]}$, $1.4^{[34]}$
$[M]_c/$:	critical concentration	$1.9^{[34]}$	$0.08^{[33]}$, $0.12^{[34]}$
	pointed end		
$k^+/(^{-1}s^{-1})$:	association	$0.23^{[33]}$, $0.16^{[34]}$	$0.6^{[33]}$, $1.3^{[34]}$
k^-/s^{-1}:	dissociation	$0.35^{[33]}$, $0.27^{[34]}$	$0.8^{[34]}$
$[M]_c/$:	critical concentration	$1.5^{[33]}$, $1.7^{[34]}$	$0.62^{[34]}$

Table 2.3: (De-)polymerization rates of ADP- and ATP-actin, values collected from references [34, 33].

2.6 The treadmilling of actin filaments:

Although filament grows faster at the plus end than the minus end, once the steady state phase is reached the G-actin concentration becomes intermediate between critical concentration value of the plus and minus ends. Lets say at the plus end critical concentration is $[M]_c^B$ and at the minus end is $[M]_c^P$
Where $[M]_c^B < [M]_c^P$ then for some intermediate concentration

$$[M]_c^B < [M] < \ [M]_c^P \tag{2.5}$$

In this situation subunits continue to be added to the barbed end and lost from the pointed end resulting in a flux of monomers in the solution from the pointed to the barbed end or equivalently a flux monomers through the filament from the barbed to pointed end.
The length of the filament remains constant, with newly added subunits travelling through the filament, as if on a treadmill, until they reach the negative end, where they dissociate. This phenomena is called treadmilling, like a dynamic instability, is a non-equilibrium behavior that requires an input of energy, which is provided by the ATP hydrolysis. So treadmilling happen when the monomer flux is observed in actin polymerization in the presence of ATP. It is believed that the irreversible process of ATP hydrolysis when bound to actin couples to the polymerization process and accounts for the difference in rate constant [35]. The possible mechanism is depicted in fig. 2.5. Researchers have found [36, 23, 37] that the filament in protruding lamellipodia are oriented in such a way that the barbed ends are found near the membrane at the leading

edge. So treadmilling of actin has been provided with much attention due to the belief that studying its connection to the protrusion of cell membrane is incisive.
We note alongside that there are different models on actin polymerization [38] which come under the general bracket named 'nucleation release model'. According to this school of thought, actin filaments are nucleated at the leading edge of the membrane. Subsequently the filaments are incorporated into a network by crosslinking and finally released towards the interior of the cell. This model proposes a large scale treadmilling of the whole network rather depending on individual treadmilling feature. Our present model mechanism has many similarities with this model. Instead of long parallel filament (as in case of treadmilling model) our model cell contains a short dense network of filament near the cell membrane (lamellipodia).

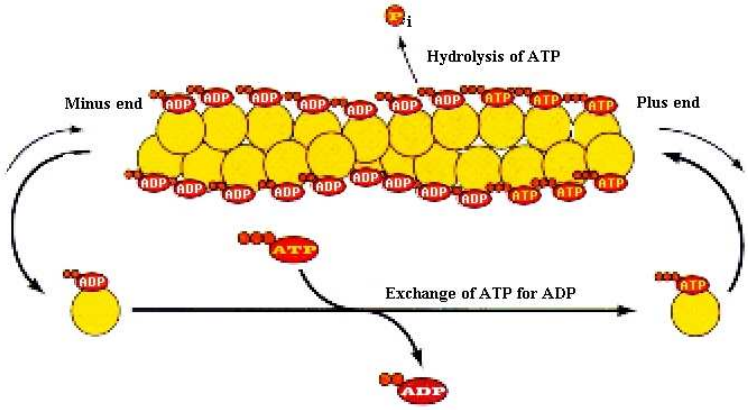

Figure 2.5: Illustration of actin treadmilling in the presence of ATP .

2.7 Actin binding proteins:

The treadmilling process is also controlled by different actin binding proteins. Fundamental cellular processes such as cytoskinesis, lamelopodial and growth cone extension, chemotaxis, endocytosis and exocytosis - are all regulated by actin-binding proteins. The total function of actin in the cell is undoubtedly more complex than treadmilling process alone and there must be more holistic(in philosophy) and refined(in implementation front) ways to describe the actin cytoskeleton. Indeed recent studies have indicated that functioning schemes of signal transduction chains are gradually becoming more clear . Furthermore these studies reveal that there is lot of actin associated or actin binding proteins that regulate actins on one hand and couple into the signal transduction chains on the other. Some of them are briefly introduced here.

2.7.1 Thymosin beta 4

It has been observed that as much as 40% of actin in an animal cell is umpolymerized. Because of its abundance in cytosol and inherent ability to bind ATP-G actin, thymosin beta 4 is considered to be the main actin sequestering protein in cells. A small protein (500MW) thymosin binds ATP-G actin in a 1:1 complex and inhibits polymerization and nucleotide exchange. Thymosin beta 4 has a much greater preference for ATP-actin over ADP-actin monomers [39]; hence the pool of unpolymerized actin in cells consists of ATP-actin and essentially no ADP-actin. The majority of quantitative assays for thymosin beta 4 binding to actin are indirect and rely on changes in the critical concentration [39, 40, 41, 42, 43, 44, 45], time courses of actin polymerization [46], nucleotide exchange from actin monomers [47], or competition with other actin-binding proteins [48]. Thymosin beta 4 also binds actin filaments, albeit weakly [49]. It is suggested that thymosin beta 4 changes the conformation and structural dynamics of actin monomers. The conformational change may reflect the unique ability of thymosin beta 4 to sequester actin monomers and inhibit nucleotide exchange. There are two opposing models defining the thymosin beta 4 (abbreviated from hereon as Tbeta 4) - binding site on actin [50, 51, 52]. Both models agree that Tbeta 4 contacts the gelsolin and profilin binding sites on the barbed end of actin monomers [53].

2.7.2 Profilin

This protein was discovered in the mid 70s. It is a small (12-15 K Da), soluble protein that is present in a high concentration (20-80 micro M) throughout the cytoplasm and has a high affinity to actin. It is known that the total actin pool in cells is composed of a filamentous and unpolymerized actin. Only a small fraction of G-actin monomers are free i.e. most of them are bound to actin binding protein [54]. A special class of phenomena is called sequestering : actin monomers are transformed into an inert state, in which they are unable to polymerize. Along with Tbeta 4 profilin act as a sequestering protein [55] but it is very weak sequestering protein. It seems that rather than sequestering the actin monomers, the main function of profilin is probably to promote assembly of actin filaments in cell [3]. Profilin interacts with membrane phospholipid phosphoinositol 4,5-bisphosphate (PIP2), and this interaction prevents binding of profilin to G-protein. Profilin binds to profilin-rich sequences that are commonly found in membrane associated signalling protein. This interaction localizes profilin actin complex to membrane. Finally, profilin also promotes assembly of actin filaments by acting as a nucleotide exchange factor. Profilin is the only actin binding protein that allowes the exchange of ATP for ADP. When G-protein is complexed with other proteins, ATP or ADP is trapped in the ATP-binding cleft of actin. But profilin binds to G-actin opposite to the ATP binding cleft, it can recharge ADP-actin monomers released from a filament. A cartoon of profilin activity is shown in fig.2.6.

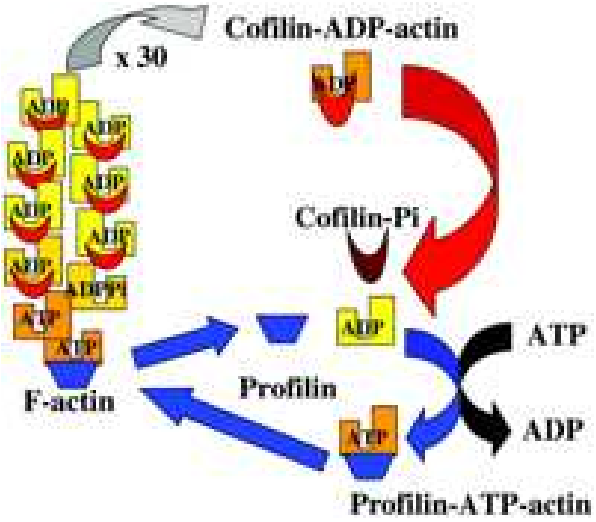

Figure 2.6: A cartoon representation the cooperative roles of ADF/cofilin (red crescents) and profilin (blue rhomboids) in regulating the turnover of actin monomers (yellow) in a microfilament containing ATP and ADP. Cofilin accelerates the dissociation of monomers from the pointed ends of filaments. Phosphorylation of cofilin (dark red) dissociates it from ADP-actin and profilin promotes the exchange of ADP for ATP that facilitates the addition of profilin-ATP-actin at the barbed end.

2.7.3 ADF/cofilin

Actin filaments can not only depolymerize, they can also be cleaved or severed. This work is performed by ADF/cofilin. The actin-depolymerizing factor (ADF), also called cofilin. It promote the disassembly of older actin filaments. ADF/cofilin family proteins appear weakly to sever filaments without capping and perhaps generate new free barbed ends to support polymerization. This protein is most active when it is not directly adjacent to the edge of motile cells but somewhat behind it. Newly assembled ATP actin subunits hydrolyze their bound ATP with a half time of 2s. Phosphate dissociation is much slower, with a half time of 350s. ADF/cofilin strongly accelerates phosphate dissociation from ADP-Pi actin filaments. Rate of phosphate dissociation depends on the concentration of active ADF/cofilin, phosphorylation of ADF/cofilin by LIM kinase downstream of PAK (p21-activated kinase) blocks this and other interactions of ADF/cofilin with actin is expected to slow phosphate dissociation and to stabilize branches. The higher affinity of ADF/cofilin for ADP-actin monomers than ADP-actin filaments provides the thermodynamic basis for their ability to depolymerize filaments. ADF/cofilin also inhibits exchange of the bound ADP. Fig. 2.6 is presenting a cartoon regarding the cooperative roles of ADF/cofilin and profilin in regulation of actin (de-)polymerization.

2.7.4 Gelsolin

Proteins of the gelsolin family are regulated by calcium which activates severing and/or capping. As cell moves through a gradient of chemotactic molecules, a cytosolic gradient of calcium is established, with a lowest concentration at the front of the cell and the highest concentration at the rear. The high calcium concentration at the rear of the cell would cause actin networks to dissemble by activating gelsolin. Severing of the actin occurs through the weakening of sufficient bonds between actin molecules within a filament to break the filament. After severing, gelsolin remain attached to the barbed end of the actin filament that can not re-anneal or elongate and thus the actin network is dissembled. PIP2 and Rac promote gelsolin uncapping.

2.7.5 Capping protein, cap Z

Another group of proteins can cap the ends of actin filaments but, unlike severing proteins cannot break filaments to create new ends. One such protein , cap Z binds the plus ends of actin filaments independently of calcium level and prevents the addition or loss of actin subunits from plus end. Capping by this protein is inhibited by PIP2, suggesting that its activity is regulated by the same signaling pathways that control cofilin and profilin. An actin filament that is capped at both ends is effectively stabilized undergoing neither addition nor loss of subunits. Such capped actin filaments are needed in places where the organization of the cytoskeleton is unchanging, as in a muscle sarcomere or at the erythrocyte membrane.

2.7.6 Arp2/3

An important set of actin regulators initiate formation of new actin filaments by a process that is called nucleation. Spontaneous nucleation is a kinetic hurdle in the process of actin polymerization and therefore, factors that can accelerate or bypass this step are important for efficient actin assembly in the cell. Among three classes of proteins which have been identified for initiating new filament polymerization one is the actin-related protein-2/3 (ARP2/3) complex . The ARP2/3 complex was first purified from Acanthamoeba castellanii [56] and was shown to consist of a stable assembly of seven polypeptides. Among seven polypeptides two of them are actin-related proteins Arp2 and Arp3 and the other five are p41-Arc/ ARPC1, p34-Arc/ ARPC2, p21-Arc/ ARPC3, p20-Arc/ ARPC4, p16-Arc/ ARPC5 [57]. ARP2/3 complex attain the active state from inactive state when nucleate the formation of new actin filaments . The mechanism of this transition and the reverse transition has been subject of intense study. Several experimental results [58, 59, 60, 61] indicated that nucleotide binding to both ARPs is important for the activity of ARP2/3 and in addition to nucleotide binding, nucleotide hydrolysis also has a role in the function of the ARP2/3 complex [62, 63, 64]. Kinetic models indicate that actin polymerization by the ARP2/3 complex is autocatalytic,

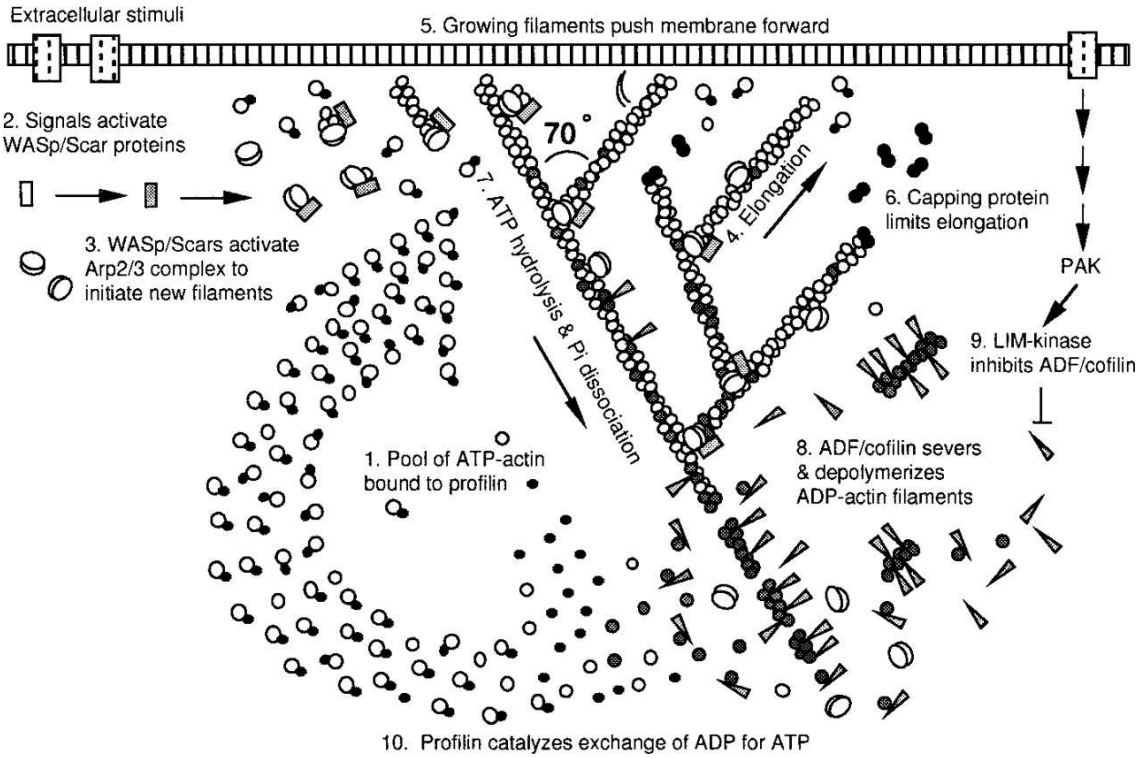

Figure 2.7: Dendritic nucleation model.

with the rate of the reaction increasing as more polymer is generated [57]. Exactly how the nucleation and branching (dendritic nucleation) activities are linked together is not very clear till now and two competing models have been suggested to explain it. One model [65] proposes that branching occurs from the sides of existing filaments, while the other [57] proposes that it occurs from the barbed ends of filaments. The most compelling experimental evidence [66, 67, 68] supports the side-branching model. According to the model ARP2/3 complex binds to the side of a filament at an angle of roughly 70 degree. Release of the mother or daughter filament from the ARP2/3 complex, known as debranching, is crucial for recycling actin networks in the cell. It has been found that ATP hydrolysis and Pi release from ARP2 has an important role in debranching [64, 63]. In chapter 4 we have discussed the branching implementation in our stochastic model. Fig.2.7 is representing dendritic nucleation model for the leading edge of a motile cell.

2.7.7 WASP

Members of the WASP(wiskott-Aldrich syndrome protein) family regulate the assembly of actin monomers into filaments; they are the key regulators of the cytoskeletal

organization and motility of cells. In activated state, many cell surface receptors induce alterations in the organization of intracellular signalling complex leading to change actin assembly and cell motility. Some recent findings tend to suggest that a limited number of cytoplasmic proteins, including WASP family members, provide focal points at which multiple signal converge to controle the dynamics of actin polymerization. The carboxyl terminus of WASP and its corresponding N-WASP(expressed in many cell types) contain a conserved VCA region consisting of a verprolin homology region(V), a cofilin homology region(C) and an acidic region(A). The acidic motif and cofilin homology region bind to the actin related protein complex Arp2/3, which initiate actin polymerization by promoting addition of actin monomers to the barbed ends of actin filament. The V region binds to monomer of complex for assembly into filaments. Fig 2.7 is representing a cartoon about WASP regulatory function in a dendritic nucleation model at the leading edge of a motile cell.

2.8 The ground state of the system :

Since our main interest is to decipher the mechanism of signalling pathway of a motile cell, we recognized the importance of forming an idea about the ground state of the system. In the absence of any positive stimuli, roughly half of the actin assemble into filaments while the rest become bound to profilin or cofilin. Even pure actin filaments are quite stable under physiological conditions in ATP. It is also known that actin subunits flux slowly onto the barbed end and of the pointed end with rate is less than 0.1 subunit per second. The combination of barbed end caps and a high concentration of profilin allows cell to maintain a high concentration of unpolymerized ATP-actin ready for elongation of barbed ends when they appear. But new barbed ends rarely appear without positive stimulus. Because profilin inhibits the initiation of new actin filaments by spontaneous nucleation factors Arp2/3 complex is inactive without nucleation promotion factors. Furthermore, the nucleation promoting factor such as Wasp are strongly autoinhibited and thus inactive in the absence of positive signals.

2.9 A probable protein regulatory network for signal transduction:

In order to respond to an extracellular signal, the cell maintains a mechanism to transfer the information across the cell membrane. The cell surface receptors bind to extracellular chemical molecules and trigger intracellular messengers. These second messengers are used to relay signals which influence the polymerization process. Cell must have three basic physiological responses: directional sensing, polarization and movement. For each individual response phenomenon cell maintains a corresponding protein regulatory network. Each regulatory network is interconnected with other regulatory networks and

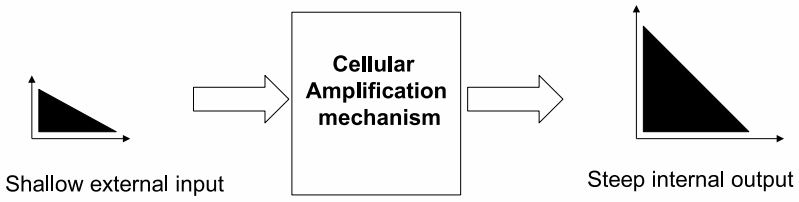

Figure 2.8: Amplification of shallow extracellular input into steep intracellular output.

a coherent coordination of different networks form a signal transduction pathway which begin at receptor and end at filament polymerization. From a reductionist point of view, it is possible to understand each process separately and then study the synergistic coordination amongst them. The first stage of this pathway is the process of sensing of extracellular signal by cell. At the next stage, cell interpret the asymmetric shape of signal in well defined front and rear part. The mechanism by which cell can transform the shallow external gradient into a steep internal response is known gradient sensing and fig.2.8 is a cartoon that depicts amplification gradient. The main components involved in this signalling pathway has been described below. Fig.2.9 is representing the flow chart of the signalling network.

2.9.1 Membrane receptor

The first step in chemotactic response involves the cAMP (cyclic adenosine 3,5-monophosphate) receptor. Although not yet identified in mammals, cAMP receptors are already well characterized in lower eukaryotes. cAR1 a G-protein-linked surface cAMP receptor, plays a central role in the development of Dictyostelium. This receptor, whose numbers vary approximately between 40-100,000 in a cell. cARs belong to the superfamily of seven transmembrane domain G protein-coupled receptors inside the plasma membrane to a trimeric guanine nucleotide-binding proteins(G protein). In leukocytes and Dictyostelium, the chemoattractant signal is perceived by G protein coupled receptors(GPCRs). The observation suggested that cAMP no longer consider only as an intracellular second messenger but also a first messenger responsible for coordinate chemical signal for cell locomotion [69].

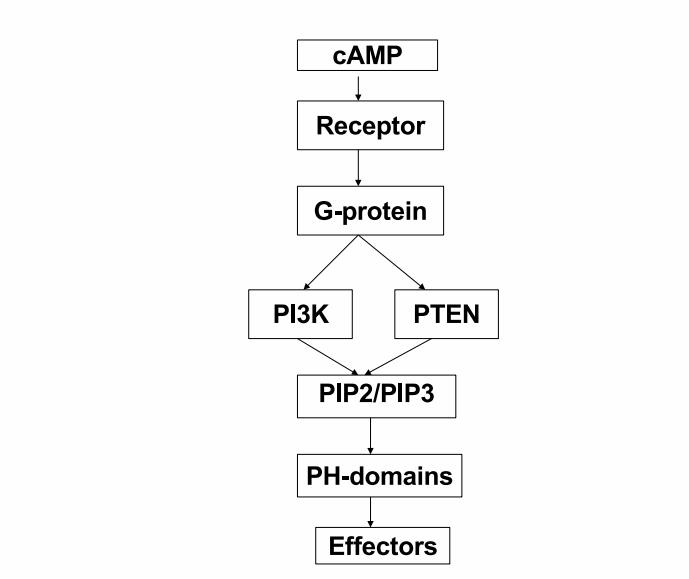

Figure 2.9: Chemotactic signal transduction pathway which regulates the adaptation and spatial sensing.

Experimental result on GFP-tagged GPCRs : Studies in both Dictyostelium and leukocytes showed that they remain evenly distributed along the plasma membrane in highly chemotaxing cells [70, 71]. This indicates that differential activation of signalling pathways in the front and in the back of cell does not depend on differential distribution of the receptors. The number of cAMP-bound receptors will mirror approximately the extracellular distribution of cAMP. In next few chapters (chapter 5, 6 and 7) we will use the term receptor occupancy, which indicate the fraction of cAMP-bound receptors in a cell surrounded by chemo-attractants. A strong and uniform presence of chemo-attractant can influence the receptor occupancies reach their saturate states and lead to a loss of directional information.

2.9.2 G proteins

G proteins which couple with receptor, function as intermediaries in transmembrane signalling. The heterotrimers G-proteins consist three subunits, labeled: α, β and γ. Under simulating condition of the receptor, the α subunit of G protein dissociates from $\beta\gamma$ subunits. These subunits are then free to signal downstream effectors. It has been shown that membrane associated G $\beta\gamma$ is distributed in only a shallow anterior-posterior gradient in highly polarized Dictyostelium cells [72], which is similar to the extracellular chemoattractant gradient. So this does not represent the mechanism of creating a spatial amplification of extracellular signal. The well known technique in this end is FRET (Fluorescence Resonance Energy Transfer), which finds substantial use in monitoring

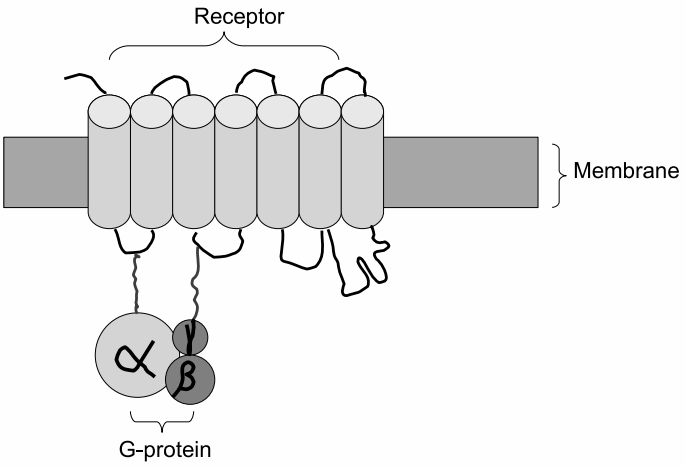

Figure 2.10: G-protein coupled receptor CAR1.

the activated G protein in living cell. FRET analysis has suggested that any significant asymmetry in amplifying the extracellular chemoattractant gradient is not the result of differential spatial activation at the level of receptor of heterometric G protein. Fig. 2.10 is presenting a cartoon of G protein coupled receptor.

2.9.3 3 ' Phosphoinositides

Phosphoinositides are a family of phospholipids which are derived by the phosphorylation of phosphatidyl inositol(PI) [73]. These membrane bound lipids have six hydroxyls on the inositol ring. Phosphorylation and dephosphorylatipon of the 3-hydroxyl is a ubiquitous second messenger in eukaryotic cells. In chemo-attractant signalling pathway, $PI(3,4,5)P_3$ is considered as a critical node. Appropriate accumulation of this membrane lipid is necessary for accurate directional sensing of extracellular source [74, 75, 76, 77, 78, 79].

2.9.4 3 ' Phosphorylation by PI3K

Phosphoinositide 3-kinase (PI3K), the 3-PI synthetic enzyme, plays an important role in linking early chemoattractant signals of G protein activation with downstream components of the chemotaxis response [11, 18]. When cAMP become simulated, PI3K

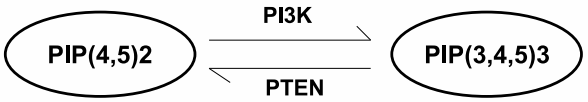

Figure 2.11: Conversion between $PI(4,5)P_2$ and $PI(3,4,5)P_3$.

is activated by G protein $\beta\gamma$ complex and then catalyzes the phosphorylation of phosphatidyl inositol(4,5)biphosphate to phosphatidyl inositol(3,4,5)triphosphate. In resting cells, most of the PI3K is found in the cytosol. After about 30 to 40 seconds of constant stimulation, PI3K then return to cytoplasm.
In the chemo-attractant gradient, PI3Ks are situated on the membrane at the front of the cell. Experiment suggested that PI3K regulation is not affected by its product $PI(3,4,5)P_3$. To be functional PI3K has to be associated with membrane binding site, which is its substrate.

2.9.5 3 ' Dephosphorylation by PTEN

The only known phosphatase that help the dephosphorylation of $PI(3,4,5)P_3$ to $PI(4,5)P_2$ is the protein encoded by a tumor-suppressor gene PTEN. The protein PTEN (phosphatase and tension homology) is found initially partly on the membrane, an attachment that requires $PI(3,4,5,)P_3$. Upon chemo-attractant stimulation, PTEN rapidly and transiently dissociates from the membrane and move to cytosol before returning to pre-stimulus levels within next few minutes. PTEN is found preferentially attached to the membrane farthest from the chemo-attractant source. Fig.2.11 is representing a cartoon of conversion between $PI(3,4,5)P_3$ and $PI(4,5)P_2$ by PI3K and PTEN.

2.9.6 PH Domains

It is now well known that 3-PIs carry out their regulatory role by activating specific effector proteins at the inner leaf of the cell membrane [73]. One such PI binding domain is known as pleckstrin homology(PH) domain. Different PIs are bound selectively by different PH-domain binding proteins. Several PH-domains which are important to chemotaxis are known to bind selectively to $PI(3,4,5)P_3$ and $PI(3,4)P_2$. One of these

PH domain containing protein CRAC was originally identified as a cytosolic regulator of adenylyl cyclase, a signaling molecule important for intercellular relay of cAMP [80, 81, 82, 83]. To monitor the action of CARC it can be fused to GFP. CRAC-GFP is found in cytosol prior to stimulation by chemo-attractants.
CARC and another PH-domain-containing protein PKB (protein kinase B) are highly localized at the leading edge of D. discoideum cells during chemotaxis [75, 79]. Similar localizations of PH-domain-containing proteins have been observed in mammalian leukocytes and fibroblasts [84, 76]. Thus, chemical gradients of extracellular signals lead to localization of PtdIns$(3,4,5)P_3$-bound PH-domain-containing proteins to the leading edge of the cell.

2.9.7 Downstream effectors:ACA

Adenylyl cyclase of aggregation (ACA) is a membrane associated protein for systhesizing cAMP. Part of this intracellular cAMP is secreted to the environment. Activation of ACA requires CRAC translocation of the cell membrane, a process mediated by G-protein induced phosphorylation of $PI(3,4)P_2$.

2.9.8 Chemotactic behavior

Adaptation

When D. discoideum cells are stimulated with a constant dose of cAMP, receptor occupancy and the G-protein activity levels rise quickly and remain above prestimulus levels. On the other hand, the response of several downstream proteins, including PI3K, PTEN and PH-domain localizations have been found to be transient. Even under the presence of sustained stimulation, signaling events terminate after a sharp increase [85]. The process of transient change in the internal states, followed by a full or partial return to the prestimulus steady state levels, in response to chemical signal is referred as adaptation. Due to presence of adaptation property a cell remains responsive to detect further changes in the cAMP concentration. The adaptation property has been found in a wide range of cells, from bacteria to mammalian cells [20, 86, 87, 88, 89, 90]. Fig.2.12 is representing example of different types of adaptation.

Gradient amplification

The directed movements of cells toward chemo-attractant or away from chemo-repellent, are crucial for many biological processes and are therefore omnipresent. To move chemotactically, a cell must perform and coordinate three basic physiological responses: directional sensing, polarization and movement. During directional gradient sensing, eukaryotic cells such as Dictyostelium and nutrophils exhibit extraordinary sensitivity to external chemical gradients. There are two different ways to sense the external gradient. Several organisms, including E.coli move among the chemoattractant field and by

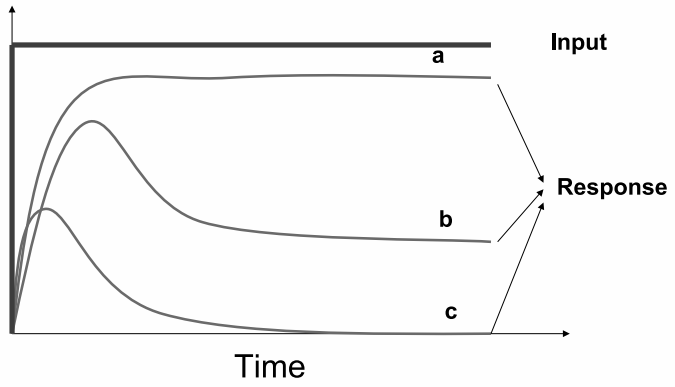

Figure 2.12: An illustration of adaptive responses to constant input signal. (a) No adaptation, (b) Partial adaptation, (c) Perfect adaptation.

comparing the receptor occupancy levels over time, detect the gradient. In case of larger cells, including mammalian neutrophils, S. cerevisiae and Dictyostelium are able to interpret gradient around them when they are immobile [75]. So it can be concluded that gradient sensing is a process independent of cell motility [75]. Both Dictyostelium and nutrophils can sense and orient accurately even when exposed to very shallow chemoattractant gradients. In cell, receptor occupancy and the G-protein activity mirror the external shallow chemoattractant gradient. Intracellular signal transduction pathway amplify the shallow signalling input into a much steeper internal response.

2.10 Some locomoting cells :

2.10.1 Keratocytes

The keratocyte is also called kerattinocyte. It is the cell of the epidermis, that is the outer most layer of the skin. It is first described in 1924 by Goodrich and due to its simple mechanism it become an important model system to study the biological features of amoeboid cell locomotion. The keratocyte is responsible for the formation of tissue and for wound healing. Actually it is the fastest cell moving with a speed of up to 30 micro meter/min. Shape of these cells are spherically symmetric and the nucleus, which is in the center of the cell, contains the genetic information and is surrounded

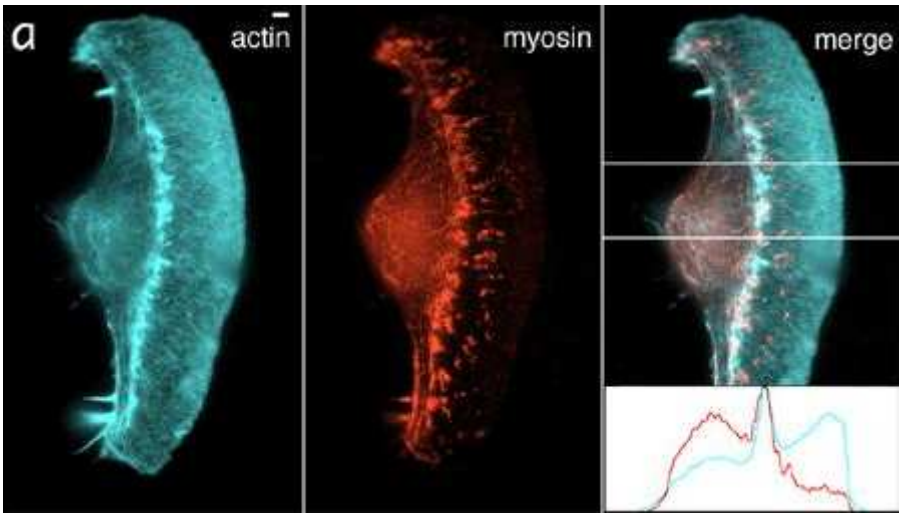

Figure 2.13: Fluorescent microscopy image of an epidermal fish keratocyte [23].

by cytoplasm. The cytoplasm consists of the intracellular fluid called cytosol and other cell organells, which involve in energy supply, cell division etc. A moving keratocyte cell form a front/rear asymmetric polar structures. The cell becomes an wing like shape depicted in fig 2.13. The width of this cell is about 150 micro meter from left to right and from front to back is about 75 micro meter.
The associated diagram shows that cells are moving from left to right direction in the two dimensional plane. Actin (cyan) and myosin (red) distributions are revealed by TRITC-phalloidin and indirect immunofluorescence staining, respectively. Overall actin and myosin II organization in a typical wing-shaped locomoting cell. They accumulate around the nucleus of the cell. And this concerned area is called cell body, which is speared from the lamella. Together the cell body and the lamellipodium form a structure like a fried egg. The white part of the egg is corresponding to the lamellipodium and the yellow part to the nucleus, respectively. The lamella is built by actin filaments. From fluorescent microscopy experiment it is known that the distribution of actin filaments in the lamellipodia is not static, rather highly dynamic [91].

2.10.2 Leukocytes

The white blood cells or Leukocytes form another important model system to study cell locomotion. The neutrophil is the most common blood leucocyte, which is responsible for primary cellular response to an acute inflammatory episode [92]. The shape of neutrophil is spherically symmetric when they are at rest. After exposing to FMLP (N-formyl-methionyl-leucyl-phenylalanine) they show a chemotactic response: neutrophils polarize and start to locomote into the direction of the source of FMLP [93]. Experimental

observations revealed that neutrophil fragments are devoid of microtubuli. It locomotes independently and reacts to chemical stimulant. It is also found that in actin based motility the Arp2/3 complex is involved in neutrophil [94].

2.10.3 Amoebae

Amoeba is a genus of protozoa that moves by means of temporary projections called pseudopods, and is well-known as a representative unicellular organism. It performs independent locomotion on two dimensional substrates [95, 96]. If Amoeba Proteus placed into a gradient of light it has been observed to prefer to travel to the darker regions. Like all other lokomoting cell it is also believed that the motile force is generated by actin filament in Amoeba Proteus.

2.10.4 Dictyostelium Discoideum

Dictyostelium Discoideum is a another protozoan cell of interest. Under normal condition it lives as a single cellular organism in the soil feeding on bacteria. But they undergo a dramatic transformation in their life cycle when they sense scarcity of food supply (or else when they sense that all the food reserve has been consumed). They build up a mechanism for signalling surrounding cells and responding to the signals from surrounding cells. The amoebae aggregate and assemble a multicellular structure consisting to approximately 100,000 cells. This multi-cellular organism subsequently go through differentiation and morphogenesis, resulting in a three dimensional fruiting body which consists of a ball of spores held high by a slender cellular stalk. The aggregation step in this process is driven by chemically guided locomotion - a process known as chemotaxis - towards cyclic adenosine, 3,5-monophosphate(cAMP). Cells are able to detect extracellular cAMP and relay cAMP signals over long distance. Observations through dark-field microscope revealed the circular pattern of outward cAMP propagation and inward cell migration [97]. These concentric rings often evolve into spirals and eventually break down into streams of cells that move into the center of aggregation regions, where they begin to form a mound. Basic processes of development such as differential cell sorting, pattern formation, stimulus-induced gene expression and cell-type regulation are common to Dictyostelium Discoideum.

2.10.5 The neural growth cone

During embryogenesis the body of higher animals is wired by the axons, that are a part of neurons. In later stage of development, when the axon connection have already been established, the connection between nerve cells may still be altered; - this phenomenon is known as neuronal plasticity, it establishes new signal transduction pathways at the expense of old ones owing to changing needs. During both processes the most advance part of the axon, the growth cone has to locomote independently from the cell body

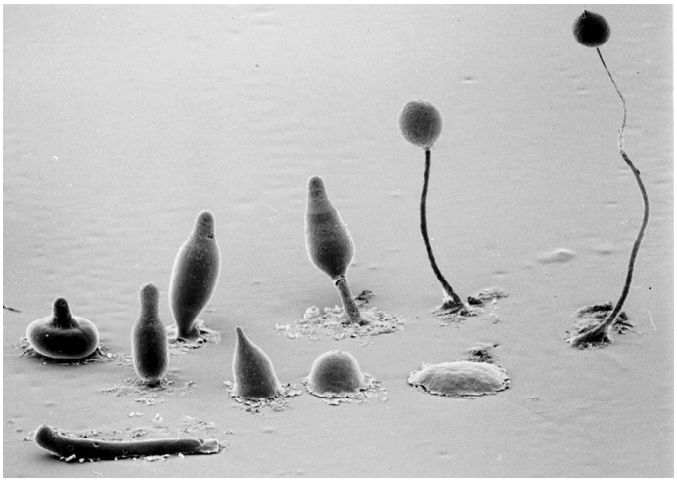

Figure 2.14: Dictyostelium life cycle.

and respond according to signal. For performing independent locomotion, the growth cone employ actin cytoskeleton and produce lamellipodia. Another protrusive structure of actin filament, the filopodia also observed in growth cones. It is known that growth cones that lack filopodia, move with distinctly higher speed [22].

2.10.6 Listeria Monocytogenes

Listeria monocytogenes is a gram-positive rod-shaped bacterium. It is the agent of listeriosis, a serious infection caused by eating food contaminated with the bacteria. It utilizes the actin cytoskeleton of an infected host cell to propel itself [98, 99]. Once inside the cytoplasm of an infected cell, Listeria " divides and induce the polymerization of host actin around them. This actin coat then rearranges into a tail located at one end of the bacterium. Actin assembly propels the bacteria inside the cytosol. When moving bacteria reach the plasma membrane, they push out long protrusions that are taken up by neighboring cells, allowing the infection to spread from cell to cell within tissues. [...] It was established (a) that polymerization takes place at the rear of the bacterium and the newly formed actin tails remain stationary in the cytoplasm and furthermore (b) the rate of incorporation of actin monomers approximates the rate of bacterial movement, suggesting that actin polymerization itself provides the energy for translocation. Listeria moves at speeds ranging from 0.05 to 0.25 per s." [99] A theoretical model by Oudenaarden and Theriot [100] propose an interesting mechanism

to break the spatial symmetry of propulsion in order to induce a persistent random bacterial walk. According to their postulation, there is a cooperative effect of growing and shrinking actin filaments on either side of the bacterium. But this mechanism is restricted by its application to the locomotion of a bacterium in the host cytoplasm: the actin cytoskeleton that is responsible for the locomotion is outside the object to be moved. But the problem of cell motility is the inverted scenario, as the actin cytoskeleton is inside the cell to be translocated. Thus an acute need for a different explanation, that cannot be derived from the cooperative effects mentioned above, is felt.

3 Numerical Method

3.1 Introduction:

Computational schemes employed in the present work revolves mainly around the implementation of Monte-Carlo simulation. Monte Carlo method aims at a probabilistic description from the outset, relying on the use of random numbers (the conspicuous correlation of gambling with probabilistic studies of random numbers; coupled with the fact that some of the great names of 20th century Mathematics and Physics, viz. Stanislaw Ulam, Enrico Fermi, John von Neuman, Nicholas Metropolis - used to like being in a casino in Monaco; - explain the origin of the name for this algorithm). In practice, of course, the 'random' numbers that this algorithm works with are not truly random but rather are pseudorandom numbers; i.e., a sequence of numbers produced on a computer with a suitable deterministic procedure. However, the pseudorandom numbers show statistical properties (nearly uniform distribution, nearly vanishing correlation coefficients, etc.) that are extremely similar to the statistical properties associated with truly random numbers, and thus a given sequence of pseudorandom numbers appears random for almost all practical purposes. Thus, from now on, the prefix 'pseudo' will be omitted and we will describe the pseudorandom numbers by 'random numbers'. Monte Carlo(MC) simulations use random moves to explore the search space to find out relevant information about the space.
It can well be understood from the discussion above that, MC simulation methods can be especially useful in studying systems with a large number of coupled degrees of freedom, such as liquids, disordered materials, strongly coupled solids and cellular structures. They are distinguished from other simulation methods (such as molecular dynamics) by being stochastic, that is nondeterministic; owing to their principal dependence on the use of random numbers as opposed to the philosophy of deterministic algorithms. On the other hand, the prevailing biological reality within cytoplasm and especially the phenomenon of cell motility, is also known to be stochastic in nature [101, 13]. Therefore the underlying process (cell motility) and the procedure concerned (MC simulation schemes), can easily be observed to share a notable similarity in their motivation. Thus the use of MC techniques in the present study becomes not only justified but also inevitable. It is also known that stochastic model is essentially a tool for estimating probability distributions of potential outcomes by allowing for random variation in one

or more inputs over time [102]. Henceforth, it becomes clear that with Monte Carlo method a stochastic trajectory can be generated through the phase space of the model considered. This approach had helped my study with significant insights.
This chapter deals with the details of the employed computational models, viz. that of the simulation techniques. Discussions based on obtained analytical results have been kept in the subsequent chapters. All the programs to implement the simulation scheme were written in Fortran90 [103, 104].

3.2 Metropolis Monte Carlo algorithm:

In 1953, Nicholas Metropolis and coworkers [105] proposed a new sampling procedure which incorporates a temperature of the system. This is done so that the Boltzmann average of a property of the system can be easily calculated. This modified Monte Carlo method is known as a Metropolis Monte Carlo simulation. To be precise, the Metropolis algorithm (Metropolis-Hastings algorithm) is a rejection sampling algorithm. It is used to generate a sequence of samples from a probability distribution that is difficult to directly sample from. This sequence can subsequently be used in Markov chain Monte Carlo simulation to approximate the distribution (i.e., to generate a histogram), or to compute an integral (such as an expected value). Helpful observation for my study was that Metropolis algorithm can draw samples from any probability distribution P(x), requiring only that the density can be calculated at x. The algorithm generates a Markov chain in which each state x(t) depends only on the previous state x(t-1). This essentially stochastic way of describing the system was precisely what the purpose of my work revolved around. The goal of this section is to introduce the Metropolis Monte Carlo Method [106, 107, 105] as applied to the computation of canonical ensemble averages.
The Metropolis Monte Carlo approach is used for generation a set of n configurations of a system $\xi_1, \xi_2, \ldots, \xi_n$ such that

$$\lim_{n\to\infty} \frac{N_\xi}{N} = P(\xi) \tag{3.1}$$

where$P(\xi)$ is a given probability distribution and the distribution follows property of Boltzmann distribution i.e $P(\xi) = Z^{-1}exp[-\beta E(\xi)]$ and N_ξ is number of configuration ξ.
The Metropolis algorithm can be described by following steps:
1) Pick a configuration ξ_n (the initial configuration can be any configuration of the system).
2)Make a trial configuration ξ_t and compute the probability ratio $R = \frac{P(\xi_t)}{P(\xi_n)}$. Pick a random number p with value between 0 and 1.
If $p \leq R$ The new configuration is accepted $\xi_(n+1) = \xi_t$
If $p > R$ The new configuration is rejected $\xi_(n+1) = \xi_n$

3)Go to step 2 replacing ξ_n by $\xi_(n+1)$ Step 3 is repeated by N times, where N is a sufficient large number.
According to Step 2 the probability of accepting a trial configuration ξ_t is

$$P_(\xi_n, \xi_t) = \begin{cases} R = \frac{P(\xi_t)}{P(\xi_n)}, when P(\xi_t) < P(\xi_n), \\ 1, otherwise \end{cases} \tag{3.2}$$

It can be shown that this algorithm indeed produces an ensemble of configurations that satisfies eq.(3.1) . If we consider ensemble of N configurations with N_ξ members of the ensemble in state ξ and apply the Metropolis Monte Carlo algorithm to each member of the ensemble by setting $\xi_n = \xi$ and $\xi_t = \xi'$ in step (2) where ξ and ξ' are any two possible states. By applying the algorithm we generate more configurations and we therefore evolve the initial distribution. In order to show that the algorithm produces an ensemble of configurations that satisfies eq.(3.1) it is needed to show that our algorithm produces an ensemble of configurations that satisfies eq.(3.1). It becomes imperative then to show that the any initial distribution $N(\xi)/N$ evolves towards the distribution $P(\xi) =$ and once such a distribution is reached it remains at equilibrium.
According to step (2), for any pair of states ξ and ξ', the number of configurations generated in state ξ' by applying the algorithm to the N(ξ) configurations in state ξ is $N(\xi)P_{\xi,\xi'}$, where $P_{\xi,\xi'}$ is the probability of accepting the trial configuration ξ' when $\xi_n = \xi$.
In addition, the number of configurations generated in state ξ' by applying the algorithm to the N(ξ') configurations in state ξ' is (1-$P_{\xi',\xi}$) N(ξ'). Therefore, the total number $\overline{N}(\xi')$ of configurations generated in state ξ' due to any other state ξ is

$$\overline{N}(\xi') = N(\xi') + \Delta N(\xi'), \tag{3.3}$$

where

$$\Delta N(\xi') = N(\xi)P_{\xi,\xi'} - N(\xi')P_{\xi',\xi} \tag{3.4}$$

is the net change in the number of configurations in state ξ', relative to $N(\xi')$. According to eq.(3.2) and eq.(3.4),

$$\Delta N(\xi') = N(\xi) - N(\xi')\frac{P(\xi)}{P(\xi')}, \tag{3.5}$$

when $P(\xi') > P(\xi)$ and

$$\Delta N(\xi') = N(\xi)\frac{P(\xi')}{P(\xi)} - N(\xi'), \tag{3.6}$$

when $P(\xi') < P(\xi)$.
Therefore, according to eq.(3.5) and eq.(3.6), $\Delta N(\xi') = 0$ when $N(\xi)/N = P(\xi)$ and $N(\xi')/N = P(\xi')$, i.e., the algorithm does not alter the relative population of the states when the ensemble distribution is equal to the equilibrium distribution. In addition,

eq.(3.5) and eq.(3.6) indicate that $\Delta N(\xi') > 0$ when $N(\xi')/N < P(\xi')$ (and $\Delta N(\xi') < 0$ when $N(\xi')/N > P(\xi')$), i.e., the algorithm evolves any arbitrary distribution towards the equilibrium distribution where $\frac{N_\xi}{N} = P(\xi)$.

3.3 Some discussion on Lattice MC method:

The main motivation behind the present model was to provide a fast (yet reliable) method to study the diffusion controlled polymerization reaction and the relevance of filament treadmilling and branching, in the context of cell motility. In this respect a lattice vesicle is designed in order to speed up the MC method by avoiding the calculation of the potential energies.
The standard Metropolis MC method for stochastic, canonical system generates equilibrium fluctuations of a set of N particles which in our case N_m number of membrane beads of lattice membrane. This has configuration $X = (x_1, \ldots, x_{N_m})$ and by taking randomly a bead $1 < j < N_m$ displace it by an amount $dx = \Delta x \times \eta$. The maximum displacement in the present scheme was kept constant Δx and η denoted a random number equally distributed on the interval $[-1 \ldots 1]$. The decisive rule behind acceptance, that is the condition for the new configuration X_n being accepted can be written as : if

$$E(X_n) \leq E(X_o)$$

Where $E(X)$ is the total energy of the system depending on the configuration X,
The above condition does not fulfill if

$$\mu < \exp(-(E(X_n) - E(X_o))/k_b T) \; . \tag{3.7}$$

where μ is a random number distributed equally in the interval $[0 \ldots 1]$.
Then the new configuration rejected and the membrane bead does not move. A MC time step is usually defined as N trials and it is expected to get the right equilibrium configuration.
From the property of polymer simulation it can be said that polymers on two dimensional lattice are reasonable model systems to study polymer dynamics [108, 109]. Generally model polymers are coarse-grained and projected onto a square or triangular lattice. A polymer is represented as a sequence of beads $r_i = (m_i\ell, n_i\ell)$, where the m_i and n_i are integer numbers and ℓ is the lattice spacing. The difference between two consecutive beads is called a bond, $b_i = r_i - r_{i-1}$. There are several algorithms that exist for the lattice bond dynamics. It should be mentioned that the polymer on lattice model is closed, $r_{N_m} = r_1$, where N_m is the number of beads on the membrane. Such a construction can be called a lattice vesicle. Generally this kind of model are used to study the diffusion of an ideal ring polymer in a network of obstacles.
In the beginning we have used one algorithm that is simple and efficient to produce all possible states: the chain segment b_i in this algorithm are placed into new configuration

by 'kink jumps' or 'hairpin moves'. Hairpins are also known as defects [24], and their configurational changes, accordingly, are called defect moves. These two moves are illustrated in fig 3.1 for a square lattice. To simulate the polymerization or branching phenomena, it is necessary to simulate the diffusion of actin monomers inside the model cell.
These actin monomers undergo Brownian motion like an ideal gas particle and exert an inner pressure to the membrane. Due to this effect the cell develops the tendency to become more and more inflated like a balloon filled with air. But as required for the present study, in order to prevent the leaving of monomer from the cell, membrane should be impenetrable for them. But this requirement leads to a different problem, namely the membrane beads become restricted in their movement if the number of free actin monomers increases. As a result cell relaxation slows down and the cell eventually becomes completely immobile at certain critical quantity of monomers.
In order to solve the problem stated above and to model the membrane more mobile it was recognized that switching over a bond fluctuation model [110, 109] (which has been discussed in next section) will be helpful. Where, as in the kinkjump/hairpin model, the bond length is kept fixed $\mid b_i \mid = 1$. Astonishingly, following this scheme of things, it turns out that kinkjump / hairpin lattice model represents a square lattice a square itself. Obviously this can only be thought of as artifact of our artificial model to mimic biological reality. Since it is easy to predict from biological knowledge that a square shaped cell does not feature amongst the list of all the probable shapes of any biological cell, we could infer easily that this particular model to study cell locomotion to be not very attractive.
A detailed discussion on the bond fluctuation approach is represented next section.

3.4 Membrane dynamics:

We wanted to model the cell membrane by a two dimensional flexible rings consisting of N_m beads (the total number membrane beads) with positions r_i(the set of real numbers in the plane). The beads are connected by polymer chains and the corresponding lattice point r_i^l is made to remain at the same point as r_i (because both are integers). In our bond fluctuation algorithm, one single monomer can move in eight possible neighboring sites. Fig 3.2 is an illustration of all possible movements (except hairpin movement) of the membrane beads with respect to its neighbors in a bond fluctuation model. The advantage that is gained from such a formulation is that it has twice more degrees of freedom to compare to earlier hairpin/kinkjump model. If we represent the position of one membrane bead by r_i, the connectivity condition can be expressed as :

$$r_{min} \geq \mid r_i - r_{i-1} \mid \leq r_{max}$$

where $r_{max} = \sqrt{2l^2}$ and $r_{min} = l$, ensures, that the cell is closed even when projected on to a lattice. The lattice constant (that is the constant distance between two lattice

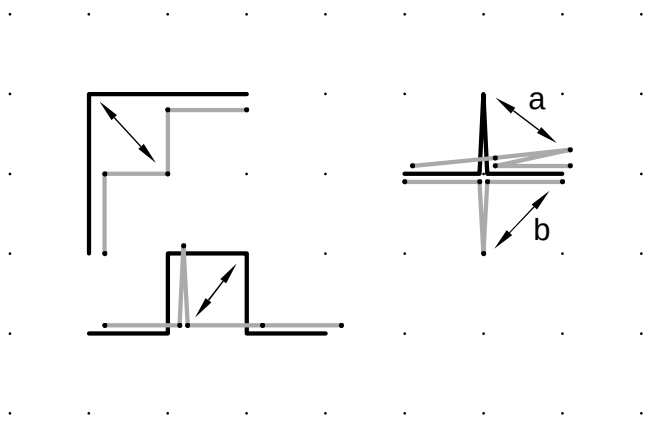

Figure 3.1: Illustration of two kinkjumps(left) and one hairpin move (right) in a lattice polymer model. The hairpin move can be restricted to a 90° turn (labelled a), but here is unrestricted, so it can rotate the hairpin by 90°, 180° (labelled b) and 270° (not shown).

point in a lattice) is represented by l.
The basic idea behind this formulation was to ensure that the monomers fail to find a 'hole' in the cell through which they can escape. Thus, in other words, to make it possible to conserve the monomers inside the cell membrane.
Equilibrium conformational fluctuations of the ring are generated by a dynamic Monte Carlo method. The corresponding protocol is described bellow :
Step-1) Each bead, either selected at random or sequentially, is randomly displaced by

$$r_i \rightarrow \; r_i + \eta \cdot \Delta \; r_{max} \tag{3.8}$$

to a nearby position, where η is a random number equally distributed in the interval $[-1 \ldots 1]$ and selected at random for each coordinate separately. The maximum displacement Δr_{max} determines the diffusive property of the ring.
Step-2) The trial movement of a single membrane bead will be accepted if neither the excluded volume interaction with actins (monomeric or polymeric form) are violated nor the restriction on the allowed range of the bond length.
Constraints imposed on this implementation scheme includes : 1) the minimum bond length between a moving particle and its nearest neighbor should not be less than 1 and 2) the maximum bond length should not be greater than $\sqrt{2}$(as l=1).
The membrane in this scheme is modelled as a set of N_m (the total number of membrane beads) beads. One Monte Carlo time step t_o is defined as N_m (randomly or sequentially)

attempted move of the membrane. The number of Monte Carlo time steps is required to move the membrane beads is defined as MC. To determine the value of MC we follow the previous successful approach [111], and note that the obtained value is 5. As this polymer ring does not follow self avoiding random walk movement, in equilibrium state it should exhibit the mean square radius of gyration $\langle s^2_{gyr} \rangle \sim N_m$. To check the dynamical properties of the model we reproduce the result of Rouse model dynamics (see appendix A) moves of the membrane.

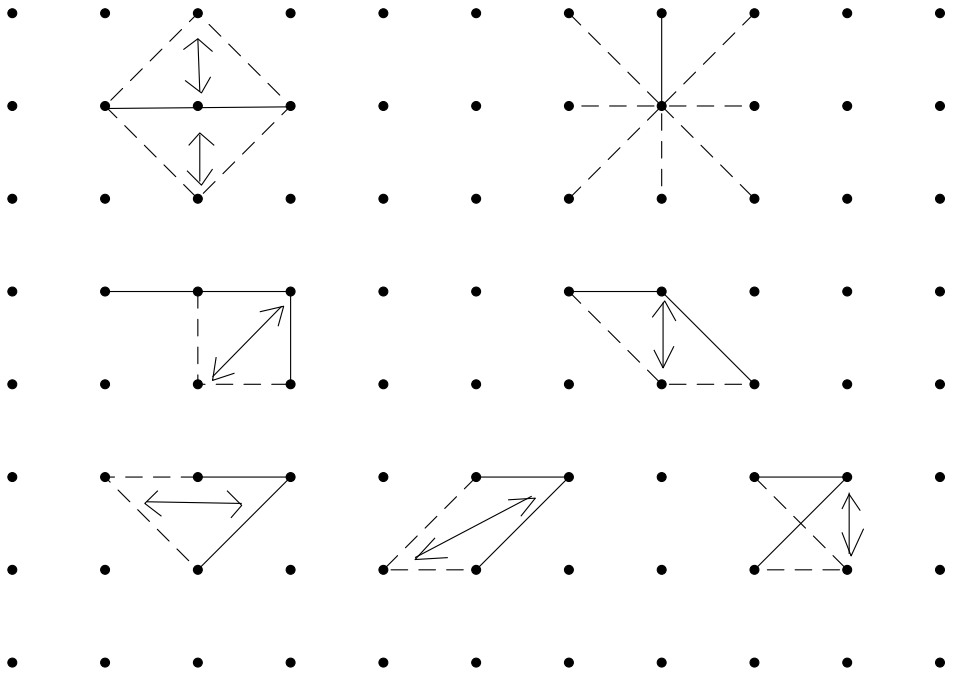

Figure 3.2: An illustration of few possible movement of the cell membrane bead. The broken line and the solid lines are indicating before/after configuration of membrane bids.

3.5 Actin dynamics:

From the biological experiments it is known that the most necessary cytoskeletal component with respect to cell locomotion is the actin molecule. Hence actin is naturally considered as the most important part of our model cell also. The total actin number

'n' is conserved. We knew further that any actin monomer can exist in two states: as a single, "free" monomer (G-actin) or as a part of a filamentous polymer (F-actin). In the previous section (see section 2.7) it had been discussed how different regulatory proteins bind to actin monomers and help in polymerization process. But for sake of programming simplicity we had opted to consider the effect of some of these regulatory proteins implicitly and had further considered G-actin as a "free" moving monomer. The term "free" is used in this study to denote actin that is not part of a filament and certainly this is a simplification. Because from biological experiment we know that actin binding proteins do a lot of things with actin monomers but for the sake of simplicity this effect is not included in present model. However we felt that this modification in the descriptional scheme of free actin molecules will not disturb the essential physical properties of a mobile cell significantly; and was thus considered.
F-actin can be treated as an immobile polymer which interacts with the G-actin pool by (de-)polymerization. G-actin then, can be considered as a freely diffusing particle on the lattice that underlies the model cell. Every time step t_o every G-actin monomer can move randomly either x or y or x and y direction in l_g lattice length, where $0 \leq l_g \geq \sqrt{2}$. Where as for F-actin diffusion coefficient $D_f = 0$.
No excluded volume constraint is imposed among G-actin molecules. Excluded volume condition, however, is imposed between membrane and G-actin molecules. This makes the membrane impenetrable for actin molecules successfully. In case of F-actin, excluded volume condition is applied between F-actin molecules and membrane also; but not between F-actin and G-actin. In case an attempt of movement of G-actin is registered as invalid, the old configuration is considered as new one. Similarly, attempt by a membrane bead to occupy a lattice site that is already occupied by any actin or other membrane bead is rendered invalid. It is true that the finite size of the polymer ring has a significant effect on diffusion coefficient of G-actin .
We notice also that owing to the G-actin molecules, additional complication arise in the model cell. The Brownian motion of the diffusing G-actin molecules exerts an internal pressure on the enclosing membrane, which leads to an expansion of the enclosed area and a stretching of the membrane. The latter effect has an influence on the shape and motility of the cell. Comparing this case to the actual biological case we notice that in the real biological cells a sophisticated balance between internal and the external pressure, produced by cytoplasm and the surrounding media, is maintained and regulated by complex signal-related protein network.
The filament is immobile and the immobility of filament takes into account the strong adhesion of F-actin to the extracellular substrate mediated by a macromolecular complex containing integrin, vinculin and other proteins, which are not included explicitly in the cell model. The immobilization of F-actin filaments represents the necessary force in order to have a traction of the cell and is necessary to break the symmetry responsible for the conservation of total momentum of the system. The reason behind this is evident, to respond in a consistent context-dependent manner with respect to the chemotactic signal, filament alignment should be asymmetric to generate a prominant front and rear

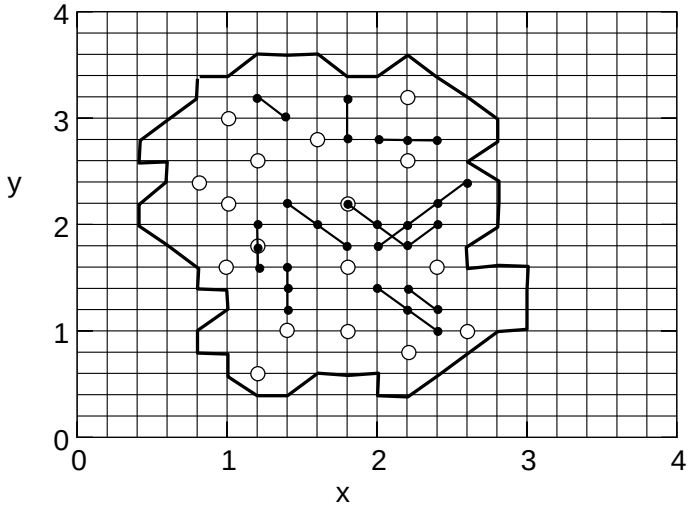

Figure 3.3: Snap-shot of the Monte Carlo lattice model : open circles are actin monomers and the filled circles are filament.

part of cell. Although, here again, the experimentally observed fact of semi-rigidity of the filament is neglected for the sake of programming simplicity. However this property is not expected to change the basic characteristic behavior concerning the asymmetry in polymerization rates and sites [111] and so does not perturb our goal of modelling the biological reality, justifying its omission.

3.6 Polymerization dynamics:

From the perspective of polymerization dynamics, the entire picture can be drawn as depicting the ways and means of interaction between actin monomers and polymers, via polymerization reactions depicted in fig. 3.4. Here monomers can be added or can be removed from any end of a filament. These processes are termed polymerization and depolymerization respectively. F-actin monomer associates to an existing filament in case of polymerization and the process of polymerization itself takes place at certain rates at the both ends. The chemical activity of the two ends of a filament are different: there is a fast growing barbed end and a slow growing pointed end. In the previous chapter(see section 2.5) is an evidence that in a locomoting cell the filaments are oriented in such a fashion that the barbed ends are directed towards the direction of motion of cell. Which imply that the barbed ends interact with the membrane at the leading edge(LE) and the pointed ends interact with trailing edge (TE) of the cell. At the LE(TE) actin monomers polymerize onto filament with a rate $k_B^+(k_P^+)$ provided they are located on the nearest neighboring lattice site of the filament. The effective polymerization rate

depends on k_B^+, k_P^+, on the density of free actins(monomers) and on the concentration of filament ends. The depolymerization reaction takes place with rates k_B^-, k_P^-, which is independent of G-actin concentration. Hydrolysis of the ATP that was bound to each actin monomer favors filament disassembly, returning actin monomers to the pool of polymerization-ready G-actin. All reaction rates are given in unit of t_o.
Some researchers [112] have given a different interpretation of polymerization. According to them the monomers can as well be considered as particles diffusing in a liquid(liquid state). The filament ends act as sources and the sinks for the monomers. Every polymerization step removes one free monomer from the liquid state into an immobile state at the tips of the filament. On the other hand, every depolymerization inserts a monomer into the liquid state. The reaction can then be understood as a diffusion controlled condensation and evaporation of actin monomers. In biological systems ATP generally assumes the role of an energy supplier. But we note alongside that ADP bound G-actin is also able to associate and dissociate from filament. The rate constant for ADP bound G-actin is different from ATP bound G-actin. For ATP bound G-actin association rate constant for barbed and pointed ends are represents as k_B^+ and k_P^+ respectively. The same hold for the depolymerization rates k_B^- and k_P^- . Thus taking all of them into account, the concentration changes according to the rate equation :

$$\frac{dC}{dt} = -k_{B(P)}^+ C + k_{B(P)}^- \tag{3.9}$$

Under equilibrium condition $\frac{dC}{dt} = 0$ and the critical concentration for barbed and pointed ends are equal. i.e.

$$C^* = \frac{k_B^-}{k_B^+} = \frac{k_P^-}{k_P^+} \tag{3.10}$$

However cells under physiological conditions exhibit ATP hydrolysis or Mg-ATP-G-actin binding to the barbed end. This leads to an asymmetry in the critical concentration at the two ends,

$$\frac{k_B^-}{k_B^+} < \frac{k_P^-}{k_P^+} \tag{3.11}$$

The critical concentration of ATP G-actin for barbed and for pointed ends are approximately $0.1\mu M$ and $0.7\mu M$ known form experimental result. The asymmetry between the critical concentration at the both ends leads to an increased association of G-actin at the barbed end and an increased dissociation of G-actin at the pointed end. This effect is well known and is termed "treadmilling". In our present model all the reaction rates are transformed into reaction probabilities.
It is obvious from the rate description of the reaction that the average length of filament will fluctuate with changing value of rate constants. For the simulation we had used

$$(k_B^+) > (k_P^+) \tag{3.12}$$

and

$$(k_B^-) < (k_P^-) \tag{3.13}$$

The total number of actin inside the cell, say n, is assumed to be constant in our model. The number of F-actin monomers n_f can be divided by n to get the average concentration of filaments. So the remaining $(n - n_f)$ monomers are free G-actin n_g . It is noticeably that all the quantities are time dependent except n, e.g. when n_g decreases by 1 due to polymerization, the n_f increases by 1. A complete picture of model cell is given in fig 3.3. In this snap-shot $n = 46, n_f = 29, n_g = 17$ and $N_m = 50$.

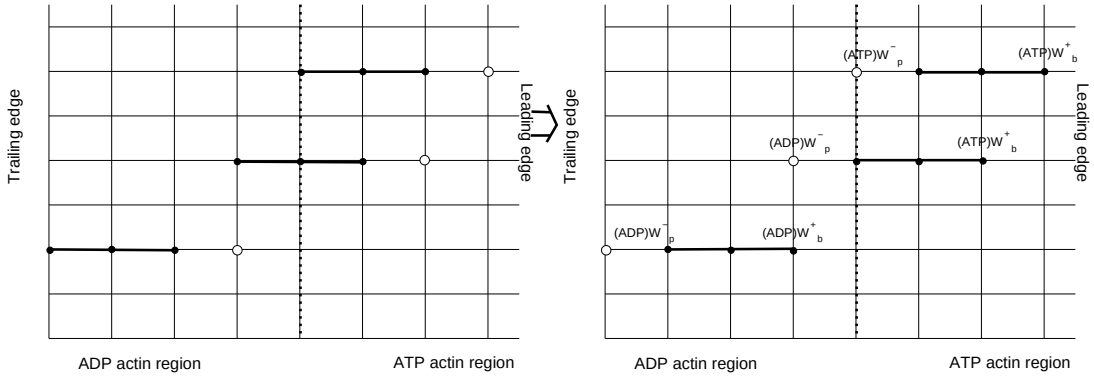

(a) (b)

Figure 3.4: Illustration of the (de-)polymerization reaction. The left hand sight of the dotted line is presenting ADP actin region and the right hand sight is for ATP actin region. The open circle is presenting the actin monomer and the closed circle is presenting the filament.

3.7 Nucleation dynamics:

Nucleation occurs in two different ways for the formation of any F-actin. The nucleation process is called the spontaneous nucleation when two G-actin monomers form a binary complex filament. Spontaneous nucleation does not have any preferable position, it can happen any position inside the cell with reaction probability W_n. The second type is called the branching nucleation or dendritic nucleation. As a result of branching nucleation a new filament is formed as a branch of a existing filament. In dendritic nucleation process actin monomer and polymer interact with each other.
It is known that the activated protein complex Arp2/3 can associate with an existing filament and can nucleate a new filament as a branch from the mother filament at an angle of about 70 degree. In the square lattice model the branching process is implemented as follows. If a G-actin is found to be on an adjacent row of an existing filament, a new daughter filament is created at the site with probability W_{br}^+. If on

that particular position already a filament exists the nucleation attempt will be rejected. When a filament becomes mother filament, the particular actin (within mother filament), which is attached with the daughter filament can not take part any other branching process unless existing daughter filament dissociates from the mother filament. The rule remains the same for the actin (within the daughter filament) which is attached with mother filament. Although, it is important to mention here that one mother filament can have more than one daughter filaments.
Based on experimental information [113] we can infer that the direction of the daughter filament should be same with the mother filament. Hence the growing tip of the daughter filament can well be recognized as the plus end or barbed end. The protein complex Arp2/3 is not taken into account in the present model because of its large concentration profile, especially near the membrane where it is activated. In the simulation a fixed range of activated Arp2/3 has been used for branching activity. Debranching happens with reaction probability W_{br}^{-}.

3.8 Summary:

property	Study in the MC model
membrane	diffusing beads connected by variable bond length
actin monomers	diffusing freely on a lattice
actin filaments	resting on a lattice
nucleation	rate constant and actin concentration dependent
polymerization	rate constant and actin concentration dependent
depolymerization	rate constant dependent
substrate	implicit due to lattice
excluded volume	lattice occupation

Table 3.1: Basic properties of MC models for cell locomotion.

4 Some General features of cell motility

4.1 Introduction:

In this chapter the first step is to understand the mechanism which is responsible for cell's persistent random walk during migration on flat substrate. In uniform concentrations of chemoattractant, cell exhibits a persistent random walk. In this type of motion cell moves in a unidirectional way for long time interval and this time duration corresponding to persistent motion is called the persistence time. One of the crucial factor for cell movement is the filament polarity and this is related with persistent random walk . The main focus of this present study is to find the cause behind the persistent random walk , and hence the cause behind the corelated change of polarity. Definitely this understanding will help later (in chapter 7)for the case of chemotactic cell movement. When the external signal is unidirectional the cell behaves chemotactically. It is known membrane bound molecule PIP3 plays an important role in case of chemotactic movement. So other than filament association and dissociation the distribution of membrane bound PIP3 is another important parameter for unidirectional motion. The filament polarity and the spatial distribution of membrane bound PIP3 molecule has a strong dependence. So furthermore we are interrested to understand the relation between the unidirectional motion (actually this represents the filament polarity) and the PIP3 distribution.

4.2 Model description:

In chapter 3 the details of the general rules of model and the modelling techniques are already described. In the current study we focus on the Persistent Random Walk(PRW) which has been discussed in chapter 2 elaborately. To avoid more computational complexity, in present case we chose to restrict ourselves to simple two dimensional model cell. In our model we neglect the intricacies of an actual biological cell body, i.e., the nucleus and other organelles. A snap-shot of the lattice model is plotted in fig 4.1. As detailed description already has given in chapter 3 , here a short summary is provided.

4.2.1 Membrane:

The plasma membrane of a biological cell is highly complex surface consisting of a lipid bilayer. We reorganized the difficulty to capture the actual complexity of the cell membrane in our model membrane. Thus in conformance with a previous study [111] we chose to model the membrane as a flexible closed ring embedded on a square lattice. The effect of free diffusing particles on model membrane in terms of internal pressure and mobility of cell was discussed in section 3.2 . Here the numbers of monomer are not very large which can make the cell inflated. The membrane beads only follow kinkjump/hairpin movement. The ring does not follow self avoiding property and it exhibits random walk characteristic. Studies of conformational changes in the ring are done using Monte Carlo methods by performing kink jump or hair pin jump.

4.2.2 G-actin:

The model membrane encloses a fixed number, n of actin molecules. Actin molecules typically have a size [114] of about 5 nm x 5 nm and is located at any of the vertices of the square lattice. The G-actin molecules diffuse freely from one lattice point to another. No excluded volume condition is imposed among G-actin molecules. But to make the membrane impenetrable for the G-actin, excluded volume condition is imposed between G-actin and the membrane.

4.2.3 F-actin:

G-actin monomers form a rigid filament by associating with each other. According to experimental results [115, 116], the filaments are assumed to be chemically coupled to the underlying substrate via membrane proteins. This attachment to the substrate provides the necessary forces (in the form of traction) for the advancement of the cell. This is the reason behind construction of immobile filament in model cell.

4.2.4 Actin-associated proteins:

A group of regulatory proteins which help to form actin network and hence control membrane protrusion are also called actin associated proteins. In section 2.7 an elaborate discussion on different actin associated proteins has been provided. Proteins of WASP/Scar families activate Arp2/3 protein complexes. It has been experimentally found that these complexes nucleate new actin filaments at the side of existing filament at an angle of 70 °.
Based on experimental observations, it is known that Arp2/3 is activated only close to the membrane. Therefore Arp2/3 induced branching process must be expected to happen only near the membrane. However the Arp2/3 molecule is not explicitly taken into account in our model because of its large physiological concentration, in particular

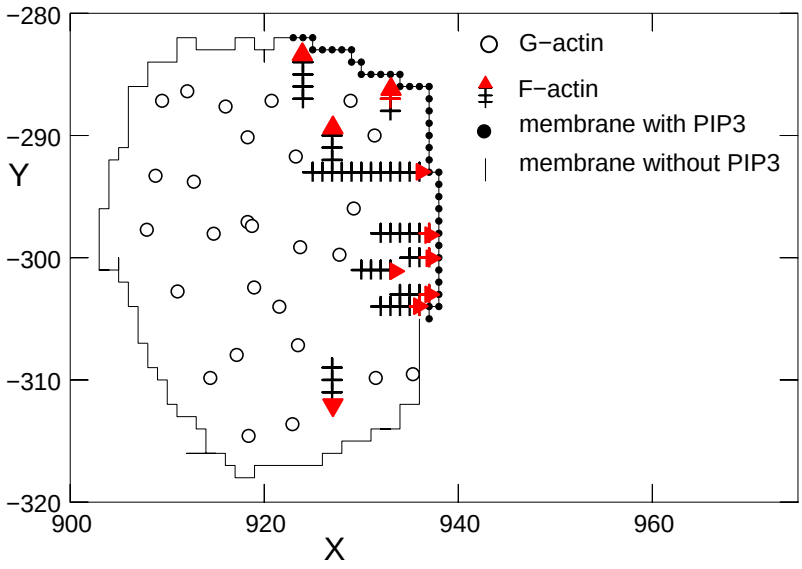

Figure 4.1: A snap-shot of model cell.

near the cell membrane, where it becomes activated. In our model, the width of the range of activation is taken to be 10 lattice sites. We chose the width of activation range by our own estimation. From the simulation result it has been seen that very narrow or very wide activation area is not effective for a efficient chemotactic motion. Accordingly the branching from an existing filaments was carried out in our scheme only if the filament extends to the range of activation near the membrane.

4.3 Probability and reaction rates:

Regarding the reaction rules we follow previous work [111]. According to the previous model diffusion of moving particles and the reactions follow different time scale. In between two reaction steps, the mobile particles and the membrane perform random diffusion for 'MC' (Monte Carlo) time steps which has already been discussed in section 3.4. In the reaction step one actin molecule is selected randomly. Then for either G- or F-type molecule, a random choice with equal probability is made for association or dissociation process. This leaves us with four possibilities :
1) If G-actin molecules and the dissociation process is selected the reaction attempt will be stooped.
2) If the association process for G-actin molecule is chosen, the successful reaction can happen provided selected G-action find a neighboring G-actin or F-actin in the selected

Quantity	*Value*
Lattice constant, a	5 nm
Typical cell size	100×100 lattice
Monte Carlo step, τ	$0.875\mu s$
W_n	0.01
W_{br}^{+}	0.1
W_{br}^{-}	0.6
W_B^{+}	1
W_B^{-}	0.0012
W_P^{+}	0.11
W_P^{-}	0.02

Table 4.1: Reaction probabilities of model cell.

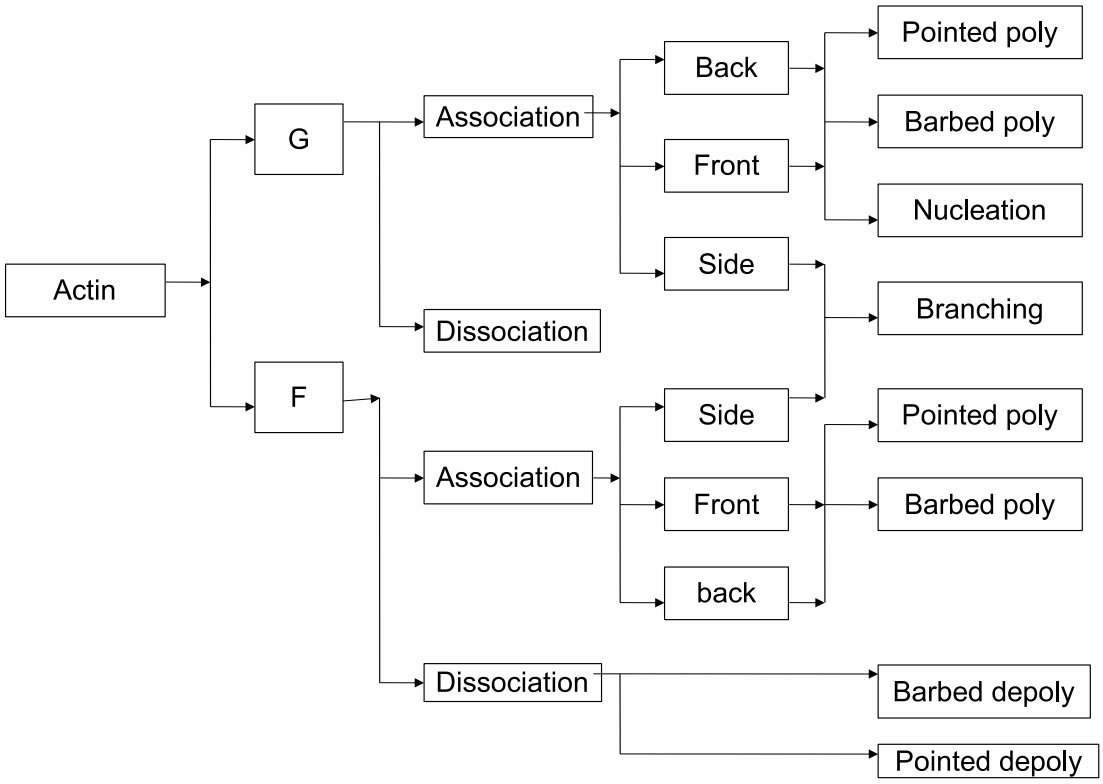

Figure 4.2: A flowchart consisting different reaction rules performing by all the actin monomers in a moving cell.

direction as shown in the reaction algorithm chart(see fig. 4.2). According to the type of molecules if the probability W_n or W_{br}^+ or W_B^+ or W_P^+ fulfill the condition $W > \eta$, where η is a random number $0 < \eta < 1$, a polymerization or nucleation (spontaneous or dendritic) takes place in the model.
3) If the association process for an F-actin is selected the successful reaction can happen if in the selected direction neighbor G-actin exists and the reaction probability satisfies the condition as described in case(2).
4) If dissociation process of a F-actin molecule is selected, the process will take place with probability W_B^- or W_P^- or W_{br}^- .

4.4 Persistent random walk and filament polarization

In presence of homogeneously distributed signal, cell shows a random but persistent motion; called 'Persistence Random Walk'(PRW). From the experimental observation [2, 117, 118] and from simulation studies [13, 111] it is known that regulatory protein complex Arp2/3-induced dendritic nucleation plays very important role for PRW of a cell. The PRW is characterized by stop and go movements: unidirectional motion with almost constant velocity over distances of the order of several cell diameters are separated by localized short time erratic movements. After each interruption of the ballistic motion, cell continues to move in a different direction. A typical trajectory of the center of the model cell is shown in fig.4.3 as an example of PRW. The persistency of the cell's random walk can be deduced from the time dependent mean square displacement of the cell and in our model is defined by

$$R^2(t) = \langle [R(t) - R(0)]^2 \rangle = \langle [Y(t) - Y(0)]^2 \rangle \tag{4.1}$$

Fig 4.3 is representing the typical mean square displacement of a cell. The behavior of r.m.s (root mean square) at short and long times are controlled by random diffusion of mobile particles and the membrane. The detail set of chatarteristics of r.m.s have been discussed in chapter 7 later. In the intermediate time, the cell motion exhibits a unidirectional drift during certain persistence time. This unidirectional motion can be explained as a result of autocatalytic dendritic polymerization [13, 119] in cell. The branching process produces a tremendous growth of filament in a certain direction which lead to membrane protrusion and as a result cell movement in the same direction. This unidirectional motion lasts only for a short persistent time and then it changes its direction. In the next section I will discuss the reason behind this dynamic instability.

4.5 Dynamic instability:

The fundamental quantity which governs the migration of the cell is its polarity and its self sustaining mechanism choosing direction of motion. The cell polarity is macroscop-

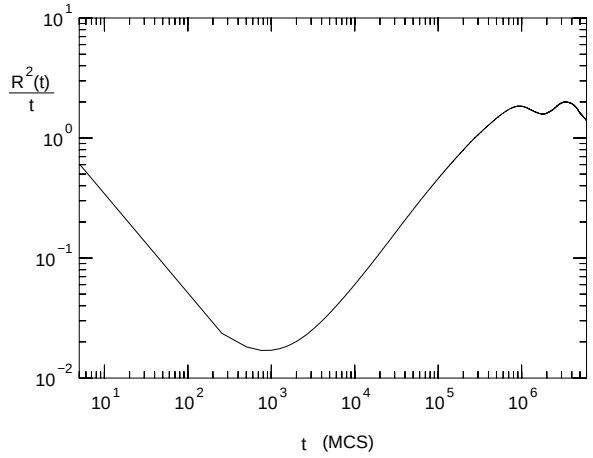

Figure 4.3: Typical mean square displacement of a cell exhibiting a persistent random walk.

ically and dynamically characterized by the formation of leading and trailing membrane edges, which in turn, are consequences of the cell's coupling to the polarity of the enclosed actin cytoskeleton. The polarity of the cytoskeleton itself is the average orientation of its filaments, where each actin filament is characterized by a polarity due to its plus and minus ends. This spontaneous internal polarity of the actin network determines the direction of cell motion and is maintained without external signals (e.g. chemotaxis) only for a certain time (persistent random walk). Specifically, the formation and regulation of cell polarity is achieved by a complex protein signalling network with positive and negative feedback loops. However since these approaches are beyond the scope of this work, we would not discuss those details. We note that different signals converge, among others, on the activation of an Arp2/3 protein complex; which leads to branching and the autocatalytic polymerization. In our present 2D model, we define the polarity of the cell by the polarity of the total actin network, i.e., by the difference in the number of filaments pointing in opposite directions. The mathematical representation of polarity 'P' is as follows,

$$P = \frac{[F^{up} - F^{dn}]}{F_{total}} \tag{4.2}$$

Where F^{up} represents the number of filaments going in the positive Y-direction and F^{dn} the same in the negative Y-direction. F_{total} is the total number of filaments in the model cell. The range of polarity parameter is $-1 \leq P \leq 1$. The trajectory of cell's randon displacement (PRW) and the corresponding polarity (dotted line, right scale) is shown in fig 4.4. From this result it is clearly noticeable that at certain times, P(t)=0 , the cell changes or tries to change the direction of its motion to the opposite side , as indicates by the corresponding displacement Y(t).

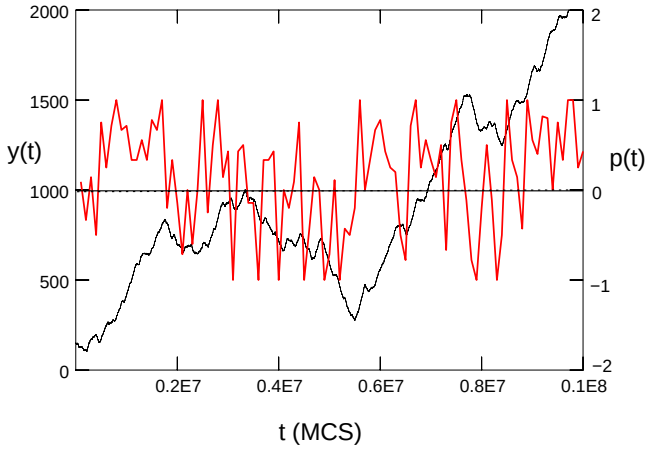

Figure 4.4: The trajectory Y(t) (full line, left scale) and polarity P(t) (dotted line, right scale) of a cell exhibiting a persistent random walk, as a function of time t in units of Monte Carlo steps, MCS.

The entire process can be understood as follows. During a spontaneous nucleation process (where two G-actin monomers form a new F-actin filament), the orientation of the new filament is determined at random. This is in contrast to the dendritic nucleation process, where the daughter filament branches off the mother filament and therefore always adopts the same direction of growth as the mother filament. Therefore, spontaneous nucleations are able to change the sign of polarity, whereas dendritic nucleation only increases the absolute value of polarity. The first leads to random motion, whereas the latter prolongs unidirectional motion. Since the polarity fluctuates in time, the spontaneous nucleation may eventually dominate and cause a change of polarity, and hence a change of vectorial motion. In other words, the vectorial motion of a cell becomes unstable due to two antagonistic processes: the spontaneous and the dendritic nucleation processes [120]. This understanding is proved by simulations of various limiting cases, which are shown in fig 4.5.

In one extreme case, the cell motion is caused solely by spontaneous nucleations. The corresponding curve is shown in fig. 4.5 by the full lines with label 's'. At two different nucleation probabilities, W_n , the mean square displacements indicate ordinary diffusion, $R^2(t)/t \approx$ constant, at almost all times. This is expected due to the random orientation of newly established filaments. A very weak persistency may be expected at small nucleation rates.

In the other extreme case, the cell motion is caused solely by dendritic nucleation. Since in this case the orientation of the filaments is preserved, the corresponding curve (dotted line with label 'd') has to exhibit a clear drift motion , $R^2(t)/t \sim t$, which takes place for times larger than a characteristic time $\tau_d \approx 7 \times 10^3$. The characteristic timescale τ_d separates periods of cell advancements and localized cell displacements ('resting'). Since

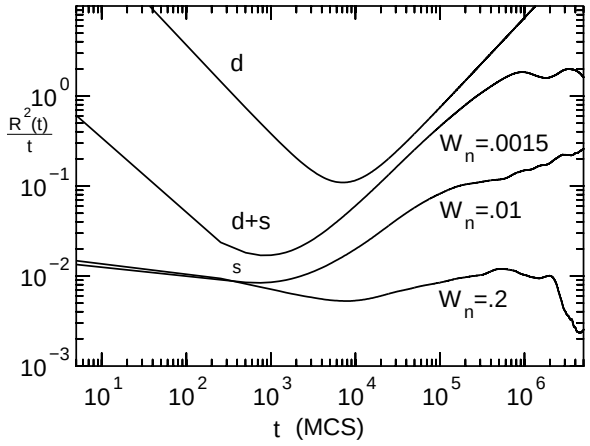

Figure 4.5: Mean square displacements of a cell under different conditions and at different probabilities of spontaneous nucleation, W_n.'s' represents spontaneous nucleation, 's + d' represents both spontaneous and dendritic nucleation, and 'd' represents dendritic nucleation only.

the activation range of Arp2/3 extends only a few lattice sites from the membrane, the rapid advancement of the leading edge of the membrane together with the rapid autocatalytic processes of branching near the leading edge, deprive this area of available G-actin molecules which are necessary for continuation of these processes. Therefore, the actin network and cell remain temporarily, during $t < \tau_d$, essentially at rest. While recruiting G-actins by diffusion from the minus to the plus ends of the filaments near the activation zone, the membrane of the cell performs random displacements around the immobile filament network, which leads to time-independent displacements of the cell, $R^2(t)/t \sim 1/t$ at $t < \tau_d$.
The interesting intermediate case, which corresponds to the persistent random walk, where a few events of spontaneous nucleation interfere with dendritic nucleations, is shown in figure 4.5 by the broken line with label 'd + s'. At a nucleation ratio of $W_n/W_{br}^+ = 0.015$, again a drift of the cell is observed up to a persistence time $\tau_p \approx 10^6$. At larger times, ordinary diffusion $R^2(t)/t =$ constant is observed, indicating the dominance of spontaneous nucleation processes. For $t < \tau_p$, the mean square displacements are qualitatively the same as for the dendritic case 'd'. The persistence time τ_p is a function of many model parameters: the length of the membrane, L, the number of actin molecules, n, the activation range of Arp2/3, and the seven transition probabilities, W, as listed in table 4.1.

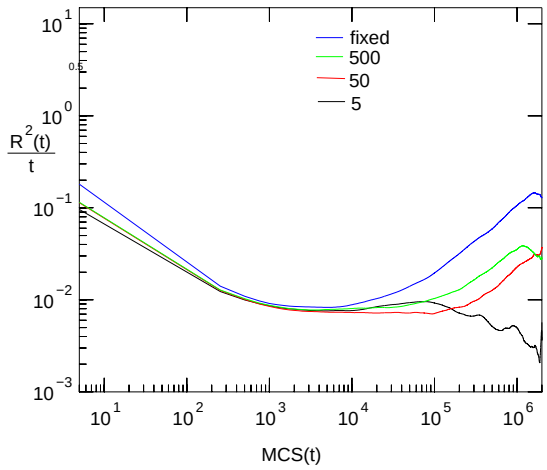

Figure 4.6: Mean square displacement of model cell with half of the membrane beads are PIP3 accumulated. Different numbers with corresponding colors are representing the PIP3 deactivation time constant in terms of MCS. And in all cases the PIP3 activation probability is 0.5.

4.6 Extracellular signal and cell motion:

To observe the reaction due to chemotactic signal on cell's motion we fix certain part (200 membrane beads out of 400 membrane beads) of the cell with artificially signal occupied receptors. After a downstream signal process, cell becomes able to produce active PIP(PIP3) on the membrane. The model under study in the present case is admittedly primitive and simple in nature. Our main aim was to observe the behavior of the cell with some PIP3 occupied membrane. In our observation it is seen that when the fixed part of the membrane is able to produce PIP3 molecule with probability constant 0.5 (maximum is 1), the actin polymerization leads to the direction of accumulated PIP3. And as a result cell moves in a unidirectional motion where front part of the cell consist PIP3 activated membrane.
The unidirectional motion becomes slightly slower when we introduce a deactivation constant of the PIP3 in terms of Monte Carlo time steps. So in this case we assume that after some Monte Carlo time steps all PIP3 will die only to be produced again with same probability constant (0.5 here). We observe the motion of the cell (in the present case it represent the trajectory of the mean square dispalecement) with different deactivation time steps such as 500, 50 and 5. Fig. 4.6 is representing the corresponding graph. When deactivation constant is 5 which means the PIP3 dilute rapidly(every 5 Monte Carlo steps). So the membrane bound PIP3 conformation changes frequently. In this case cell does not show a strong unidirectional motion towards the accumulated PIP3, rather it shows a random motion. With increasing the deactivation time constant the unidirectionality become stronger.

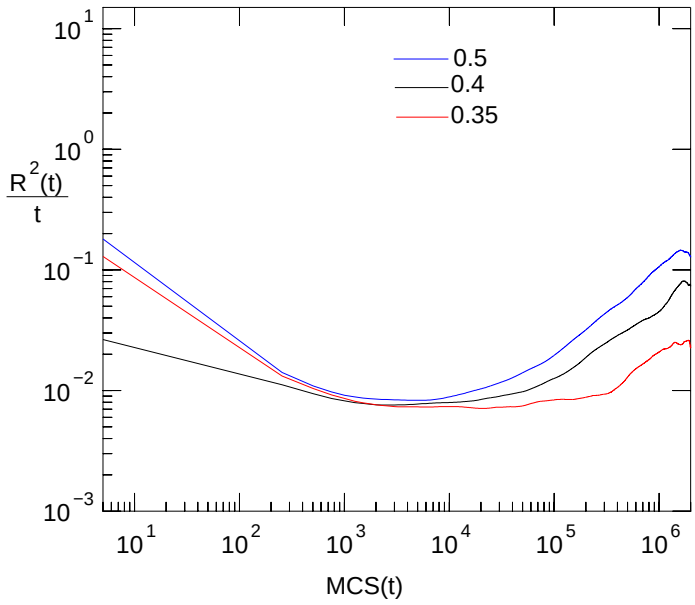

Figure 4.7: Mean square displacement of model cell whose part (50 % of total cell membrane) of cell membrane is accumulated by PIP3 molecules and the cell is under different PIP3 activation probabilities. The numbers are indicating the PIP3 activation probability.

Before finding the possible explanation behind the aforementioned behavior of cell with different deactivation time steps, we require to observe another situation. In this case we do not introduce any deactivation time step, rather we systematically change the activation probability of PIP3. We start to decrease the activation probability from 0.5 to magnitudes below than that. It's found that upto probability constant's magnitude 0.35, the cell is able to respond chemotactically. The corresponding graph is represented in fig. 4.7 . From these two observations, it can be concluded that to generate a unidirectional chemotactic motion cell depends more on a stable conformation of membrane localized PIP3 rather than a unstable conformation of the same. If the stable conformation contains comparatively less dense membrane bound PIP3 compared to an unstable but dense PIP3, the first conformation helps the cell to move a unidirectional motion.

To quote a previous researcher [121] : "D. discoideum amebae do not orient during the first several minutes of gradient formation in our chamber if the gradient is formed by removal of cAMP at the sink. The rate at which the cAMP concentrations decrease is greatest during this period. Subsequently chemotaxis was observed, although it was somewhat weaker than in the gradient formed by addition of cAMP through the source fiber ". From this observation it appears to be a clear suggestion that the amoebae are unable to respond to chemotactically decreasing concentration, if the concentration falls down more rapidly than the motility that the cell can be identified with. The hypothesis

above, made by previous researchers, also point out some other information. This set of information is narrated here. To polarize itself towards the chemotactic source, cell needs some time and if the change of external signal concentration is faster than the required time, it is then difficult for cell to respond correctly with the changing chemotactic source. Our observation supports this suggestion that instability in membrane bound PIP3 production is unfavorable for cell's unidirectional motion. Furthermore, a careful study on our framework of result implies that the time required for cell to polarize itself appropriately with concentration of external signal, depends on many parameters. These parameters include nucleation rate constant, polymerization and depolymerization rate constant etc. In our present model when external signal gradient concentration changes frequently due to low deactivation constant, cell fails to secure enough time to make a proper actin network towards the highest concentration signal. But the situation changes when the deactivation time steps increase and cells get sufficient time to accommodate the motility with the existing gradient. Although in chapter 6 we will see that the gradient sensing for a short distance source, where due to finite distance between source and the cell and continuous changing position of cell, the gradient concentration along the cell changes and according to that cell shows PIP3 accumulation on the membrane. This is also intersting to point out that the rapid changing of source concentration does not effect the generation of PIP3.

4.7 Summary:

In this chapter the first step was taken to form a model that is capable to explain amoeboid locomotion in terms of stochastic process. Some important features viz. treadmilling and branching of actin filaments are included too. The dynamics of moving cell is dominated by random diffusion at short time and at longer time cell shows drift motion. The filaments grow at both ends with treadmilling rate and branching in both direction leads to a persistent random walk. From our observation it has been found that the whole phenomena is controlled by two antagonistic nucleation processes during the polymerization of cell's actin cytoskeleton : the spontaneous nucleation and the dendritic nucleation processes. The spontaneous nucleation introduces randomness in cell's motion whereas the dendritic nucleation or branching helps to move in a unidirectional way. So in case of uniformly stimulated cell (which is our present case) the cell moves in a persistent direction due to the dendritic nucleation unless the spontaneous nucleation dominates over it.
In the second phase of study the cell is stimulated not uniformly but in a direction-specific manner. In this unidirectional movement cell motion follows the concentration of PIP3 on membrane. The simulation technique in the model is very primitive. The distribution of PIP3 accumulated membrane is changed by changing the deactivation time constant of PIP3 and the PIP3 activation probabilities. In both cases the expected unidirectional movement of cell shows the same nature of characteristic . To achieve the chemotactic

motion the stable distribution of PIP3 plays more dominant role than an unstable PIP3 distribution. Although this primitive model are able to point out some basic feature of cell chemotaxis motion but it is not possible to get the more complete picture by using this model. In case of cell's unidirectional motion one very very important feature is the amplification of the gradient signal into a strong intracellular response (PIP3). And this property is heart of many theoretical models where researchers concentration tremendously focus on it , and need less to say this important feature is absent in our present model. This may be the first reason why we need a real protein regulatory network which can amplify the weak extracellular signal and definitely is sensitive to signal changing.

5 Response To Uniform Homogeneous Signals in Stochastic LEGI Models

5.1 Introduction:

A number of mathematical models have been proposed to explore numerous potential mechanisms for gradient sensing, spatial localization and adaptation in eukaryotic chemotaxis. A common pattern of mechanism in many of these models is the interplay between a local activator and a global inhibitor [12, 122, 123, 124]. The present work has proposed a stochastic lattice model for eukaryotic cell based on the model proposed in a previous work [9]. In the present model both local activation and global inhibition pathways are activated through the same receptor activity. When cell is exposed to a uniform concentration of chemo-attractant, it has been found to adapt fully or partially.

5.2 Model description:

The basic philosophy of LEGI(Local Excitation Global Inhibition) model is pair of reaction mechanism called local excitation, global inhibition response. In the LEGI model, upon receiving the signal through receptor, the response is mediated through the balance between 1)a fast and local excitation and 2) a slower and global inhibition process. The faster local excitation rises with receptor occupancy, leading to an increase in the response. As the level of slower inhibition rises, the response subsides(in case of uniform homogeneous signal with proper parameter set this leads to perfect or near perfect adaption). The main players involved in LEGI model are as follows : R(cAMP receptor), E_{PI3K}(exciter of PI3K), E_{PTEN}(exciter of PTEN), I_{PI3K}(inhibitor of PI3K), I_{PTEN}(inhibitor of PTEN), BS_{PI3K}(binding site of PI3K), BS_{PTEN}(binding site of PTEN), PI(3,4,5)P3 and PI(4,5)P2 (for simplicity rest of the text we mention them as PIP3 and PIP2 respectively). In LEGI model two LEGI mechanisms act independently and in parallel. Fig.5.1 is representing model for regulation of PIP3 through complementary LEGI (LEGI-PI3K and LEGI-PTEN) mechanism. These two LEGI mechanisms regulate the membrane binding/activation sites for PI3K and PTEN upon chemo-attractant stimulation in complementary way.
The first LEGI mechanism generates PI3K binding sites on the membrane which has been described in details by Huang [77]. In this reaction the molecule involved in the fast excitation (E_{PI3K}) is confined only to the membrane, whereas the slower inhibitory

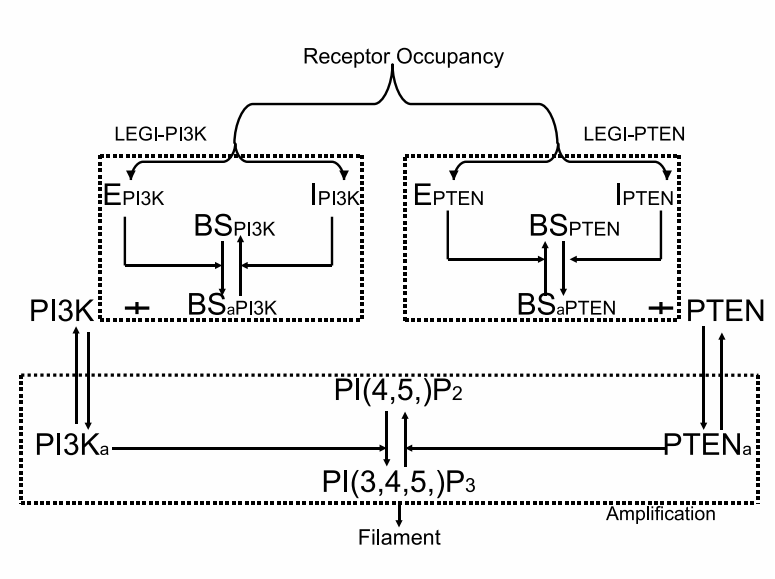

Figure 5.1: Illustration of LEGI model.

molecule (I_{PI3K}) is allowed to diffuse freely in the cytoplasm. This mechanism allows a transient increase of PI3K binding sites in response to uniform chemical stimulus and an accumulation of active PI3K binding sites on the side of cell facing the chemo-attractant gradient.
The other LEGI mechanism controls the activation of PTEN binding sites by using separate excitation (E_{PTEN}) and inhibition (I_{PTEN}) molecules. But in this case, the response regulator destroys active binding sites. From fig. 5.1 we can notice that PTEN binding sites are regulated in inverse way compare to regulation of PI3K binding sites. This event of destruction leads to a transient decrease of PTEN binding sites in response to uniform homogeneous signal and furthermore accounts for an accumulation of active PTEN binding sites on the opposite side of cell facing maximum chemo-attractant. It is already known from experiment [125] that PTEN and cAMP concentrations are inversely correlated. It is assumed here that there is no cross link in between two reaction mechanisms. This assumption is justifiable to satisfactory extent because the mutual independence of working schema of PTEN and PI3K, was established recently [77, 126]. The reactions involved in LEGI model are formulated as follows. Where "a " is indicating the active state of the corresponding molecule.

$$Signal + R \rightarrow R^a \tag{5.1}$$

$$R^a \rightarrow R \tag{5.2}$$

(activation probability = W_R^a, deactivation probability = W_R)

$$R^a + E_{PI3K} \rightarrow E^a_{PI3K} \tag{5.3}$$

$$E^a_{PI3K} \rightarrow E_{PI3K} \tag{5.4}$$

(activation probability = W^a_{EPI3K}, deactivation probability = W_{EPI3K})

$$R^a + E_{PTEN} \rightarrow E^a_{PTEN} \tag{5.5}$$

$$E^a_{PTEN} \rightarrow E_{PTEN} \tag{5.6}$$

(activation probability = W^a_{EPTEN}, deactivation probability = W_{EPTEN})

$$R^a + I_{PI3K} \rightarrow I^a_{PI3K} \tag{5.7}$$

$$I^a_{PI3K} \rightarrow I_{PI3K} \tag{5.8}$$

(activation probability = W^a_{IPI3K}, deactivation probability = W_{IPI3K})

$$R^a + I_{PTEN} \rightarrow I^a_{PTEN} \tag{5.9}$$

$$I^a_{PTEN} \rightarrow I_{PTEN} \tag{5.10}$$

(activation probability = W^a_{IPTEN}, deactivation probability = W_{IPTEN})

$$E^a_{PI3K} + BS_{PI3K} \rightarrow BS^a_{PI3K} \tag{5.11}$$

$$I^a_{PI3K} + BS^a_{PI3K} \rightarrow BS_{PI3K} \tag{5.12}$$

(activation probability = W^a_{BSPI3K}, deactivation probability = W_{BSPI3K})

$$I^a_{PTEN} + BS_{PTEN} \rightarrow BS^a_{PTEN} \tag{5.13}$$

$$E^a_{PTEN} + BS^a_{PTEN} \rightarrow BS_{PTEN} \tag{5.14}$$

(activation probability = W^a_{BSPTEN}, deactivation probability = W_{BSPTEN})

$$PI3K + BS^a_{PI3K} \rightarrow PI3K^a \tag{5.15}$$

$$PI3K^a \rightarrow PI3K \tag{5.16}$$

(activation probability = W^a_{PI3K}, deactivation probability = W_{PI3K})

$$PTEN + BS^a_{PTEN} \rightarrow PTEN^a \tag{5.17}$$

$$PTEN^a \rightarrow PTEN \tag{5.18}$$

(activation probability = W^a_{PTEN}, deactivation probability = W_{PTEN})

$$PI3K^a + PIP2 \rightarrow PIP3 \tag{5.19}$$

$$PTEN^a + PIP3 \rightarrow PIP2 \tag{5.20}$$

PIP3 activation probability = W_{PIP3}, PIP3 deactivation probability = W_{PIP2})
In our lattice model we have used the probability constants (see table 5.1) instead of kinetic rate constants used by the previous model [9]. However, owing to the lack of experimental data Iglesias group used their reaction rate by using data fitting method from experimentally observed PI3K and PTEN localization. So our conversion of probability constants do not strictly follow their reaction rates exactly. However, since we are more interested on qualitative property of the system than quantitative result, the discrepancies that might have had crept into the calculation owing to the aforementioned cause; we assume, won't be perturbing the system characteristics to anything but negligible extent. In stochastic lattice LEGI model, all the reactive particles can be divided into two groups. In one group, the particles diffuse freely inside the cell and these particles are involved in global interaction. The PI3K, PTEN and their respective inhibitors belong to this group. We have taken into account these diffusive particles explicitly in the present model. Whereas the other group consists of all the non-diffusive particles. The receptors of cAMP, exciters and binding site of PI3K and PTEN and PIP3/PIP2 belong to this second group. All these non diffusive particles are not taken into account explicitly in the membrane. In our model a cluster of membrane bound particles are represented by each membrane bead. A description about these non movable particles has been given in next paragraph.
It is known that approximately $40-80$ thousand cAMP receptors exist in Dictyostelium. In LEGI model proposed by Iglesias, the approach was to use a large concentration of cAMP receptors along the membrane. The concentration of surface bound molecules e.g. E_{PI3K}, E_{PTEN}, BS_{PI3K}, BS_{PTEN},PIP2/PIP3) are also found to be very high in their kinetic model [9]. To make variables of our model to be consistent with real situation, we tried to keep the ratio of concentration of all the membrane bound particles almost the same as them. In our lattice polymer model, each membrane bead effectively represented a cluster of membrane beads which consisted of implicitly fixed numbers of E_{PI3K}, E_{PTEN},BS_{PI3K}, BS_{PTEN}, PIP2/PIP3. Every cluster contains 7 receptors, 10 exciters, 10 binding site of PTEN and PI3K respectively and 100 PIP3/PIP2. In case of diffusive particles, their concentration in real cell is known to be very high [9]. But due to the limitation of model technique, membrane polymer movement has been limited; which resulted in a constrained stretching extent of the membrane (membrane can not be stretched after certain limit). Hence in extreme case, the shape of the cell resembles that of a gas filled balloon. This inflated cell shape hampers the movement of whole cell. In order to control this problem, in the present lattice model each diffusive particle has been made to represent effectively a group of many diffusive particles. With the implementation of this modification the cell membrane ceases to become extremely stretched due to highly populated cytocolic particles. The following table 5.1 represents the probability constants of the model cell.
According to the LEGI mechanism, at steady state the concentration of active binding

Receptor	W_R^a	**1.0**
	W_R	**0.75**
Exciter	W_{EPI3K}^a	**0.5**
	W_{EPI3K}	**0.4**
	W_{EPTEN}^a	**0.5**
	W_{EPTEN}	**0.5**
Inhibitor	W_{IPI3K}^a	**0.003**
	W_{IPI3K}	**0.0000002**
	W_{IPTEN}^a	**0.003**
	W_{IPTEN}	**0.00000005**
Binding site	W_{BSPI3K}^a	**0.3**
	W_{BSPI3K}	**1.0**
	W_{BSPTEN}^a	**1.0**
	W_{BSPTEN}	**0.09**
PI3K	W_{PI3K}^a	**1.0**
	W_{PI3K}	**0.85**
PTEN	W_{PTEN}^a	**1.0**
	W_{PTEN}	**0.85**
PIP3	W_{PIP3}	**0.6**
PIP2	W_{PIP2}	**0.2**

Table 5.1: Reaction probabilities of the PIP3 mediated signalling network in model cell

site of PI3K along cell perimeter (nm) can be defined by

$$BS^a_{PI3K}(nm) \propto E^a_{PI3K}(nm)/I^a_{PI3K}(nm) \tag{5.21}$$

From several experimental results [127, 77] it is known that PI3K concentration is maximum at the front of the cell where the signal intensity has also found to be highest. PI3K is regulated by active binding site of PI3K. Therefore such result indicates unambiguously that BS_{PI3K}(nm) is directly proportional to the source intensity along the membrane.

$$BS^a_{PI3K}(nm) \propto S(nm) \tag{5.22}$$

It is also known

$$E^a_{PI3K}(nm) \propto S(nm) \tag{5.23}$$

However the $I^a_{PI3K}(nm)$ depends not only on nmth membrane bead but on the whole cell perimeter N_m . It is also found [9] that the activation of inhibitors are directly related to signal intensity. Thus to satisfy the condition 5.21 we need to keep the value of $I^a_{PI3K}(nm)$ (with respect to time) to a constant or near-constant level. In the previous model [9] the same has been achieved by using very high diffusion coefficient of inhibitors, implying thereby that the number of I^a_{PI3K} at all membrane beads, will be almost constant. However, our model shifted slightly from the previous model. Our aim was to observe the importance of diffusion coefficient on a cell which is exposed to uniformly homogeneous source . So instead of keeping the value of diffusion coefficient very high we preferred to keep the magnitudes of the deactivation probability (W_{IPI3K}) of inhibitors to a significantly small level, so that irrespective of the signal value, activated inhibitors reach its saturation states. This modelling, in a strict sense, actually violates the real situation. Since it is known that in real cell, the number of total inhibitors are much larger compared to activated inhibitors. But due to our computational limitation and lack of experimental data we have not able to use a very dense concentration of inhibitor particles. According to our understanding, in real situation, due to slower rate of activation and inactivation of inhibitors compared to exciters, the effect of inhibition does not vary much with differentially varying signal intensities. Thus in that case, the condition of our model becomes comparable to the actual situation. In case of uniformly distributed source, we observe that the adaptation of cell can as well be seen as a function of diffusion coefficients (relevant results have been shown later). From this result it can be hypothesized that the large diffusion coefficient is able to make perfect or near perfect adaptation compared to the same with small values diffusion coefficient . Hence what was an assumption in our previous model, has been found as a result with our model. According to our understanding adaptation property also helps a cell to become sensitive with varying signal intensity in case of gradient source. Thus we believe that there can be genuine ground in accepting our current assumption about inhibitors action, which has been found to be adequate in making the cell signal sensitive in case of gradient source also.

Since both the binding and activation of PTEN are regulated by similar mechanisms as PI3K, where the role of excitation and inhibition are reversed; we can write :

$$BS^a_{PTEN}(nm) \propto I^a_{PI3K}/E^a_{PI3K}(nm)/ \propto 1/S(nm) \tag{5.24}$$

And finally

$$PIP3(nm) \propto BS^a_{PI3K}(nm)/BS^a_{PTEN}(nm) \tag{5.25}$$

5.3 Effect of density:

It is known that PIP3 accumulation on membrane depends on relative concentration of the cytosolic signaling proteins as PTEN and PI3K [128, 78]. PTEN deficient cell shows higher accumulation of PIP3 on membrane and as a result produce an impaired chemotaxis in case of gradient signal [128, 78]. However PI3K inhibitors are known to restore (at least partially) the chemotactic response in PTEN- cell [129]. The adjacent diagram fig.5.2 is depicting the response (PIP3) concentration with respect to the concentration ratio between PTEN and PI3K for immobile and mobile cell respectively. We observe that the nature of graphs are the same in both cases. which tend to imply that the transition of PIP3 concentration is an inherent property of cell. According to our understanding, the reason behind this phase transition is as following :
Due to constant inhibitor concentration, the production of BS^a_{PTEN} does not vary with varying concentration of PTEN and in any way conversion of BS_{PTEN} from inactive state to a active state does not depend on concentration of PTEN. Even if the PTEN concentration becomes lower than PI3K concentration, still the number of available active BS_{PTEN} remains always almost at the same level. In this situation, the diffusion coefficient of moving particles plays an important role. If the diffusion constant is higher enough , the PTEN can be observed to move very rapidly towards membrane and bind to the active BS_{PTEN} which happen to result in a negative regulation of the production of PIP3 on membrane. Henceforth, despite the lack of PTEN concentration, the higher diffusion coefficient can be able to make up the availability of PTEN to the membrane bound active BS_{PTEN}. According to our work, for every diffusion coefficient there is a transition concentration (PTEN/PI3K) region. For example, in the present case, the PIP3 transition occurs when the corresponding PTEN/PI3K values are between 0.4 to 0.5 for diffusion coefficient is 15 in case of mobile cell (see fig.5.2(b)). When the relative concentration ($\frac{PTEN}{PI3K}$) reaches this region, the diffusion constant no more finds itself to be able to supply enough free PTEN particles to active BS_{PTEN}. As a result PIP3 concentration starts to increase very rapidly and it reaches its saturation level very fast. In case of higher diffusion coefficient the transition of PIP3 happens at relatively lower value of relative concentration , compared to the case when diffusion coefficient is smaller. It also noteworthy to mention that the association time of membrane bound PTEN plays another important role regarding this transition. In the present case, the

association time per 100 Monte Carlo steps has been kept fixed at 15. This lower value of association time also helps to compensate the effect of lower concentration of PTEN.

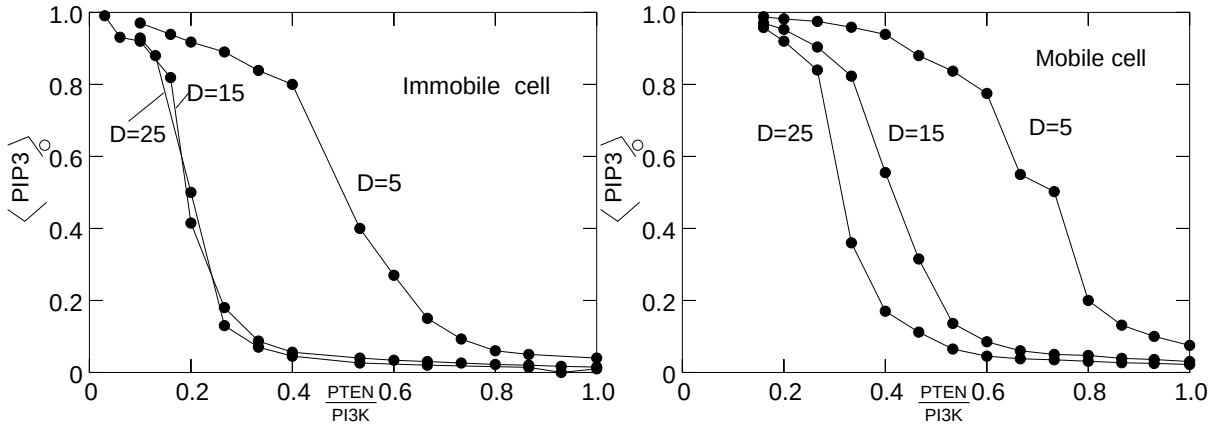

(a) (b)

Figure 5.2: Phase Transitions :PIP3 vs PTEN/PI3K for different diffusion coefficients D, and for (a) immobile and (b) mobile cells.

5.4 Global amplification:

Cell has a fascinating ability to detect shallow gradient of extracellular molecules and to link that sensing to change cell motility. These capabilities are the central to polarization and chemotaxis [130]. Amplification is defined the mechanism by which the weak extracellular signal is converted into much stronger intracellular responses. In chapter 2 fig.2.8 represents a cartoon of signal amplification. In case of homogeneous uniform source the input extracellular signal as well as the output intracellular response both are distributed allmost homogeneously throughout the cell membrane. Due to absence of any local accumulation of the the input and output we redefined the amplification here as 'global amplification'. In the following we consider the relation between the output parameter average PIP3 concentration (which we call "response intensity") as function of the homogeneously distributed input signal intensity P_s (amount of cAMP).
With regard to chemotatic signaling the homogeneous case seems to be of less importance, because there the amplification of a gradient of PIP3 as response to gradient of P_s is of interest. This is discussed in the following chapter . But we will show later (see section 6.2.1 in chapter 6), from the relation between PIP3 and P_s for the homogeneous case one can already anticipate, qualitatively, how strong a gradient of P_s would produce a gradient of PIP3 at the front and at the back of a cell when the mean P_s value is same for both cases. So study of PIP3 amplification for the homogeneous case

is not so trivial as it seems. From the observation it is found that amplification is a nonlinear phenomena, i.e., with increasing strength of the signal, the response increases nonlinearly. Fig. 5.3 is representing the corresponding situation with various diffusion coefficients D.

We did not find any experimental evidence of this kind of amplification of PIP3 for a uniform homogeneously signal exposed cell. Because researcher did not concentrate on this area. It is obvious that the relation between PIP3 and P_s depends among other parameters including the association times T and the kinetic reaction rates k in the system. But for simplicity we have restricted here to one of the important parameters, which is D.

In the present case both output response PIP3 and input signal P_s are normalized by their maximum values respectively. In fig.5.3 The broken lines are indicating zero amplification. So the value of PIP3 above the broken line representing the amplified response for the corresponding input signal. From result it has been shown that (in case of moving cell) for high diffusion coefficient the PIP3 amplification is very small (D=5) or nil(D=10, 15). As the value of D started to decrease the amplified response started to increase. From fig.5.3 we can conclude that the amplification of PIP3 is inversely related with the diffusion coefficient of moving particles. This diffusion coefficient actually represent the global inhibitory effect. So for high D value global inhibition dominates over local excitation.

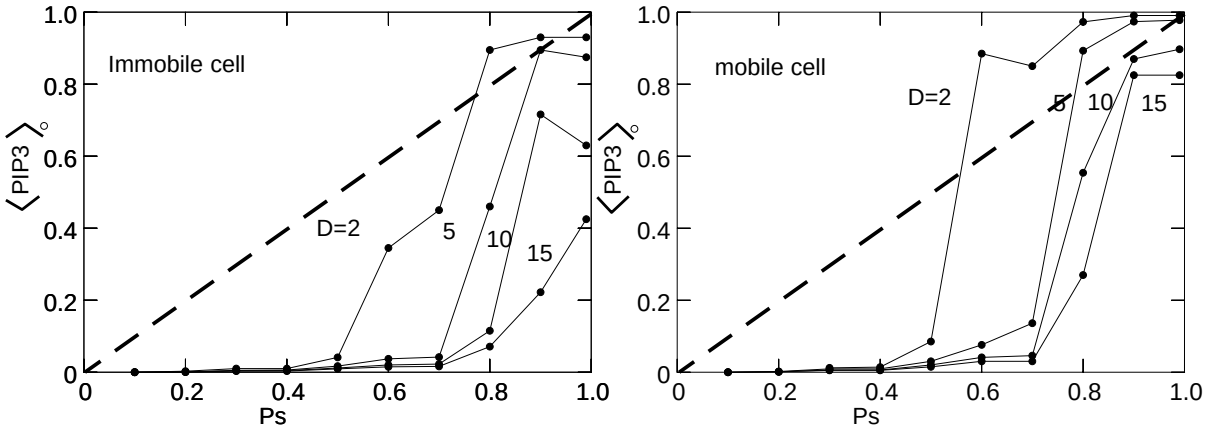

(a) (b)

Figure 5.3: Global amplification of PIP3 versus P_s for different diffusion coefficients D, and for (a) immobile, and (b) mobile cells. Here the dashed line is indicating no amplification. (PTEN/PI3K=1).

5.5 Binding site and diffusion coefficient:

It is known that the binding sites of PTEN and PI3K are the earliest point from where signal asymmetry starts in case of gradient source. In a uniform homogeneously exposed cell the spatial asymmetry of the distribution of these binding sites along the membrane is not possible. But we think that the study of nature of active BS_{PI3K} and BS_{PTEN} as function of varying signal strength has important aspect to understand the LEGI mechanism more clearly. The following figure fig.5.4 is representing the total number of active binding sites(normalized by maximum active binding sites) of PI3K and PTEN with respect to changing signal for various diffusion coefficients of mobile cell.
In case of gradient signal PTEN become active at the rear of the cell where signal intensity is lowest. For regulation of PTEN, BS^a_{PTEN} is responsible and at the rear part of the cell this binding sites are most active. So activity of BS_{PTEN} is inversely proportional to the signal strength. And on the other hand PI3K is mostly active at the front part of the cell where BS_{PI3K} is also active. Several studies indicate that the PI3K activation is directly proportional to the signal strength along the membrane perimeter. In case of homogeneous signal the active binding site of this two enzymes along the cell periphery are allmost uniform and there is no spatial asymmetric distribution. So we calculate the average active binding site and plot them with respect to different signal (P_s). From the picture 5.4 it is clearly visible that with increasing signal strength the number of BS^a_{PTEN} is dropping down towards zero and number of BS^a_{PI3K} is increasing with increasing signal. In case of very low diffusion constant such as when D= 2 the the decreasing of active binding site is faster than the higher diffusion constant when D=10. In case of low inhibitor diffusion constant the exciter plays dominant role over inhibitor on the cell membrane. According to LEGI mechanism PTEN exciter regulates the inactivation of BS^a_{PTEN}. In case of higher diffusion constant the inhibitors get more chance to regulate the PTEN binding site on membrane , as a result deactivation of BS^a_{PTEN} becomes much slower than the case of low diffusion constat. For PI3K binding site things are just reverse. In this process exciter is responsible for the PI3K binding site activation and inhibitor regulate the deactivation. This explain the increasing number of of BS^a_{PI3K} with increasing signal strength.

5.6 Global adaptation:

In many experiments it is observed that after a sustained constant stimulation of the cell, the amount of receptor occupancy and activated signaling proteins, including PI3K, PTEN and others, relaxes towards their new steady-state values after a significant increase above these values. This process of transient change in the internal states, followed by a full or partial return to pre stimulus steady-state levels, in response to a persistent uniform stimulus is referred to in biology as ‘adaptation’. The advantage of adaptation is that cells remain responsive and are ready to detect further change of the stimulating

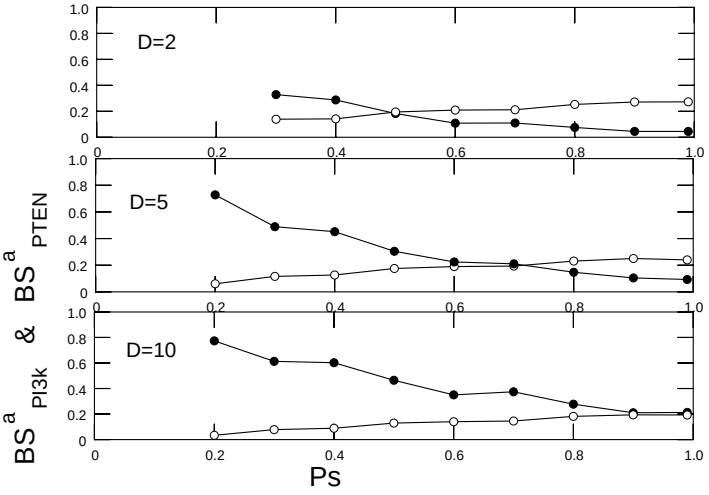

Figure 5.4: Active binding sites versus signal intensity. The open circle and the closed circles are representing the number of BS^a_{PTEN} and BS^a_{PTEN} respectively.

signal. It allows the system to distinguish between constant mean levels of external signals from variations in the concentration of external stimuli. Therefore, adaptive sensory systems can measure relative signal differences instead of the absolute value of signal intensities.

The efficiency of an adaptive systems can be measured by the adaptation time τ_{Ad}. The adaptation time τ_{Ad} is the time the system needs to relax between the old and the new steady-states. Fig.5.5(a) is depicting the different ranges of adaption(full, partial and zero adaption) with different diffusion coefficients D for a particular P_s (0.6) value for a mobile cell. This figure demonstrate that as the diffusion coefficient decreases, the peak response in PIP3 levels increases, as does the steady-state levels and adaptation time τ_{Ad}.

In fig.5.5(b) we can see the nature of adaptation of PIP3 and the corresponding BS^a_{PI3K}, BS^a_{PTEN} concentration around cell periphery . According to Iglesias LEGI mechanism for uniform homogeneous signal the response does not depends on particular concentration of external chemoattractant at steady state. In our stochastic model adaptation is also robust but for very high P_s value the response lose it adaptation. In LEGI model the excitation has a smaller time constant and thus rises faster than inhibition and as a result the response increases transiently.

After the excitation and inhibition approach their steady state values, this make a balance between production and degradation of response. At that moment response gradually reaches to a steady state which is exactly or allmost same to its pre stimulus level. In fig. 5.5(b) active BS_{PTEN} is representing the slower global inhibitory effect where

active BS_{PI3K} is representing the faster local excitation. Which explain the adaptation of response PIP3 followed by a transient increase. Contrast to Iglesias result regarding adaption some experimental results [84, 131, 132] as well as theoretical model [133] of eukaryotes suggest that only partial adaptation occurs. The nature of the graph in fig. 5.5(b) is very similar to the graph produced by another theoretical model [133] in respect to adaption.

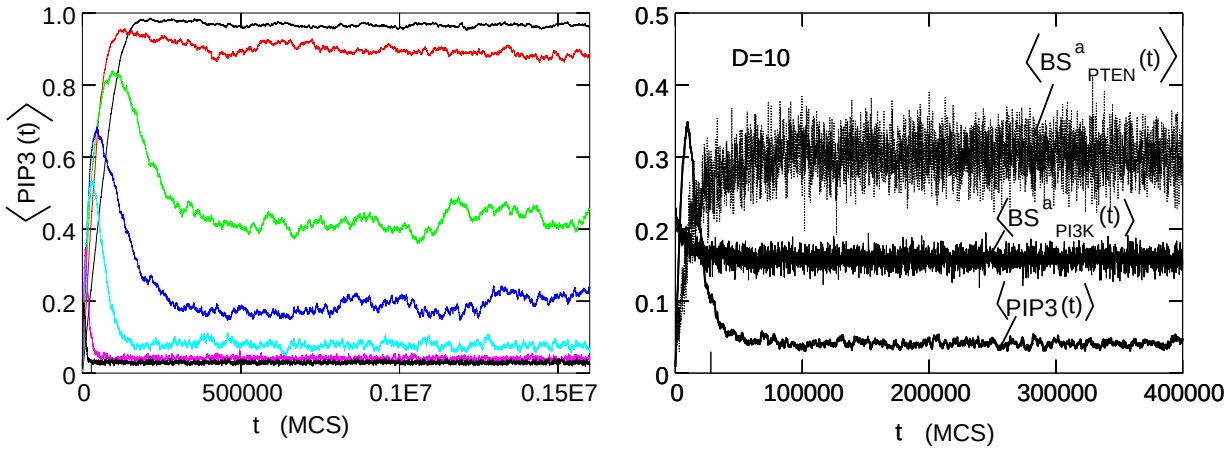

(a) (b)

Figure 5.5: (a)Relaxation (global adaptation) of PIP3(t) *versus* time t for different diffusion coefficients D.(Ps=0.6, PTEN/PI3K=1) .
(b) Relaxation (adaptation) of PIP3 and active $BS_{PI3K}(t)$ and $BS_{PTEN}(t)$ versus time t for mobile cells.

5.7 Adaptation and diffusion coefficient :

According to Iglesias model for uniform homogeneous signal at steady state the excitation E, inhibition I and response 'Response' have no spatial dependence. So according to their assumption these three components are defined roughly as follows

$$I(t) \approx constant1 \times S \tag{5.26}$$

$$E(t) \approx constant2 \times S \tag{5.27}$$

Where S is representing the source.

$$Response(t) \approx \frac{E(t)}{I(t)} +' transientpart' \tag{5.28}$$

$$Response(t) \approx constant \tag{5.29}$$

where ['transient part' =0 and $\frac{E(t)}{I(t)}$ = constant at t =∞]
So when S is homogeneous 'Response' does not depend on S at steady state. But in this particular model our observation indicates an interesting point which does not taken into account in the previous model. It is well known that for homogeneous uniform signal the response does not associate spatial variation. Exciters are membrane bound particles and excitation is a membrane dependent phenomena. Although inhibitors diffuse throughout the cell, but its effect is measured at the membrane. As a result response measurement is also membrane dependent. So inhibition action on membrane become very efficient when it has large diffusion coefficient . As a result the inhibition and excitation effect balance each other and response approaches to its pre stimulus level almost irrespective of signal intensity. But when inhibitor diffusion coefficient is very small the effect of inhibition on membrane is not very global and is mild compare to excitation effect. As a result response does not reach its pre stimulus state irrespective of signal intensity. Even in gradient signal we have seen the same tendency of adaptation with respect to different diffusion coefficients. Fig.5.6(a) is representing graph of the adaptation time τ_{Ad} versus different diffusion coefficient D for a mobile cell , and fig.5.6(b) is showing the adaptation time τ_{Ad} with respect to varying signal intensity P_s for different D value of motile cell.

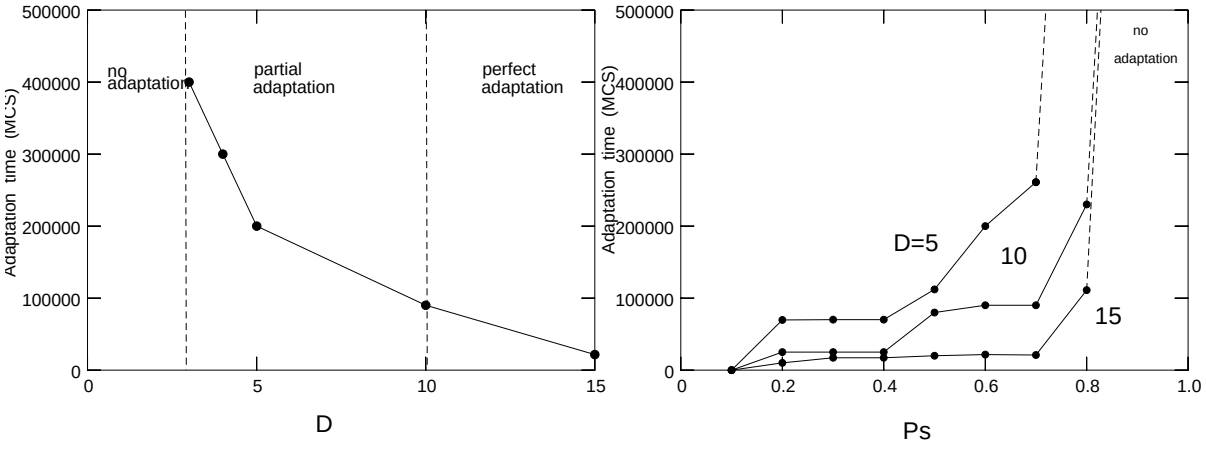

Figure 5.6: (a) Adaptation time τ_{Ad} versus change in diffusion coefficient D at fixed signal intensities $P_s = 0.6$.
(b) Adaptation time τ_{Ad} versus change in signal intensity P_s.

5.8 Cell's random movement:

In chapter 4 the model cell exhibited random movement when it exposed to a uniformly homogeneous signal. This characteristic is considered to be basic property of a uniform

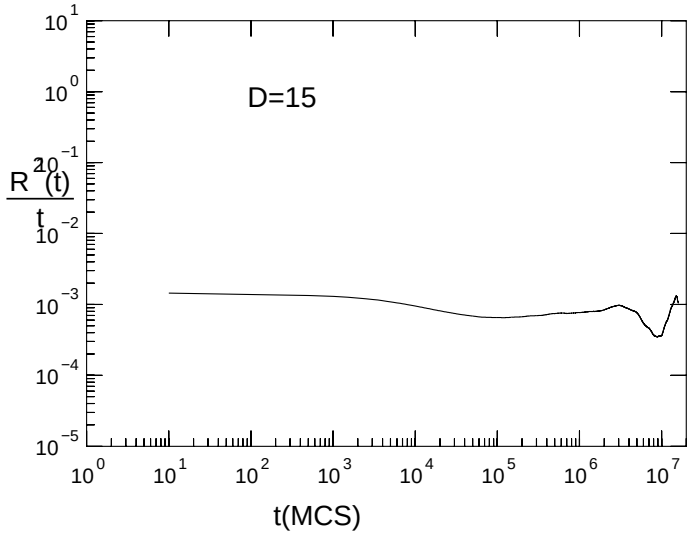

Figure 5.7: Plot of $R^2(t)/t$ (mean square displacement) versus time t (Monte Carlo steps)

exposed cell. Although in a uniformly exposed cell the moving particles inside the cell body diffuse randomly , still it is an interesting point to observe the movement of the cell to see whether there exist any prefferred direction for cell movement. Fig. 5.7 is representing the mean square displacement of the model cell with respect to Monte Carlo steps. And it is clear from the concerned figure that in case of uniform signal the diffusing particles diffuse homogeneously throughout the cell and this random diffusion reflects the random motion of the cell.

5.9 Summary:

It is well known that PTEN deficient cell shows an impaired chemotactic movement. PTEN and PI3K work complementary way to produce PIP3 on membrane. So when PTEN concentration is less than PI3K concentration definitely the production of PIP3 also increases. Our simulation results show that PIP3 amplified in a non linear fashion when $\frac{PTEN}{PI3K}$ decrease gradually. And this transition of amplified PIP3 depends on the diffusion coefficient of moving particles.
Furthermore from the simulation result it is also observed that in normal situation the uniformly exposed cell shows the same nonlinear tendency of amplification of PIP3. As the corresponding signal is uniformly distributed so the amplification is termed as global amplification. And this global amplification depends on the value of D. For low D value the PIP3 amplification is large and high D value can not produce amplified PIP3.
Similar to global amplification the corresponding adaptation is termed as global adaptation. It is observed that the global adaptation inversely related with the diffusion

coefficient. As the diffusion coefficient of the moving particles inside the cell has complementary effect on response amplification and on adaptation, so according to our hypothesis there should be an optimal diffusion coefficient of moving particles.

6 Response To Inhomogeneous Signals

6.1 Introduction:

To explain gradient sensing mechanism Parent and Devreoles [134] had conjectured the principal driving impetus of PIP3(response) localization to be the interaction between two processes. One of these two key processes originate out of activating the response due to locally acting exciters, whereas the second corresponds to response becoming activated due to globally acting inhibitors. The activator/exciter binds to the membrane at a rate proportional to the local degree of receptor activation. Hence, taking into consideration the facts established earlier in the work, it can well be expected that more activator will be bound at the front than at the rear of the cell in case of gradient source. The inhibitor, on the other hand, will surely respond to the integrated receptor activity. Its activity, therefore, will be proportional to the average concentration of attractant across the length of the cell. Typically, the global inhibitor is assumed to be a rapidly diffusing protein or small molecule in the cytosol. In case of the gradient source, the cell determines its front and rear by comparing the local concentration of the activator on the membrane relative to the global concentration of the inhibitor. At the front, the concentration of the activator is greater than the inhibitor and vice-versa at the rear. The popularity of the local activator/global inhibitor model is owing to the fact that it provides a simple mechanism for explaining how a cell can distinguish its front and rear from a common signal.

6.2 Homogeneous gradient of cAMP:

In the case, when the cell is exposed to a homogeneous gradient of cAMP, it can be described as if the case corresponds to that when the presence of source is at infinite distance. Since we do not simulate explicitly diffusing cAMP in the extracellular environment, we can assume that the cAMP-receptors are stimulated with probability:

$$P_s(\mathbf{r}) \equiv P_s(y) = exp[-(y_0 - y)^2/\lambda^2] \tag{6.1}$$

The parameters λ and y_0 determine the range and the intensity of the gradient. Our model is a 2D lattice model, and we assume that source vary only along the y-coordinate.

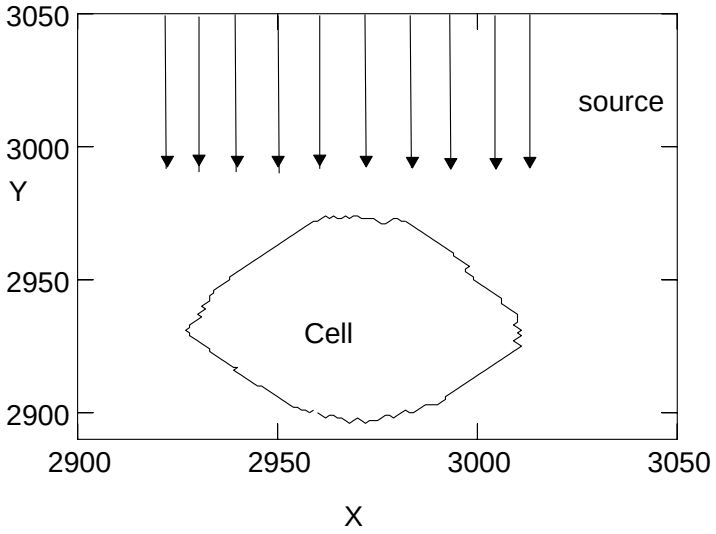

Figure 6.1: Cartoon of a cell exposed to a homogeneous gradient source.

As our assumption is that the source is placed at infinite distance, the effect of source along x axis is same for a particular y-coordinate. In the above expression of probability, y_0 and y represent the corresponding y-coordinate of source and the membrane bead, respectively. We do not use cAMP explicitly in our model. The present set up is easier to calculate from the computational point of view. Fig. 6.1 is representing a cartoon of a cell exposed to a homogeneous gradient source.

6.2.1 Amplification:

The definition of amplification, along with a brief exposition of the same in the present context has already been provided earlier (see chapter 5). Some biological terms which have been used often in the following part are described in short in appendix C.
To understand gradient sensing mechanism clearly, it is imperative to know how precisely the shape of cAMP gradient affects the distribution of activated receptors and the receptor-induced distribution of PIP3 molecules along the membrane. It is known experimentally that the overall chemotactic response depends on the steepness of the concentration gradient of cAMP across the cell [121, 135]. Along with this, a few theoretical studies, notably by Iglesias group [9] had attempted to address the problem.
However, the set of answers derived from all these efforts do not exactly provide an elaborate and complete framework to understand the scope and depth of the aforementioned question.
In particular we address the question how a special type of cAMP signal (eq.6.1) yields a particular distribution ("shape") of activated receptors, along the contour nm of the

cell membrane, and the induced response of activated PIP molecules along the contour, $PIP3(nm)$. Typical results from computer simulations for different signal distributions $P_s(nm)$ are shown in fig.6.2.
One useful way to characterize the shape of $P_s(nm)$ is by defining its maximum value P_s^{max} , and its minimum value P_s^{min} , which are the concentrations of signal at the top and the bottom of the cell (compare fig.6.1), respectively. The significance of P_s^{max} and P_s^{min} was also indicated by experiments [121, 135]. There it was shown that the shape of the "response gradient" (or synonymously,"response amplification"), $\Delta P_r \equiv PIP3^{max} - PIP3^{min}$, where $PIP3^{max}$ and $PIP3^{min}$ are defined analogous to P_s^{max} and P_s^{min} , depends on both "midpoint concentration" of the signal, P_s^{max} , and the "concentration gradient" of the signal, $\Delta P_s \equiv P_s^{max} - P_s^{min}$.
It is very instructive to consider the following cases :

1) Fig.6.2(a) and fig.6.2(b) show the dependence of the response PIP3(nm) on P_s^{max} for two different signal gradients $\Delta P_s = 0.1$ and $\Delta P_s = 0.35$, respectively. The results in fig.6.2(a) and fig.6.2(b) were obtain by using different diffusion constants, D=15 and D=5.

2) Fig.6.2(c) and fig.6.2(d) show the dependence of the response PIP3(nm) on various signal differences ΔP_s at constant P_s^{max} for two cases, P_s^{max} =0.93 and P_s^{max} =0.71, respectively.

3) Fig.6.2(e) and fig.6.2(f) show the dependence of the response PIP3(nm) on various signal differences ΔP_s at constant P_s^{min} for two cases, P_s^{min} =0.1 and P_s^{min} =0.39, respectively.

A. Sensitivity of signal amplification depends on maximum signal P_s^{max} .

Fig.6.2(a) and fig.6.2(b) show that with increasing P_s^{max} and constant ΔP_s , the response PIP3(nm) varies considerably. In fig.6.2(a), the shapes of PIP3(nm) are more or less flat except for the case P_s^{max} =0.9 (curve c), where PIP3(nm) exhibits significant amplification, which is localized in the range $50 < \text{nm} < 150$. This is of importance for chemotaxis, because only in the case of strongly localized amplification a unidirectional motion of the cell can be expected. This is discussed in more detail in chapter 7 .
From fig.6.2(a) we can notice that when the signal steepness is $\Delta P_s = 0.1$, the corresponding ΔP_r is large (0.38) if $P_s^{max} = 0.9$, but not detectable if $P_s^{max} = 1.0$. This result agrees with the experimental result [121], where it has been shown that ΔP_r depends on ΔP_s . The experimental result had suggested that cells "measure" not only the signal difference ΔP_s , but also the maximum of the signal P_s^{max} . These observations agree with our results.

Figure 6.2: Spatial distribution of the response PIP3 (red lines) for a mobile cell exposed to inhomogeneous signals P_s (black lines). The label *nm* indicates the position along the membrane. (a) $\Delta P_s = 0.1$ (b) $\Delta P_s = 0.35$. (c) P_s^{max} =0.93. (d) P_s^{max} =0.71. (e) P_s^{min} =0.1. (f) P_s^{min} =0.39.

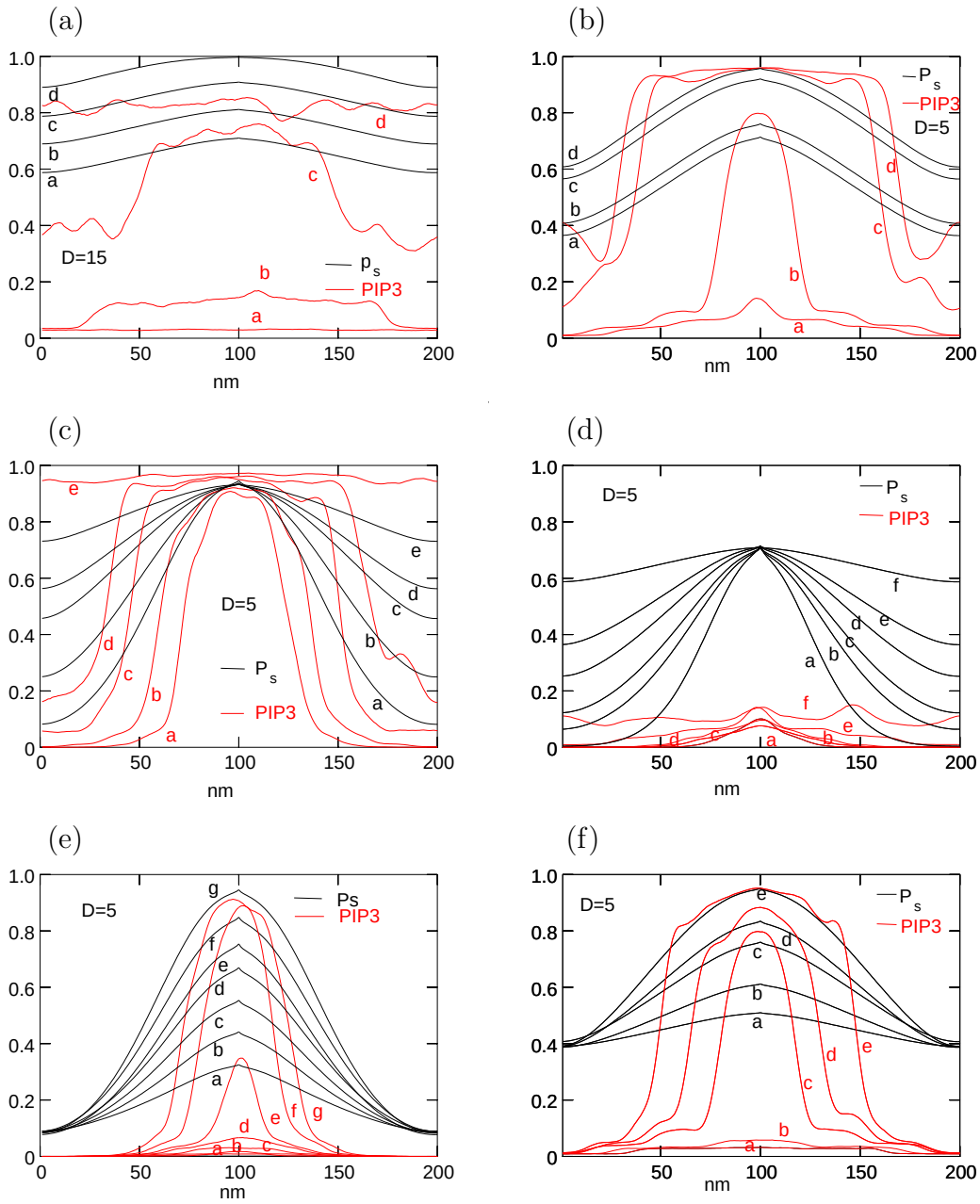

B. Spatial localization of PIP3 depends on signal gradient ΔP_s and maximum signal P_s^{max} .

Figs.6.2(c)–(f) show how the spatial distribution of the response PIP3(nm) depends on the maximum and minimum of the signal, P_s^{max} and P_s^{min} , for various sizes of the signal difference $\Delta P_s = P_s^{max}$ - P_s^{min} .
Fig.6.2(c) and fig.6.2(d) show the results of studies when P_s^{max} is kept constant while P_s^{min} is gradually decreased, whereas fig.6.2(e) and fig.6.2(f) show the results when P_s^{min} is kept constant while P_s^{max} is gradually increased. All these investigations show that the response difference ΔP_r decreases with decreasing steepness of signal ΔP_s . It is observed that ΔP_r becomes completely insignificant when the corresponding ΔP_s is very shallow (< 0.2). It is important to note that in certain cases the response PIP3(nm) can assume very high magnitudes although the signal gradient ΔP_s is very small. More importantly, the response gradient ΔP_r can be highly localized in a narrow range on the membrane. As an example compare fig.6.2(f) (curve c), where the response is $PIP3^{max} \approx 0.8$ and which is restricted to a narrow range of $75 <$ nm < 125.

C. Response ΔP_r depends on diffusion constant D of inhibitors.

Since large diffusion coefficients of the inhibitor particles can be expected to produce large global inhibition, this effect can diminish the response amplification ΔP_r . Therefore, it is of interest to investigate the dependency of the ΔP_r on the diffusion coefficient D. The results are shown in fig.6.3. It shows that with increasing P_s^{max} , the response

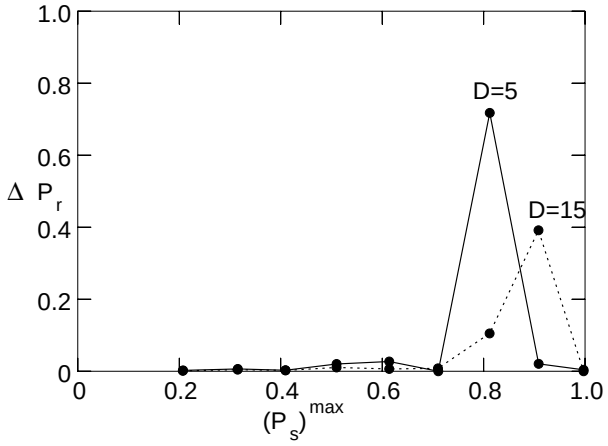

Figure 6.3: Graph of response amplification ΔP_r *versus* P_s^{max} at fixed signal gradient ΔP_s =0.1 for two different diffusion constants of the inhibitors D=5 and D=15. The depicted data correspond to the results shown in fig.6.2(a) and fig.6.2(b).

difference ΔP_r starts to increase from zero to a maximum value, which depends on

the diffusion coefficient D of the mobile particles inside the cell, predominantly the inhibitors. The maximum depends on the diffusion coefficients, and it is larger for D=5 than for D=15. From this, one can conclude that the response amplification ΔP_r is inversely dependent on D and that larger diffusion coefficient will necessarily produce shallower response.

D. The response amplification ΔP_r exhibits a transition as function of signal gradient ΔP_s .

Using the data shown in fig.6.2, one can calculate the response amplification ΔP_r as function of the signal gradient ΔP_s , which is depicted in fig.6.4. The two curves in fig.6.4 summarize the data shown in fig.6.2(c) and fig.6.2(e). The full line in fig.6.4 corresponds to the case where the maximum value of the signal is kept constant, P_s^{max} =0.93, and the broken line corresponds to the case where the minimum value of the signal is constant, $P_s^{min} = 0.1$.

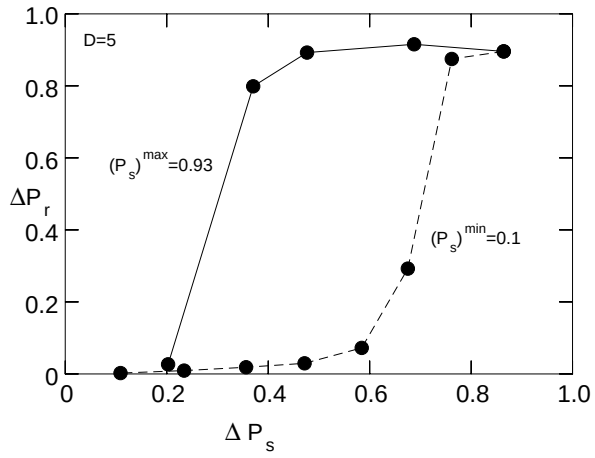

Figure 6.4: Plot of ΔP_r *versus* signal difference ΔP_s at fixed signal maximum P_s^{max} =0.93 (full line) and at fixed signal minimum P_s^{min} =0.1 (broken line). The depicted data correspond to the results shown in fig.6.2(c) and fig.6.2(e).

Fig.6.4 yields the important and new result that the response amplification ΔP_r exhibits a transition from an "inert" state at shallow signal gradients to a strongly responsive state at large ΔP_s . The threshold of the transition depends on the maxima and minima of the signal, P_s^{max} and P_s^{min} . It would be of interest to examine the nature of transition. From the present data it is not possible to decided whether the transition is a true phase transition. If the transition is caused by a cooperative many-body effect (in this case, the interaction among mobile particles and membrane-bound particles), then larger system sizes would have to be investigated in order to elucidate the nature of the transition.

This, however, would have required the development of new computer programs, which are suitable for larger cells and for performance on parallel machines.

E. Response intensity $\langle \mathbf{PIP3} \rangle$ depends on signal intensity $\langle \mathbf{P}_s \rangle$.

In general, one can assume that the transition, as shown in fig.6.4, is determined, besides P_s^{max} and P_s^{min} , also by the variation of the shape of the signal, which can be captured by the average signal $\langle P_s \rangle$. Here, the brackets $\langle ... \rangle$ denote the average of P_s(nm) along the contour nm of the membrane. One may also call this quantity "signal intensity". Similarly, $\langle$PIP3$\rangle$, the response intensity, is the average of PIP3(nm). In the following we discuss the relation between the response intensity, $\langle$PIP3$\rangle$, and the signal intensity, $\langle P_s \rangle$. Fig.6.5 shows the collection of data, which are presented in figs.6.2(c-f), for

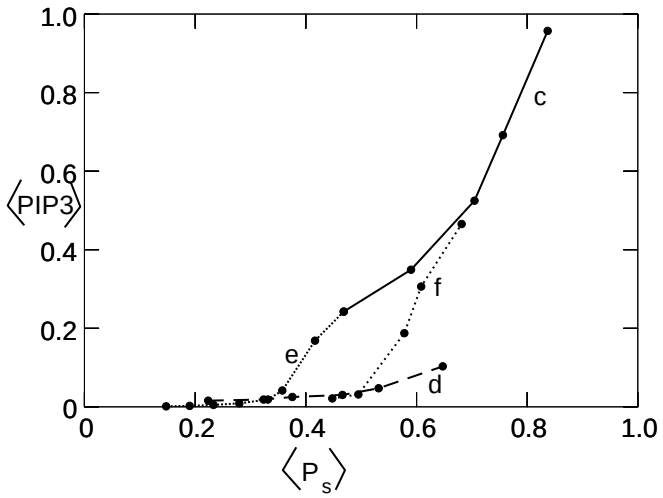

Figure 6.5: Plot of average response $\langle PIP3 \rangle$ *versus* signal intensity $\langle P_s \rangle$. The plot numbers (c-f) refer to the results shown in figs.6.2(c-f).

$\langle$PIP3$\rangle$ *versus* $\langle P_s \rangle$. The label at each curve corresponds to the label in fig.6.2. The result shows that all curves do not follow a simple scaling behavior. It is not know whether certain combinations of P_s^{max} , ΔP_s , and $\langle P_s \rangle$ could lead to the collapse of all curves to a single master curve.

In our study one question of interest is whether globally amplified $\langle$PIP3$\rangle_0$ (see fig.5.3(b)) has any significant relation with gradient amplified PIP3 for the same $\langle P_s \rangle$. Our study regarding amplification of PIP3 in case of homogeneous signal and gradient signal reveals that there is a relation between $\langle$PIP3$\rangle_0$ and $PIP3^{min/max}$ for the same $\langle P_s \rangle$.
To make the above conclusion more clear, an example is illustrated in fig. 6.6. Here we observed the spatial distribution of PIP3 and P_s along the cell periphery for a gradient and homogeneous source exposed cell , where $\langle P_s \rangle$ in both cases are almost same, 0.4.

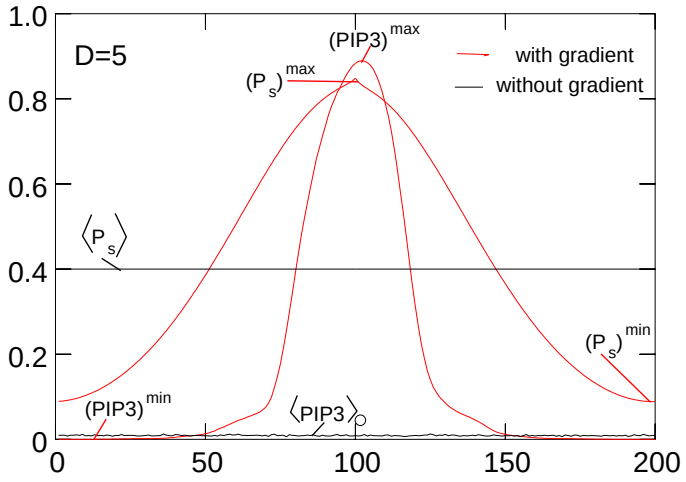

Figure 6.6: Spatial distribution of response (PIP3) and signal, P_s, along the membrane for steeper gradient and the black line is corresponds to homogeneously distributed signal. In both cases $\langle P_s \rangle \approx 0.4$.

If

$$\langle P_s^{homo} \rangle \approx \langle P_s^{grad} \rangle \approx \langle P_s \rangle \tag{6.2}$$

From fig. 6.3 and 6.2

$$P_s^{min} < \langle P_s \rangle < P_s^{max} \tag{6.3}$$

Our simulation result shows that if $\langle P_s \rangle \ll P_s^{max}$ then we get

$$PIP3^{max} \gg \langle PIP3 \rangle_0 \tag{6.4}$$

Similarly for $\langle P_s \rangle \gg P_s^{min}$

$$\langle PIP3 \rangle_0 \gg PIP3^{min} \tag{6.5}$$

Fig.6.7 is representing $PIP3^{max}$ and $\langle PIP3 \rangle$ for gradient source exposed cell and cell which is exposed to homogeneous source respectively verses $\langle P_s \rangle$. In that figure the ΔP_s of homogeneous gradient signal is approximately equal to 0.1. So $\langle P_s \rangle$ is not much smaller or greater than P_s^{max} and P_s^{min} respectively. This is the reason why for higher and lower $\langle P_s \rangle$ the response $\langle PIP3 \rangle_0$ and $PIP3^{max}$ are almost equal. So as a general rule we can predict the relation between $\langle PIP3 \rangle_0$, $PIP3^{max}$ and $PIP3^{min}$ as

$$PIP3^{min} \leq \langle PIP3 \rangle_0 \leq PIP3^{max}, \tag{6.6}$$

irrespective of all signals.

Some existing models[12, 124, 123] had predicted a steady-state response (PIP3 accumulation on membrane) which is invariant with respect to changing of signal relative

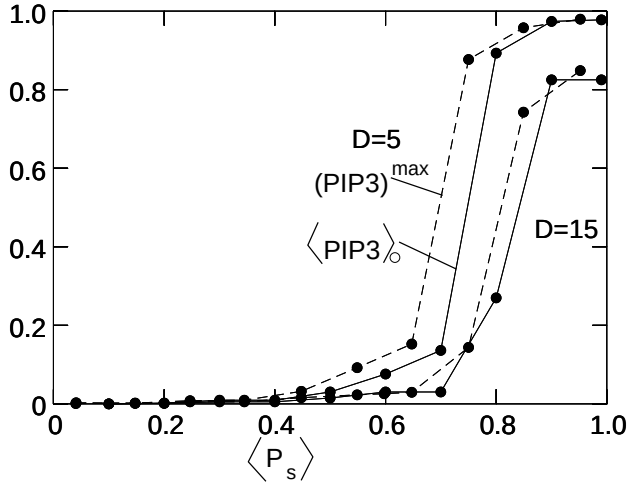

Figure 6.7: Comparison of amplifications between the cases of homogeneously distributed signals ("global amplification") and signals distributed according to a homogeneous gradient ("front amplification"). The graph shows $\langle PIP3\rangle_0$ (solid line) and PIP3^{max} (broken line) *versus* $\langle P_s\rangle$for fixed signal gradient ΔP_s =0.1 and two different diffusion coefficients, D=5 and D=15.

gradient. The other set of models were not exactly illuminating while addressing cell's ability to sense varying gradient midpoint concentrations [136]. But changes of response spatial localization due to changing of corresponding signal concentration along the membrane can logically be considered as one of the necessary and inherent properties of a chemotactic cell [9]. The stochastic LEGI model proposed here, seems to have addressed this question to some satisfaction. From the above observation it is very clear that the nature of response amplification is completely nonlinear and the relation with the signal parameters is quite complex. So at least qualitatively we can predict that the main controlling parameters of response amplification are as follows.

$$\Delta P_r = f(\Delta P_s, P_s^{max}, \langle P_s\rangle) \tag{6.7}$$

6.2.2 Molecular mechanism of amplification

In the previous section I have discussed the importance of P_s localization in context of response gradient amplification. In the present section I am going to discuss the mechanism behind the difference of response localization for same $\langle P_s\rangle$.

To study this we need to observe carefully the temporal as well as spatial response of PIP3. Fig.6.8(a) depicts the temporal response of PIP3 for two cases: a cell with uniformly distributed signal and a cell exposed to a gradient signal. In both cases the mean concentration of the signal is almost equal, $\langle P_s\rangle \approx 0.4$. From the result it is

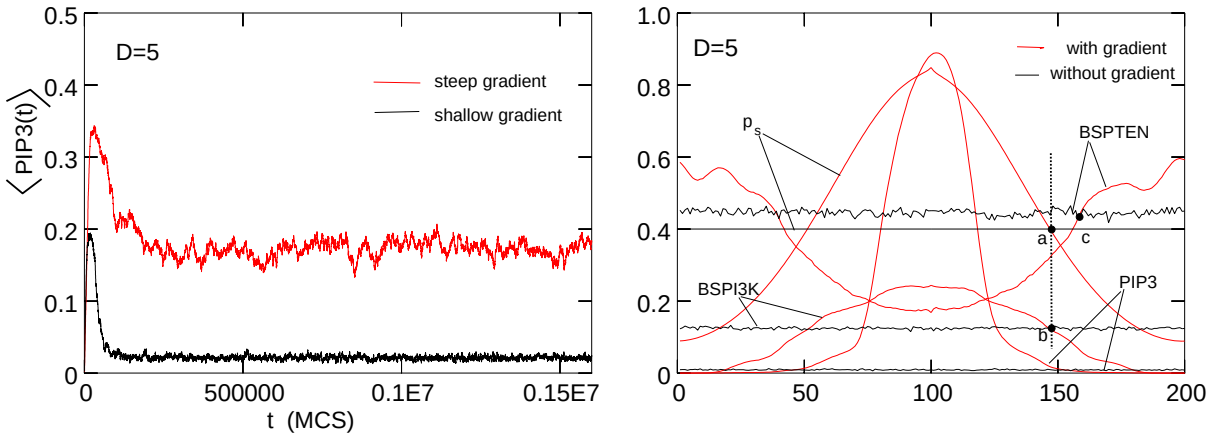

(a) (b)

Figure 6.8: (a) Temporal response,⟨PIP3⟩ (t), when the signals are homogeneously distributed, $\Delta P_s = 0$ (black line), and when the signal source has a homogeneous gradient, $\Delta P_s > 0$ (red line). (b) Spatial amplification of PIP3 along the membrane boundary. The spatial distributions of the signal P_s and of the activated binding sites for PTEN and PI3K, BS^a_{PI3K} and BS^a_{PTEN}, respectively. The red and black lines correspond to the cases of homogeneous signal gradient, $\langle P_s \rangle = 0.4$, and homogeneous signals, $\langle P_s \rangle = 0.41$, respectively.

clearly seen that, although the mean concentration is same for both cells, the average accumulation of PIP3, ⟨PIP3⟩ (t), exhibits a huge difference in these two cases. The gradient exposed cell has a higher average accumulation of PIP3, with respect to time, than the homogeneously exposed cell. Even without seeing the spatial response of these two cells, only from this result we can expect that also the spatial response will be very much different for both cases. The reason behind this different accumulation of PIP3 is the localization of activated binding sites of PI3K and PTEN, BS_{PI3K} and BS_{PTEN}, which is explained in next few paragraphs in detail.

In fig.6.8(b), the localization characteristics of response gradient in two cases are plotted, which shows altogether different traits for the two systems. Fig.6.8(b) shows the distribution of activated binding sites, BS_{PI3K} and BS_{PTEN}, along membrane.

We had concluded in the previous sections that the steepness of response gradient, ΔP_r , depends on the corresponding P_s^{max} and other parameters as ΔP_s and $\langle P_s \rangle$. The results presented in fig.6.8(b) vindicate such assertion by qualifying as another proof conforming to the obtained conclusion. Here, from fig.6.8(b) it is observed, that ΔP_s and P_s^{max} are larger for the cell, which is exposed to a gradient signal source, than the cell, which is exposed to a uniform signal source. The LEGI mechanism yields that the response depends on the ratio of excitation over inhibition processes. The excitation and inhibition reactions represent the local and the global (average) receptor occupancy, respectively.

In the present case, it is observed that the mean concentration is almost equal in both

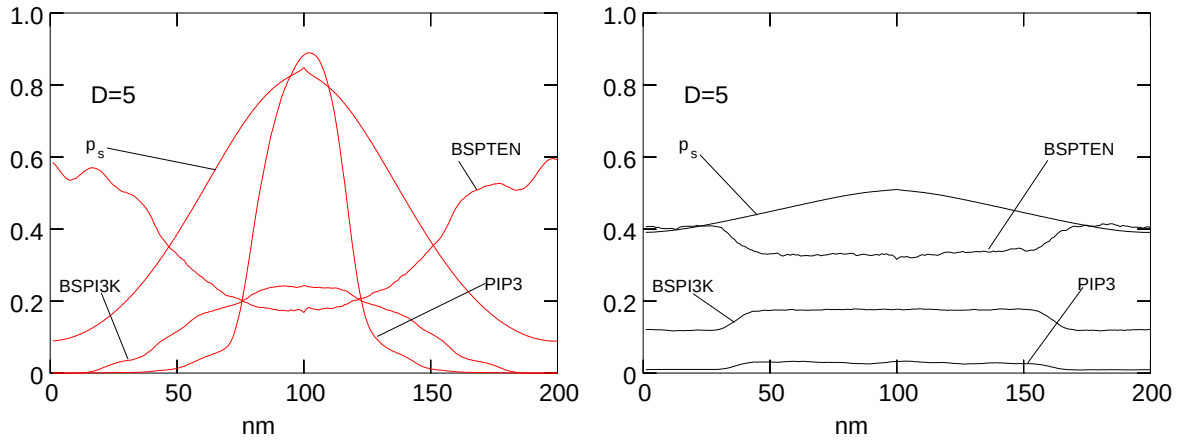

Figure 6.9: Responses with homogeneous gradient sources , the sources have almost same mean concentration ($\langle P_s \rangle \approx 0.41$) but different gradient steepness where red line corresponds to steeper gradient and the black line corresponds to shallower gradient.
(a) Spatial distribution of PIP3 , signal P_s and BS^a_{PI3K} and BS^a_{PTEN} along the membrane for steep gradient $\Delta P_s = 0.72$.
(b) Spatial distribution of PIP3, signal P_s and BS^a_{PI3K} and BS^a_{PTEN} along the membrane for a shallow gradient $\Delta P_s = 0.1$.

cases, which implies, that the global inhibition effect is almost same for both the cells. This is because global inhibition depends on the average receptor occupancy [11, 9]. However, the local receptor occupancy varies for each case, which serves as the causal point of inception of difference in production of PIP3 at the membrane. In the case of homogeneous gradient source, the exposed cell has a greater local excitation effect at the front due to larger receptor occupancy than the uniformly exposed cell. From fig.6.8(b) we can make out clearly that due to the difference of local receptor occupancy, where the average receptor occupancy are same in both cases, the production of active binding sites also becomes different in these two cases. This result supports the existing suggestion put forward by previous researchers [137] in that the binding site of PTEN and PI3K may be the earliest point of signal asymmetry during directional sensing. Our study therefore assumes a newer dimension of importance as it can successfully prove the existing theories from a different point of view.

We could also detect a similar phenomenon when we compare the effects of two different gradient sources, one with large gradient and another one with a shallow gradient. The results are shown in fig.6.9. Here both the cells are exposed to homogeneous gradient sources with different gradient steepness, but with almost equal mean signal, $\langle P_s \rangle \approx 0.41$. We study this situation for a better understanding of the relation between PIP3 amplification and the signal mean concentration in LEGI mechanism. The simulation result also supports our earlier finding: the response gradient, ΔP_r , corresponding to

shallower signal gradient could expectedly be seen to be smaller than in the case of a the steeper signal gradient.

From fig.6.8(b), fig.6.9(a) and fig.6.9(b) we can observe one unexpected behavior of active BS_{PTEN}. The spatial accumulation of BS^a_{PTEN} is inversely proportional to the signal activated receptors along the membrane. If we focus on the y coordinate of fig.6.8(a), where both signal gradients intersect (see point a) each other, the corresponding active binding site of PTEN and PI3K should intersect at the same y position. From this figure we can see that BS^a_{PI3K} of both signal intersect at the point (see point b), where it is expected. But for BS^a_{PTEN} the situation is not exactly same. The corresponding BS^a_{PTEN} intersection point (see point c) is shifted a bit from the expected point. According to our observation we can explain this discrepancy as follows. It is mentioned by researchers that the spatial distribution of active BS_{PI3K} is directly proportional to the spatial distribution of the signal, where the spatial distribution of active BS_{PTEN} is inversely proportional with the same. The regulation of active BS_{PI3K} and BS_{PTEN} are two complementary processes. In case of active BS_{PI3K}, its production depends on the ratio of PI3K exciter effect over PI3K inhibitor effect. As these exciters are membrane bound particles, so movement of membrane as well as inhibitors do not affect the production of active BS_{PI3K} much. On the other hand, the active BS_{PTEN} production depends on the ratio of PTEN inhibitor effect over PTEN exciter effect. So the diffusion of PTEN inhibitors are able to vary the number of active BS_{PTEN} more effectively. This is the probable reason for this discrepancy of spatial distribution of active BS_{PTEN} in case of gradient signal. In fig.6.9(a) and fig.6.9(b), both BS^a_{PI3K} and BS^a_{PTEN} interaction point had undergone a minor shift from their expected intersection point.
This set of of results is indicating explicitly that in case of gradient exposed cell, the effect of signal's mean concentration become shadowed by local receptor occupancy, where the local receptor occupancy depends on the relative signal gradient and the gradient midpoint concentration.

6.2.3 Adaptation

The definition and the importance of adaptation in cell motility has been discussed in the previous chapter (see section 5.4) already. Generally researchers focus on adaptation of response in case of cell exposed with uniform homogeneous signal. It should also be taken into consideration that in some particular cases, the cell exposed with gradient source may achieve this adaptation state. For example in case of homogeneous gradient source cell can adapt. Unlike point source or inhomogeneous gradient source, in this case, the receptor occupancy does not change quite often with movement of cell. It is also true that receptor occupancy changes when cell changes its shape or starts to move in a different direction. But the present case is very simple and no filament is introduced. Thus the shape and the direction of movement does not change very significantly with respect to time. Through this set of process, cell is able to reach a steady state and we

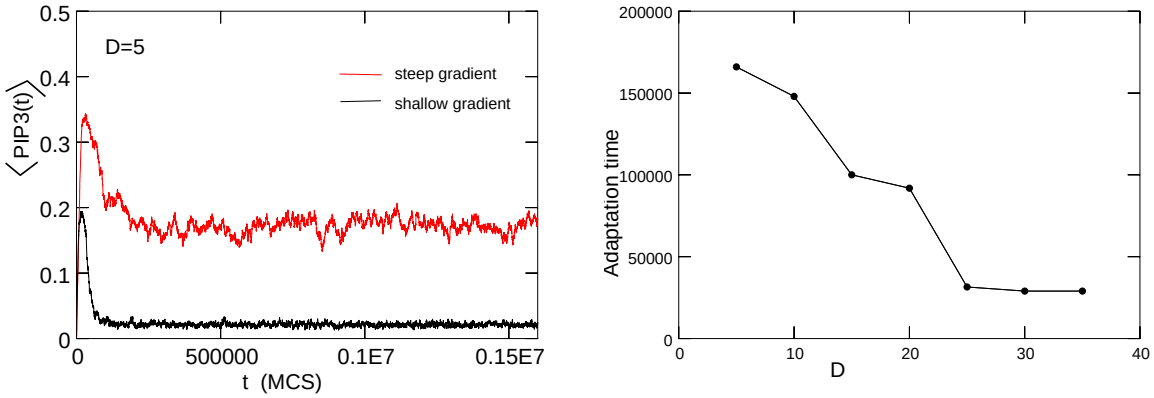

(a) (b)

Figure 6.10: (a) Temporal responses with homogeneous gradient sources. (b) Plot of adaptation time τ_{Ad} versus change in different diffusion coefficients D .

measure the adaptation time of the corresponding cell. In the present work our principal aim was to observe the effect of diffusion coefficients of moving particles on motility and for this reason we had to vary the magnitude of D gradually. Fig. 6.10 depicts the corresponding case. From the result we notice that diffusion coefficient is inversely proportional to adaptation time τ_{Ad} . So from both gradient source and uniform source results we can conclude that inverse relation between τ_{Ad} and D is inherent to the cell.

6.3 Inhomogeneous gradient of cAMP

In this section, we intend to discuss the performance of our model with a more general case, namely upon the exposure of cell periphery to an inhomogeneous gradient of cAMP, which originates from a point source at $\mathbf{r}_s$, within a short finite distance. We assume that the cAMP-receptors are stimulated with probability

$$P_s(\mathbf{r}) = exp[-(\mathbf{r}_s - \mathbf{r})^2/\lambda^2] \tag{6.8}$$

The parameter λ determine the intensity of the gradient. And $\mathbf{r}_s$ is the position of the source where $\mathbf{r}$ is the position of the membrane bead. It is easily understandable that when cell is situated very near to the source , or the distance is finite between the source and the cell, small distance change between the membrane receptor and the source produces a significant change of accumulated cAMP on receptors.
We study the adaptation and amplification at various distances between cell and source including the case where the cell may reach the source.

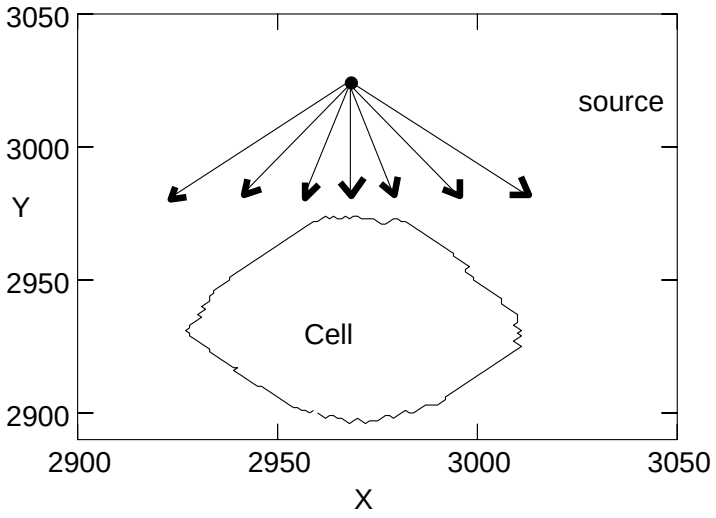

Figure 6.11: Cartoon of a cell exposed to an inhomogeneous gradient source.

A. The moving cell does not reach a steady state in case of inhomogeneous gradient source.

In case of inhomogeneous gradient, the distance between the point source and the cell is finite. Without having filament polymerization, cell does not become polarized, because cell polarization needs not only proper gradient sensing, but also asymmetric filament polymerization. Due to signal activated regulatory proteins the filaments grow very

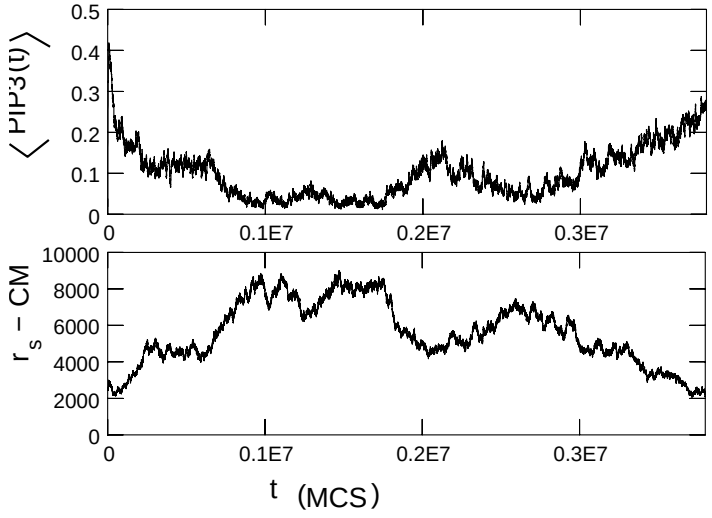

Figure 6.12: (Upper part) Response intensity,⟨PIP3⟩ (t), as function of time (Monte Carlo steps, MCS) for an inhomogeneous gradient source. (Lower part) Time-dependent distance between point source r_s and the center of mass of the cell, CM.

rapidly at the front of the cell as compared to that at its rear. At the rear part, filament polymerization is suppressed. So filament polymerization (in other words, filopodia and lamellipodia formation) produces a driving force for the cell to move towards the source. Without having filament the cell moves in a random way. Due to randomness of motion, the distance between source and cell changes continuously with time. Therefore the response intensity ⟨PIP3⟩ (t) fluctuates considerably, much larger than in the case of a homogeneous signal gradient (compare fig.6.8(a)). For changing concentration of cAMP at various points on the cell surface the shape of signal gradient also changes. We observe in this study that continuously changing signal gradient affects the response gradient spatially and temporally in both ways. Fig.6.12 (upper part) shows the temporal response of the PIP3 intensity, ⟨PIP3⟩ (t). The lower part of figure 6.12 shows the distance between source and the center of mass (CM) of the cell as a function of time. From this figure it is clearly observed that when the cell is far from the source, the average PIP3 accumulation is less compared to PIP3 accumulation in case of shorter distances between source and the cell. This is because shorter distances between source and cell makes the receptor occupancy higher and as a result PIP3 accumulation at the front part of the cell becomes higher. Thus, the moving cell does not reach any persistent steady state in case of inhomogeneous gradient source. We define a steady state as a state where the average spatial accumulation of PIP3 along the membrane PIP3(nm) and the average accumulation of total PIP3 ⟨PIP3⟩ with respect to time remain approximately constant, i.e., the relative fluctuation δPIP3/⟨PIP3⟩ <1. The relative fluctuation

in the steady state (fig.6.8(a)) is δPIP3/$\langle$PIP3$\rangle$ $\approx$0.2, whereas in the non-steady state (fig.6.12) δPIP3/$\langle$PIP3$\rangle$ $\approx$1.

To measure the spatial response, we select some short time interval between when the PIP3 production is persistent and the distance between source and the cell does not vary much. Fig.6.13 is representing the corresponding graphs.

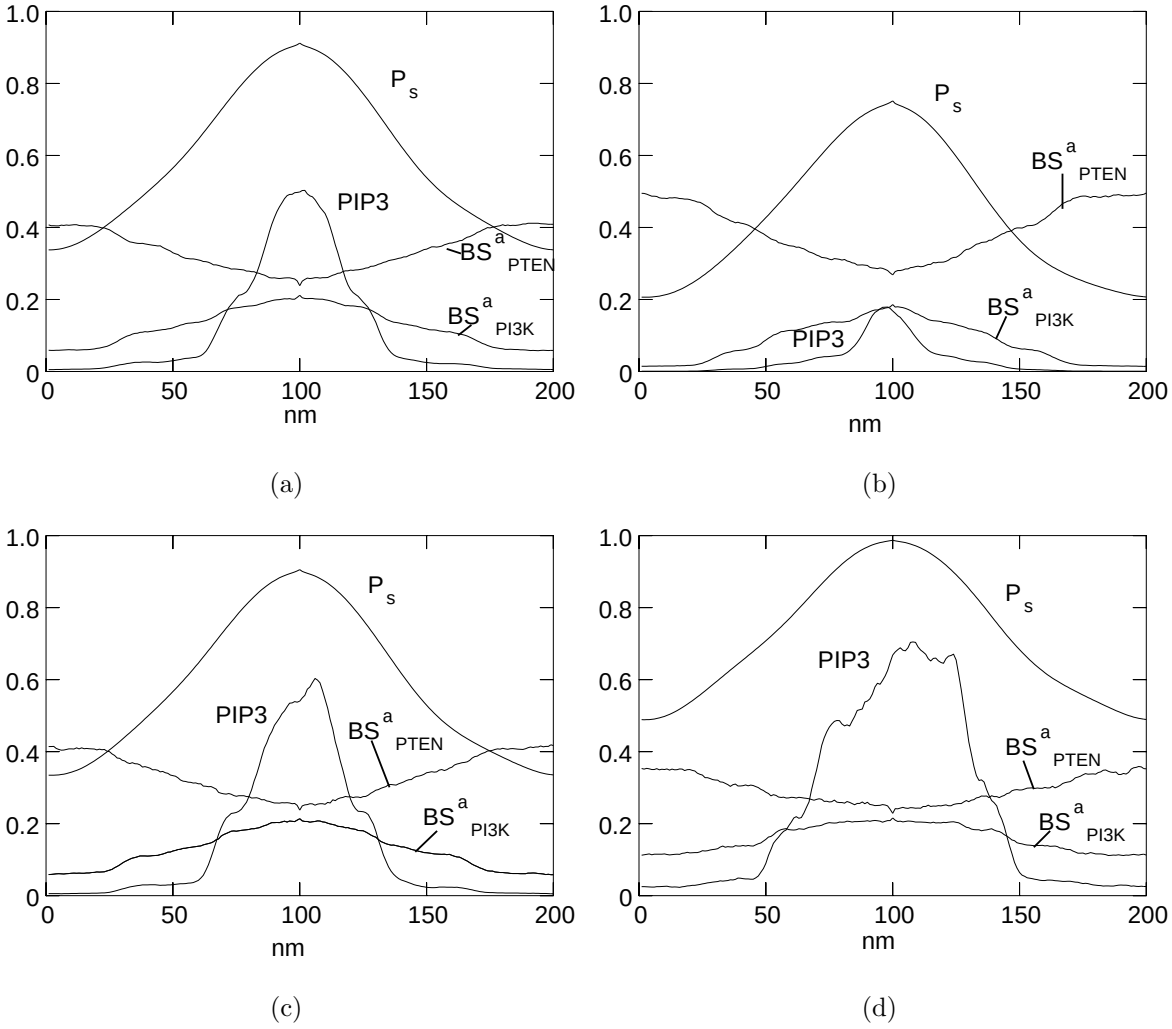

Figure 6.13: Spatial amplification of the response, PIP3(nm), as a function of membrane periphery, nm, for 4 different time intervals of about 5×10^5 MCS selected from fig.6.12. Corresponding spatial signals P$_s$(nm) and BS^a_{PI3K}(nm) and BS^a_{PTEN}(nm) are plotted as well.

B. Inhomogeneous signals produce decreased directional sensing of a cell.

In fig.6.13(a), the signal gradient as well as response gradient, assume greater magnitude as compared to time intervals, for example in fig.6.13(b). The process evidently becomes more interesting after certain time intervals when cell approaches the source. Then the signal gradient increases and so does the response gradient. Fig.6.13(c) and fig.6.13(d) show the profiles of gradients as this process takes place. From the plot of activated BS_{PI3K}(nm) and BS_{PTEN}(nm), we can discern that when the response concentrations at the front of the cell are not much compred to its maximum possible concentrations, the difference between the front concentrations of BS^a_{PI3K} and BS^a_{PTEN} are larger than the case when the concentrations of response at the front of the cell assume greater magnitude. Some experimental findings [138] have also reported that cells, especially amoebae fail to respond chemotactically to decreasing concentrations.

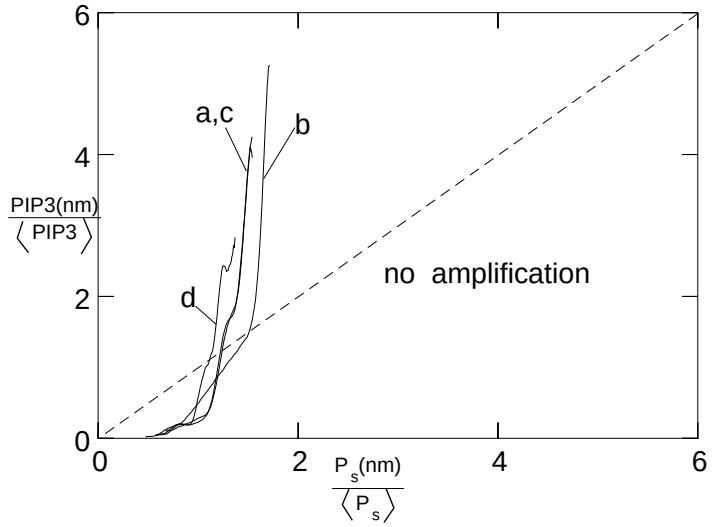

Figure 6.14: Plot of response, PIP3(nm)/⟨PIP3⟩ , *versus* the relative signal, P_s(nm)/$\langle P_s \rangle$. The broken line is representing no amplification line. The number (a-d) refer to fig.6.13(a-d).

Experimental results [138, 121] suggested furthermore that amoebae are unable to respond chemotactically to decreasing concentrations if the signal gradient concentrations decrease more rapidly than it can be accommodated by the motility of the cell. From the result obtained by our model we can conclude that decreasing concentrations of signal produce decreasing directional sensing too. Thus, the inability of a cell to move accordingly fast with decreasing signal concentrations along the cell periphery is not due to the improper directional sensing. Other proposed models indicate that the rear part of the cell becomes inhibited and is unable to sense the change in stimuli [123]. In our stochastic model the change of signal concentrations at the front part and the rear part

of the cell both are responsive. This result is similar to some experimental result on latrunculin-treated cell [125].
To measure the degree of response amplification in case of chemotactic signals, the relation between input signal and output response can be plotted [9]. Fig.6.14 shows the relative response, PIP3(nm)/$\langle$PIP3$\rangle$, as function of the relative signal, P_s(nm)/$\langle P_s \rangle$. The data are the same as shown in fig.6.13. The plotted curves are showing the relationship between input and output and have an almost identical shape which indicates that this property is inherent for mobile cell. This result matches qualitatively with previous result for immobile model cell [9]. In fig.6.14 the broken line describes the case with no amplification. Although the difference is extremely small, to the point of being microscopic, a careful observation enables us to notice from fig.6.14 that, when the cell is near the source the amplification slope is more steeper than the case when cell is going away.

C. Cells exposed to inhomogeneous signals perform random motions.

Fig.6.15 is representing the mean square displacement and the trajectory of CM (center of mass) of the moving cell . From the nature of displacement and the trajectory, we can conclude that the motion of the cell is completely random. Although the asymmetric distribution of the moving regulatory particles (PI3K and PTEN) is expected here, but this asymmetric distribution is not sufficient to produce any persistent movement of cell.

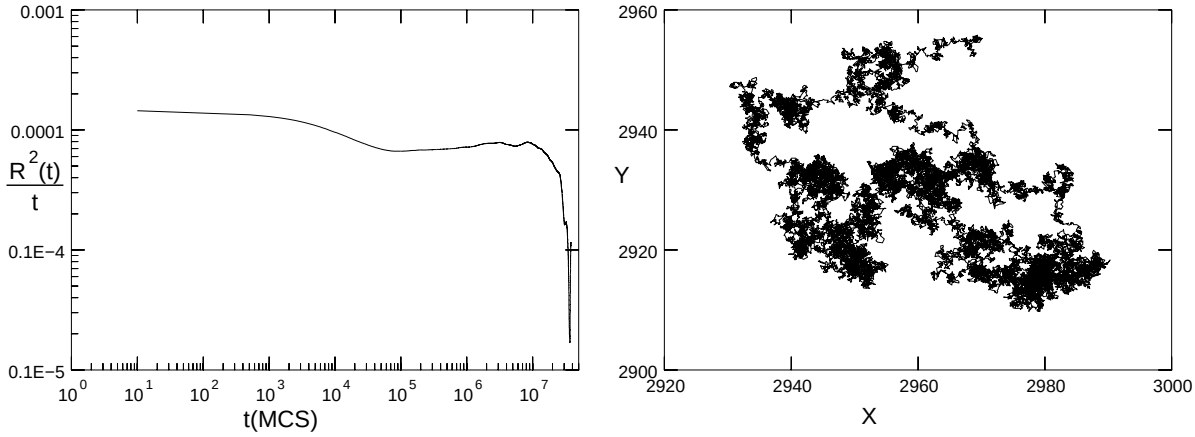

(a) (b)

Figure 6.15: (a) Mean Square Displacement (MSD) *versus* Monte Carlo steps (MCS). (b) Center of mass (CM) trajectory of the cell.

6.4 Summary

The relation between output response (PIP3) and input signal (P_s) is completely non linear. ΔP_s, P_s^{max} and $\langle P_s \rangle$ are important signal parameters for controlling the respose gradient amplification. It has been found that the signal localization plays very important role for producing response gradint. So slight change of signal localization on membrane can produce huge difference on above mentioned signal parameters and as a result an abrupt change in response gradient occurs.
Although cell exposed to uniform homogeneous signal does not get enough attention in terms of directional sensing compare to cell exposed to gradient signal, but from our simulation result we have noticed some important fact regrading them. The average response concentartion $\langle PIP3 \rangle_0$ corresponding to cell exposed to uniform signal can predict the limit of maximum or minimum response concentartion at the back and at the front of the cell respectively.
Cell's directional sensing does not hamper with the change of gradient signal. One drawback of our model is that in case of inhomogeneous signal gradient the change of signal gradient is out of our control. Although from the result we can conclude that the cell can adapt the change of signal gradient but we are not able to make any comment on how fast the cell can adapt the change of external signal in their internal regulatory pathway. From the adaptation study it can be concluded that the adaptation time τ_{Ad} and diffusion coefficient D of moving particles inside the cell are inversely proportional. In appendix B a literature study for probable candidates involved in LEGI mechanism has been discussed.

7 Signal induced cell migration : Chemotaxis

7.1 Introduction:

In the previous chapter (chapter **??**)it has been discussed about the directional sensing of a chemotaxis cell. In chapter 2 it is also mentioned that cell motility is a collective result of directional sensing and cell polarization. In the present chapter I present some basic properties of cell polarization along with directional sensing. Polarization defines the propensity of the cell to assume an asymmetric shape with a defined anterior and posterior. Molecules associated with the "leading edge" include actin and actin-binding proteins Scar, WASP, filopodin, cofilin, and coronin, whereas molecules associated with the"trailing edge " include myosin II and cortexillin [139, 140, 141, 142, 143]. In polarized cells the anterior surface is more sensitive to chemoattractants than other regions. Cells migrating directionally toward a chemoattractant source display a highly polarized cytoskeletal organization. Although directional sensing does not require actin polymerization, polarity depends critically on a signal input as well as a reorganization of the cytoskeleton. So it is suggested that establishment of polarization involves a dynamic, coordinated interaction of directional sensing events with the activities of the cytoskeleton. Cells display various degrees of polarization that may also change with conditions. In general, neutrophils are immobile until exposed to chemoattractant. Then they polarize, acquire a distinct leading edge and uropod, and begin to move [144, 145, 146, 147]. Growth stage *D. discoideum amoebae* are unpolarized and move randomly without exogenous chemoattractant. These cells can still sense direction and carry out chemotaxis. As they differentiate, they become elongated, motile, and highly chemotactic [148]. Polarization can also be enhanced by a period of directed movement in a gradient.

7.2 Model description:

To study the cell polarization and finally the cell's chemotactic movement, we use the same stochastic LEGI model, as discussed in the previous chapter, for directional sensing. In the present model actin particles has been added. For actin molecules the nucleation (spontaneous and dendritic), polymerization and depolymerization follow the same rule as described in the model description section of chapter 4. To make the actin movement

consistent with the membrane movement we introduce six additional degrees of freedom instead of two as in chapter 4.

Quantity	*Value*
Lattice constant, a	5 nm
Typical cell size	100×100 lattice
Monte Carlo step, τ	$0.875\mu s$
Diffusion constant, D	5 MCS
W_n	1
W_{br}^+	1
W_{br}^-	0.6
W_B^+(ATP)	1
W_B^-(ATP)	0.002
W_B^+ (ADP)	0.1
W_B^-(ADP)	0.009
W_P^+(ATP)	0.1
W_P^-(ATP)	0.002
W_P^+(ADP)	0.01
W_P^-(ADP)	0.06

Table 7.1: Reaction probabilities of model cell.

According to our stochastic model, first each membrane bead will be activated by corresponding signal probability. As described in the previous chapter, each membrane bead represents a cluster of membrane bound particles. Every cluster contains 7 receptors, 10 exciters, 10 binding sites of PTEN and PI3K, respectively and 100 PIP3/PIP2. A short description regarding all these particles responsible for directional sensing is given in appendix C. We keep the same ratio of membrane bound particles as in previous work [9]. In the LEGI mechanism first receptors become activated according to signal probability of corresponding membrane bead. According to our previous parameter selection, one membrane bead is activated by 100% signal probability, where all the corresponding 7 receptors are active. Until the signal probability decreases from 1.0 (maximum) to 0.875, all receptors remain active. Since seven receptors represent 100% signal probability, each receptor takes in account effectively more than 14% signal difference, which makes the model cell not very signal sensitive. So with this parameter set the minimum signal difference between front and back is 14% which the cell can sense. On the other hand, it has been suggested that a cell has the ability to sense a signal difference as small as 1-5% [134, 84]. So to improve the signal sensitivity of the model cell, we increase the number of membrane bound particles in each cluster by a factor of 10. In present model each receptor activation represents 1.4% signal probability difference, which implies that the cell's ability of directional sensing is improved more than earlier (chapters 5 and 6).

In section 7.4 we will see that the directional sensing of the cell indeed is improved with present parameter values as compared to previous parameters.
From the literature it is known that even monomeric actin with bound ADP can also aggregate to form filaments, albeit at a slower rate [149]. To make our present stochastic model more realistic we introduce ADP-actin (de-)polymerization for barbed ends and pointed ends. To determine the value of the probability constant we have used the experimental rate constants [34, 33], which are shown in table 2.3. Table 7.1 contains some of model parameters and the reaction probabilities used in the simulation.

7.3 Mean square displacement:

It is known that the dynamics of a cell is governed by two completely different time scales. One characterizes the random diffusion of the moving particles inside the cell, and the other is related to (de-)polymerization events. In order to understand the relation and the relative dominance of these two time scales (we call it diffusion time scale and the reaction time scale), it is important to study the mean square displacement of center of mass of the cell (CM). The mathematical expression of the mean square displacement [150, 151] is

$$R^2(t) = \langle (R(t) - R(0))^2 \rangle = 4Dt + 2v^2\,\tau_p\big[t - \tau_p\big(1 - \exp(-t/\tau_p)\big)\big]\,. \qquad (7.1)$$

τ_p is the persistence time of the random walk and v is the drift velocity. In fig.7.1 the mean square displacement is plotted as a function of time t. For short times, it is $R^2 = 4Dt$. This indicates that for short times the random diffusion of the mobile particles and the membrane dominates the motion of the cell. Then, for $0 < t < \tau_t$, the behavior of the cell is subdiffusive. Due to 'substrate attachment' of the filaments, the random movements of the cell membrane are restricted and slowed down. After the attachments of the F-actin filaments have been released through depolymerization. This state is just prior to the states when filaments grow autocatalytic way towards the signal activated direction. This behavior is not included in the equation 7.1. After the time τ_t the cell starts to move persistently and for $\tau_t < t < \tau_0$ cell moves with drift velocity. The upper limit of the ballistic regime of the mean square displacement is τ_0. And again cell goes to diffusive regime for $t < \tau_0$ due to persistent random motility.

7.4 Polarized cell with different signal gradient:

It has been reported that directional sensing does neither require a change in the morphological of the cell shape nor a change in the cell motility [152]. It is not possible to predict the nature of cell's motility from directional sensing response excluding the polarization event. Polarization involves the asymmetric distribution of filaments along the membrane (nm) . These asymmetrically distributed filaments produce protruding

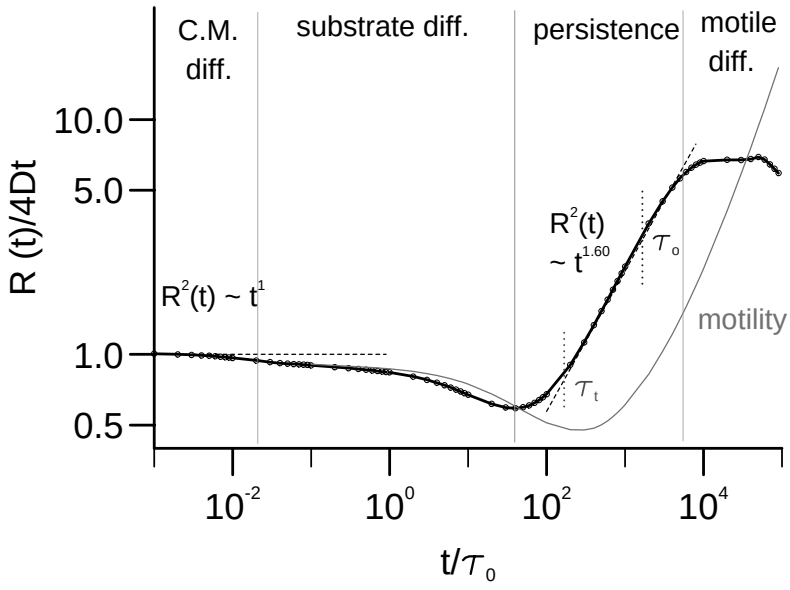

Figure 7.1: Typical mean square displacement of a two dimensional simulation of a persistent random walk model.

force towards the signal activated membrane and as a result cell moves. So to get a complete understanding of cell motility polarization study for a mobile cell in necessary. The downstream proteins network responsible for cell's polarization get input signal from directional sensing response.

7.4.1 Cell velocity and signal activated section of the cell membrane

Only 40% to 60% of total actins are found as F-actin filaments in a cell [153, 154]. Our simulation result shows on average 55% actins are involved in filament network. To study the polarization we keep P_s^{max} constant (0.93) and constantly decrease the gradient steepness ΔP_s , similar to the studies discussed in the previous chapter (fig.6.2(c)).
In the model description section, the reasons behind the change of membrane bound parameter values is mentioned. The difference between two parameter sets in terms of cell's sensitivity towards the signal difference is clearly noticeable in table 7.2. The input parameter ΔP_s transfers to output parameter ΔP_r by using amplification network. As the receptor activation is the first step of amplification process, so first input signal P_s is converted into receptor activity. We measure the receptor activity by calculating the difference between number of active receptors (Δr) at the front (r^{front}) and at the back (r^{back}) of the cell. r^{front} is representing the number of active receptors at the highest activated membrane bead and r^{back} is the same for lowest activated membrane bead.

When Δr (r^{front} - r^{back}) is zero the corresponding situation indicates that the input signal P_s is effectively uniform.

ΔP_s (%)	Δr (previous)	Δr (present)
88	3	21
72	3	18
50	2	13
39	1	10
34	1	9
28	0	7
21	0	5
17	0	4
12	0	3

Table 7.2: percentage of signal difference ΔP_s between front and back of the cell and average difference in numbers of signal activated receptors Δr (r^{front} - r^{back}) between front and back of cell with previous and present parameter.

From table 7.2 we notice that with present parameter set the cell is able for directional sensing even with a shallow gradient, where ΔP_s is almost 10%. So we believe that by increasing the number of membrane bound particles in each cluster, it is possible to make the cell more sensitive even for 1-5% signal difference. It should be noted that this do not change the basic characteristic properties of cell polarization or cell motility. So we do not continue this subject anymore.
Fig.7.2(a) depicts the graph of drift velocity versus ΔP_s. The figure shows that when ΔP_s is minimal, the signal gradient is small and the drift velocity is small too. With increasing ΔP_s the drift velocity increases sharply until a maximum. After the maximum the drift velocity decreases very slowly with increasing ΔP_s . In the following I will explain this dependency of v on ΔP_s .
As I have mentioned above, the present situation is similar to the case shown in fig.6.2(c). From this figure it is noticeable that when ΔP_s decreases, the corresponding PIP3 accumulation along the membrane approaches its saturation level. Although saturated PIP3 accumulation along the whole cell periphery implies that many filament polymerization events must take place and, in particular, a large number of barbed ends by dendritic nucleation is generated. According to our result we can hypothesise that production of filament barbed ends is not the only parameter regarding the velocity of chemotactic cell. Cell motility is a more complex phenomena. According to our hypothesis the amount of accumulated PIP3 at the cell periphery is also very important. This important phenomenon has been observed in several other situations which I will discuss in next few sections of the present chapter.
Generally, depending on the P_s(nm) concentration on the membrane, the cell has different PIP3 concentration, $PIP3(nm)$, along the membrane. The cell has the ability to

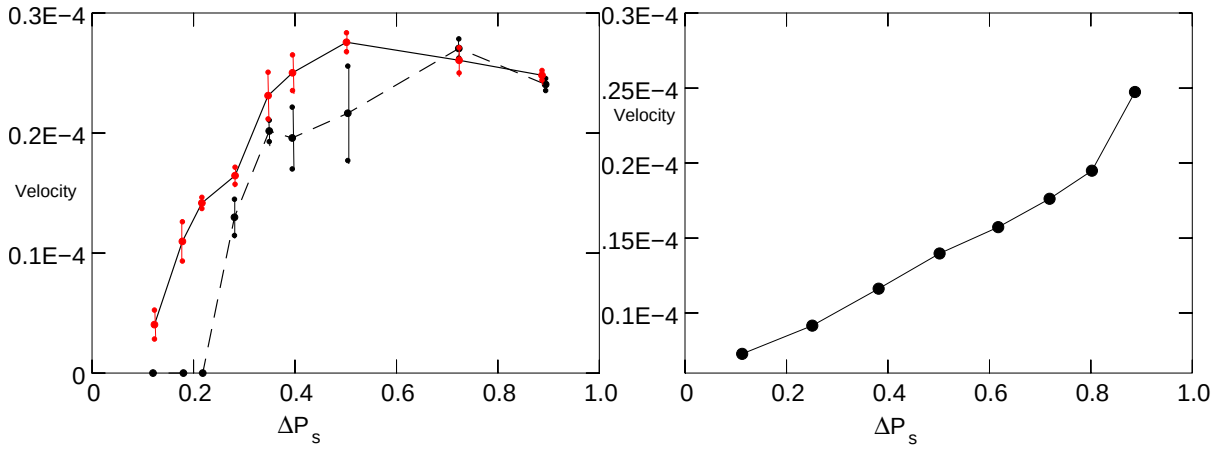

(a) a (b) b

Figure 7.2: (a) Plot of drift velocity versus signal gradient for a mobile cell when the corresponding signal midpoint (P_s^{max}) is constant. The solid line indicates the data with present parameter value and the dashed line is representing the data for previous parameter values. (table 7.2). The velocities have been plotted with error bar. (b) Drift velocity versus signal gradient for a mobile cell for fixed P_s^{min}=0.1.

detect the region with highest PIP3-concentration among whole PIP3 accumulated cell periphery. In our model cell we call this most PIP3 concentrated cell perimeter as the "PIP3 accumulated effective cell perimeter", when the PIP3 concentration is more than $\langle PIP3 \rangle$. For the remaining part of my thesis I will mention this 'PIP3 accumulated effective cell perimeter' as 'PIP3 accumulated cell perimeter'. Due to PIP3 accumulation the area near the cell membrane becomes rich of filaments (specially ATP-filaments). The growing barbed ends of these filaments lead to the directed movements of the signal activated (PIP3 accumulated) membrane. In the case of very steep signal gradients, ΔP_s , the section of the membrane containing PIP3 is much smaller as compared to the whole cell perimeter (see the curve 'a' in fig.6.2(c)). So the production of barbed ends on that particular part of cell membrane is not enough to drag the whole cell towards the source with highest velocity. In the case when P_s^{max}, is same but signal gradient is shallower, the PIP3 accumulated membrane perimeter increases (see the curve 'c' in fig.6.2(c)). It is easy to understand that this increment of PIP3 accumulated membrane perimeter leads to an increase of polymerizations at the branched and the barbed ends. This increased amount of PIP3 populated membrane helps the cell to move faster than in the earlier case when PIP3 activated membrane was smaller. Figures 7.3(a) and (b) (solid line) represent the PIP3 accumulated cell perimeter and the production of ATP barbed ends, respectively, *versus* ΔP_s.

There are some theoretical papers [111, 155] in which it has been suggested that the maximum velocity can be achieved by an optimum balance between the number of filaments needed to push the membrane and the number of free monomers which are

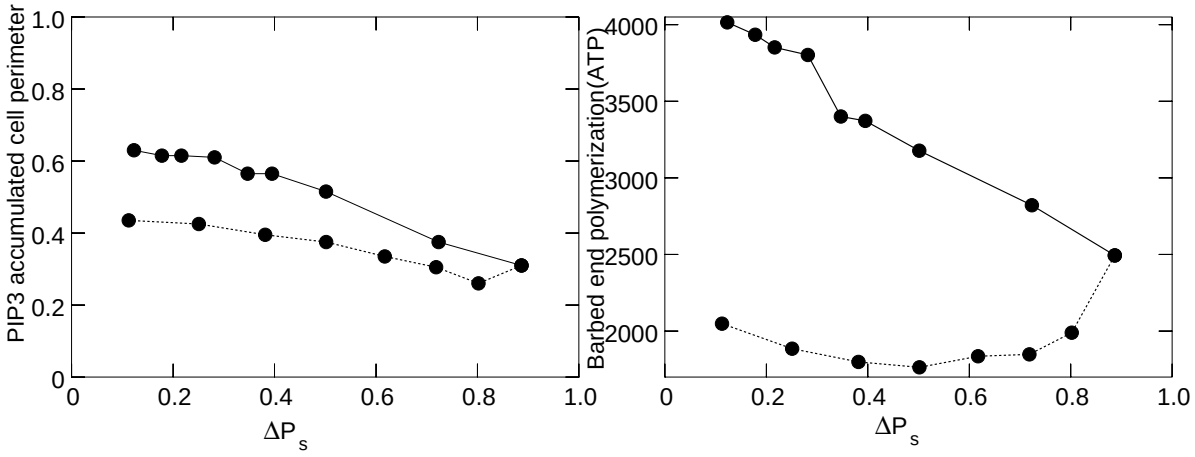

(a) (b)

Figure 7.3: (a) Membrane perimeter with active PIP(PIP3) as a function of different signal gradients of a moving cell, where the signal midpoint concentration, P_s^{max} , is constant for solid line and P_s^{min} is constant for dotted line. (b) Production of ATP barbed ends *versus* ΔP_s when $P_s^{max} = 0.93$ (solid line) and $P_s^{min} = 0.1$ (dotted line).

needed for maintaining the treadmilling process. However, in this study first we observe that in the case of maximum cell velocity there is a significant role of PIP3 accumulated membrane perimeter. The maximum velocity depends on an optimum balance between signal activated membrane perimeter and the filament growing ends to protrude. I will discuss this below in section 7.5 again.

I have also studied the drift velocity v by varying ΔP_s while keeping constant $PIP3^{min}$ (0.1) (see fig.7.2(b)). In this case ΔP_r increases nonlinearly with increasing value of ΔP_s (compare fig.6.4 (broken line)). In this case the drift velocity also increases with increasing ΔP_s. In the previous paragraphs I have hypothesized that the role of PIP3-accumulated membrane perimeter and the filament barbed ends are significant for the drift velocity. Fig.7.3(broken line) represents the above mentioned parameters in this situation. From fig.6.4 (broken line) we can notice that up to certain value of ΔP_s (0.6), ΔP_r is very small and after then with increasing ΔP_s, ΔP_r starts to increase very sharply. This is the reason why in fig.7.3(broken line) instead of decreasing PIP3 accumulated membrane perimeter the production of barbed ends increase. At highest ΔP_s the PIP3 accumulated membrane perimeter is 30% of total membrane perimeter, but the production of barbed ends is maximum and this combination provides the maximum of the drift velocity. This study makes our claim more strong that the drift velocity depends on the relative nature of PIP3 accumulation at the cell membrane.

7.4.2 Effect of relative PIP3 concentration

In the previous chapter we have seen that, when we keep ΔP_s constant and gradually increase P_s^{max} , the response gradient ΔP_r starts to increase very slowly from zero to a certain maximum value (fig.6.3). Further increment of P_s^{max} causes the drop of ΔP_r very rapidly from its maximum. In the present study we have calculated the corresponding drift velocity of the model cell in this situation. Fig.7.4(a) represents the corresponding graph. In case of a minimal value of P_s^{max} the drift velocity does not assume its lowest

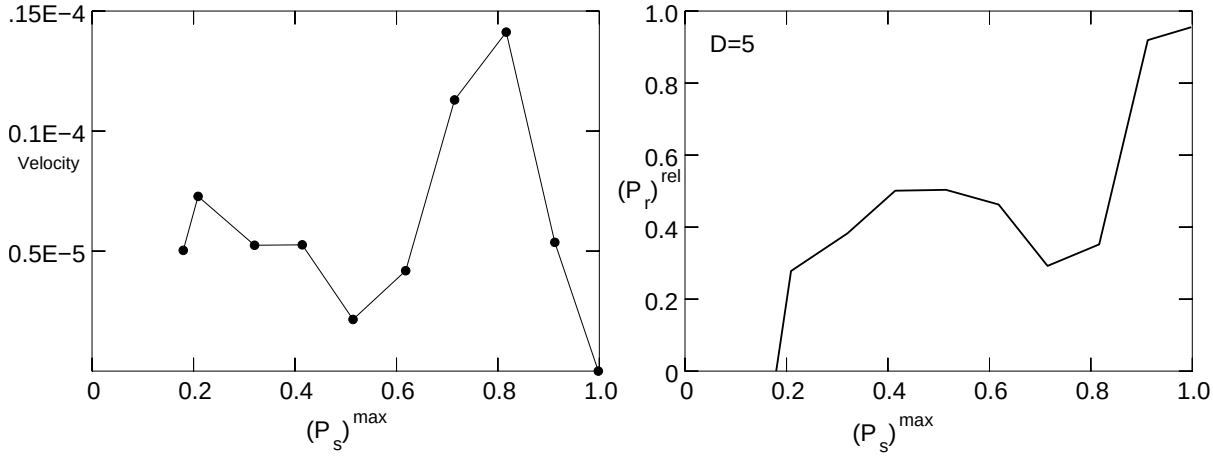

Figure 7.4: (a) Plot of drift velocity versus P_s^{max} for a mobile cell when ΔP_s is fixed (0.1). (b)$P_r{}^{rel}$ *versus* P_s^{max} .

value as the corresponding lowest response gradient ΔP_r . The drift velocity has a certain starting value and it is not zero. When the ΔP_r starts to increase very slowly (see fig.6.3), the corresponding drift velocity gradually decreases from its starting value(see fig.7.4(a)). When ΔP_r starts to increase relatively rapidly, again the drift velocity starts to increase very rapidly. For the maximum ΔP_r the corresponding drift velocity is also maximal. After reaching its maximum value, the response gradient as well as drift velocity both starts to decrease very rapidly. According to our understanding, when P_s^{max} is very small, the corresponding ΔP_r is also small, which implies that the number of PIP3 (accumulated at signal activated membrane) is also very small. When the concentration of PIP3 at the front part of cell is very low, the corresponding rear part of the cell contains almost null PIP3. To measure the difference between front and back concentration of PIP3 I have calculated the relative response $P_r{}^{rel}$ which is defined by

$$P_r{}^{rel} = \frac{PIP3^{min}}{PIP3^{max}}, \tag{7.2}$$

Where $PIP3^{max}$ represents the accumulated PIP3 at the front and $PIP3^{min}$ the accumulated PIP3 at the rear part of the cell. Fig.7.4(b) shows the graph of $P_r{}^{rel}$ versus

P_s^{max} . From fig.7.4(b) and fig.6.3 it can be noticed that when ΔP_r is lowest, the corresponding ${P_r}^{rel}$ is also minimal. Although the front accumulation of PIP3 is reduced, the cell still can move in a chemotactic way, although at small velocity because the intensity of the signal coming from accumulated PIP3 is very weak and thus produce only a small amount of barbed end filaments. With gradual increase of P_s^{max} the response gradient starts to increase very slowly and the corresponding PIP3 accumulation at the back and at the front both also increase. This increment of PIP3 synthesis at the back of the cell makes ${P_r}^{rel}$ larger. From the fig.7.4(b) we can see that with increasing value of P_s^{max} , the value of ${P_r}^{rel}$ starts from minimum and then gradually increases, which indicates that the ratio of accumulated PIP3 at the front and at the back is not large. This leads to the decrease of the drift velocity which is shown in fig.7.4(a). After a certain P_s^{max} value, the response difference ΔP_r starts to increase (for example see curve 'c' in fig.6.2(a)) and ${P_r}^{rel}$ as well starts to decrease again. The reason behind this sudden decrease of ${P_r}^{rel}$ is not fully understood. In the previous chapter we have seen that the localization of P_s along the membrane plays a very important role for the response amplification. Therefore, we can imagine that in the present case, instead of the same ΔP_s , some localization of P_s is able to produce a huge amplification of the response as comprared to other localization (see curves 'b' and 'c' in fig.6.2(a)). As a result, the PIP3 concentration at the front is quite large as compared to PIP3 concentration at the back. That is the probable reason behind the decrease of ${P_r}^{rel}$ and the concomitant rapid increase of the drift velocity. When P_s^{max} reaches its maximum level, the difference between back and front accumulated PIP3 again becomes quite small as ΔP_s approaches its saturation level along the membrane. This causes the decrease of the response gradient ΔP_r very rapidly and an increase of ${P_r}^{rel}$. It should be noticed that ${P_r}^{rel}$ only measures the relative PIP3 concentration at front and back of the cell, which yields the fact that the minimum of ${P_r}^{rel}$ does not correspond to a maximal drift velocity. The drift velocity is controlled, besides ΔP_s , by other important parameters.

7.5 Drift velocity of a polarized cell:

Although filament dissociation does not contribute directly to cell's drift velocity, it plays nevertheless an important role in cell's motion by controlling the F-actin concentration. Dissociation helps the cell in recycling monomers from the rear of the cell to the lamellipod at the front. During the study of the cell's drift velocity as function of F-actins concentration at different signal gradients, a specific rate constant W_P^- for pointed end F-actins was chosen. The value of W_P^- for ADP F-actin is quite large compared to other dissociation probabilities (see table 7.1). ADP-F-actin dissociates from filaments rapidly [156] because this process is catalyzed by filament regulatory proteins [157, 158, 159] which have a high affinity to the ADP-F-actin ends of filaments. From our result it is observed that the drift velocity exhibits a maximum at slightly varying (0.06 to 0.08) W_P^- for different ΔP_s and P_s^{max} =0.93. This is shown in fig.7.5(a).

Fig.7.5(b) shows the total number of ATP-barbed ends as function W_P^- for different ΔP_s .

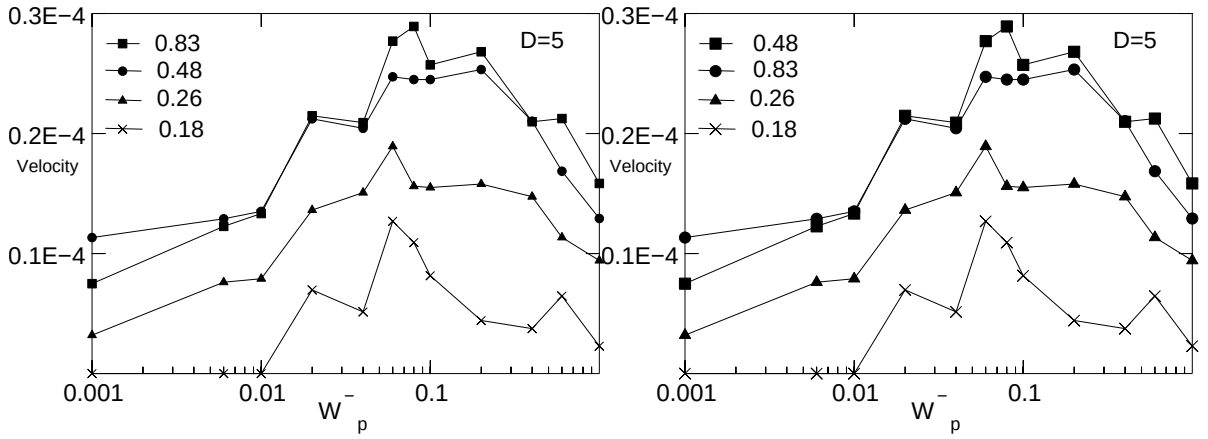

Figure 7.5: (a) Plot of drift velocity as a function of pointed end (ADP) depolymerization probability W_P^- for different signal gradient in a moving cell. (b)Total number of filament barbed end (ATP) polymerization versus pointed end (ADP) depolymerization probability W_P^- for different signal gradient in a moving cell (The number inside the graph is indicating the value of ΔP_s) .

At W_P^- =1.0, the corresponding concentration of F-actins (n_f) is the lowest (10% of the total concentration of actins).

Fig.7.6 shows the fraction of F-actin, n_f/n, as function of W_P^- for various ΔP_s . Due to large values of W_P^- the life time of individual filament becomes extremely short. This is not favorable for neither dendritic nucleation nor barbed end polymerization. Due to very unstable and short filament network the production of barbed end is hampered, although the spontaneous nucleation happens maximum at this large value of W_P^- for large concentration of actin monomers. So less filament polymerization as well as less barbed ends produce little force to protrude the membrane forward. As the value of W_P^- gradually decreases, the filament concentration starts to increase (fig.7.5(b)). As a result, the drift velocity gradually increases with increasing concentration of F-actin, n_f/n (fig.7.7). After reaching a maximum value, the drift velocity again started to drop down with further decrease of W_P^-. Due to treadmilling mechanism the barbed ends of filaments are more prone to associate new actin monomers and the pointed ends are more prone to dissociate actins from the filaments. Decreasing value of W_P^- is able to change this treadmilling event. Due to small value of W_P^- the pointed end depolymerization occurs very rarely compare to barbed end polymerization, which implies that the life time of existing filaments become very long. From our study we found out that when the value of W_P^- is 0.001, irrespective of ΔP_s, the concentration of F-actins becomes

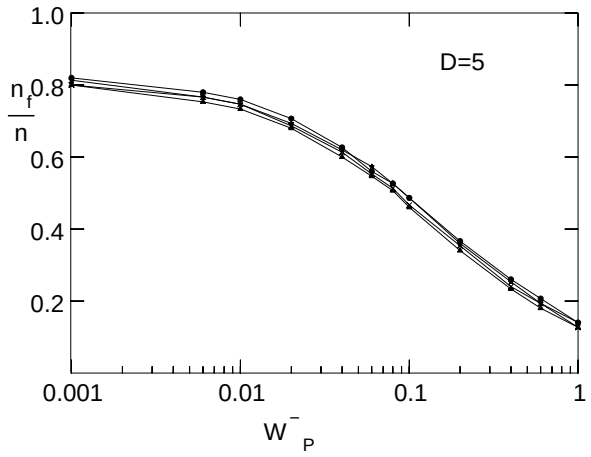

Figure 7.6: Fraction of F-actin (n_f) as a function of pointed end (ADP) depolymerization probability W_P^- for different signal gradient in a moving cell.

around 80% of the total actins concentration. But this large concentration of filaments does not produce maximum number of barbed ends or branched filament. Fig.7.8 shows the production of barbed ends and branching filaments with varying concentration of filaments n_f/n. This situation implies that at low values of W_P^- the actin networks exists as very long probably single or almost single cluster inside the cell. A similar explanation was reported by other theoretical studies [111] also.

We denote the particular W_P^- by W^* when corresponding drift velocity becomes maximal. When $W_P^- > W^*$ or $W_P^- < W^*$, in both cases the number of barbed ends is smaller than the total barbed ends of corresponding W^* (≈ 0.08). So it can be concluded that the origin of maximum velocity is barbed end induced pressure on the cell membrane. However, we observe that besides the barbed end production, there is another important factor which also controls cell motility. From fig.7.5(b) one can notice that when ΔP_s is maximal (sharpest signal gradient), the production of barbed end polymerization is minimal as compared to the case when ΔP_s is minimal, irrespective of all W_P^- values. I am explaining this phenomena. In the previous chapter we have seen that for a constant P_s^{max} , the ΔP_r decreases when ΔP_s changes from maximum to minimum (fig.6.3(b) solid line). In that situation the response gradient in terms of PIP3 accumulation at the membrane has been measured. So according to signal gradient the PIP3 accumulation along the membrane is different. The sharpest signal gradient produces very large amount of PIP3 concentration at the front and extremely low PIP3 concentration at the back of the cell. In our simple model we define the front and the back of the cell by the closest and the furthest point of the cell from the source respectively. As for example, fig.6.2(b) shows the average PIP3 accumulation along the cell membrane and the corresponding signal intensity. So the membrane perimeter, covered by accumulated PIP3,

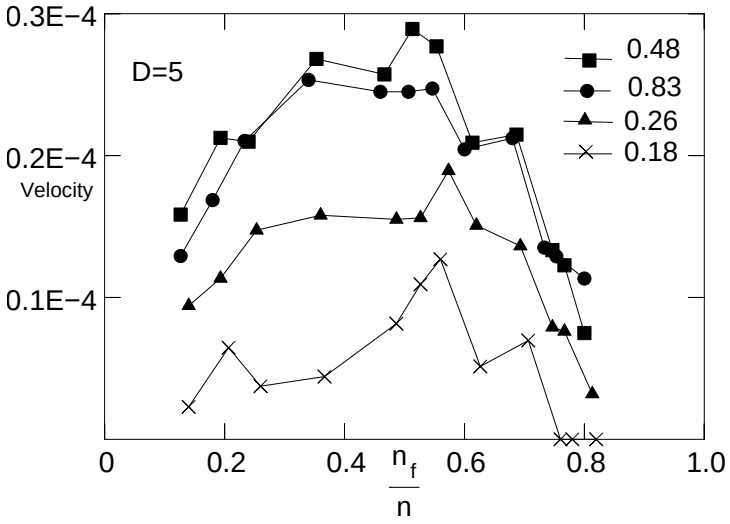

Figure 7.7: Drift velocity as a function of the fraction of F-actin, n_f/n for different signal gradients. The number inside the graph shows the values of of signal gradients ΔP_s .

is different for different signal gradients. The measurement of this membrane section is important because actins get necessary signals for branching or ATP-induced polymerization from this part of the cell membrane. ATP-F-actins exert a pressure on this membrane perimeter. Although there exist ADP-F-actin also, but generally their concentration is very small as compared to ATP-F-actin and do not produce significant force to move the cell forward. Fig.7.3(a) (solid line) shows the membrane perimeter covered by active PIP(PIP3) versus the varying signal gradient ΔP_s . When the signal gradient is shallowest, the PIP3 accumulated effective perimeter is 61% of total membrane beads, which is 200 membrane beads. This large amount of PIP3 accumulated perimeter for the shallowest gradient is the reason behind the huge number of barbed ends and branched filament production. So when signal gradient $\Delta P_s = (P_s^{max} - P_s^{min})$ is shallow, the PIP3 populated membrane perimeter is much broader than the PIP3 populated membrane perimeter resulted from steep signal gradient. And this broader activated membrane is the reason behind the large number of branching and ATP-barbed end polymerization.

It should be noted here that in other theoretical models [155, 111] the maximum barbed end production implies maximum filament concentration. So in these models, when barbed end production became maximum, then due to the lack of freely available G-actin monomers the velocity of cell drops very rapidly. Our present model differs in that respect. From fig.7.5(b) and fig.7.6 we can notice that when the filament concentration is maximal, the corresponding barbed ends production is not maximal. Very low value of W_P^- can produce large concentrations of F-actin. The reason behind less barbed end production, observed in the present study, has been discussed in the previous section

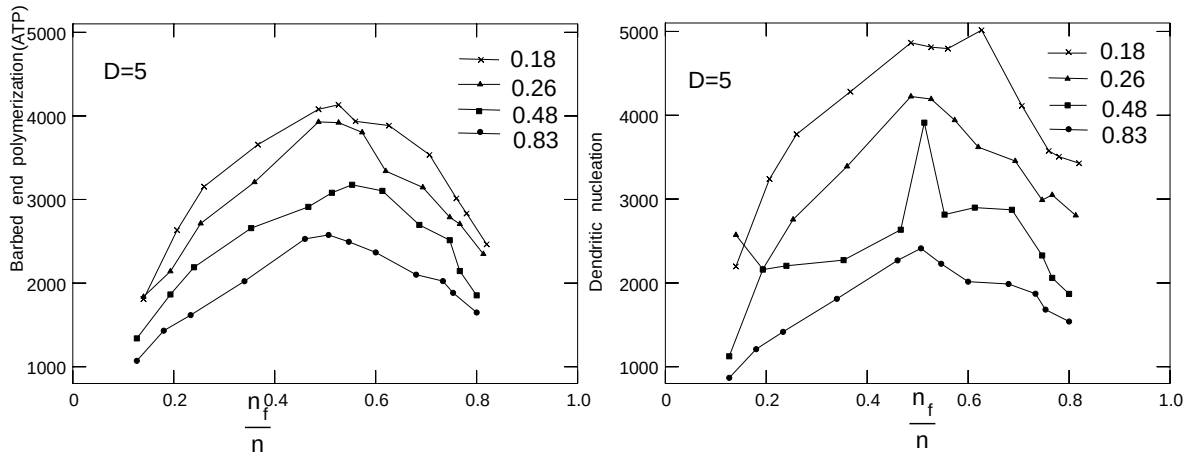

(a) (b)

Figure 7.8: (a) Total number of filament barbed end (ATP) polymerization *versus* fraction of F-actin ($\frac{n_f}{n}$) for different signal gradient ΔP_s in a moving cell. (b) Total number of filament dendritic nucleation *versus* fraction of F-actin ($\frac{n_f}{n}$) for different signal gradients in a moving cell.. The number inside the graph shows the values of signal gradients ΔP_s .

already. However, the main result of the previous studies [155, 111], that the filament barbed ends are responsible for the cell movements, and that an optimum balancing between the filaments and the actin monomers is needed for maximum velocity, is in agreement with our observations also.

It has been seen for a particular ΔP_s , when the barbed end production is maximal, the respective cell shows a maximum drift velocity. But in case of shallowest signal gradient, the corresponding barbed end production is maximum and its drift velocity is allways smaller than the drift velocity of steeper signal gradient whose barbed end production is smaller than it (see fig.7.5(b)). The origin behind this apparent contradiction, which is as follows. When ΔP_s is maximal (the steepest signal gradient) the PIP3 accumulated cell perimeter is quite small compared to the whole cell perimeter. The neighboring part of this membrane perimeter is rich at stable F-actin network. As the dense F-actin network exist only along short membrane perimeter, the rest of the membrane can fluctuate often and cell moves forward. When signal gradient becomes relatively shallow, the membrane perimeter with accumulated PIP3 becomes broader. With this increased membrane perimeter the filament network also spread out. Due to this broader cluster of filaments, the membrane fluctuations gradually decrease. In other theoretical paper this kind of phenomena was described as barbed end induced suppression in membrane fluctuation [111]. So there must be a critical balancing between membrane fluctuation and the membrane perimeter covered by active PIP molecules. When stable actin filaments exist along a very short range of the membrane, the rest of the membrane can fluctuate

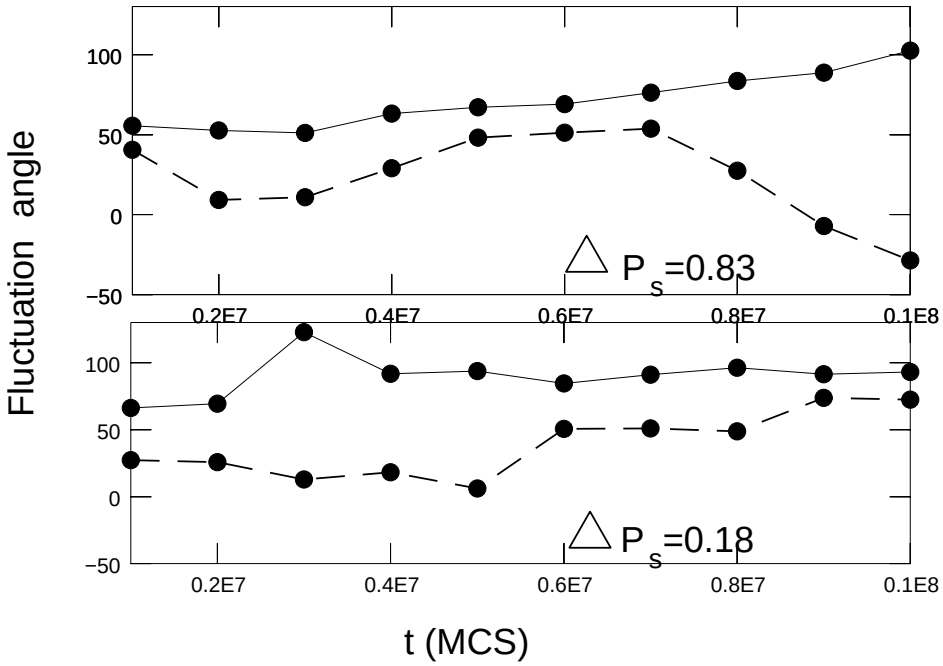

Figure 7.9: Plot of fluctuation angle as function of Monte Carlo time steps (MCS) for different signal gradients ΔP_s . The dashed line presents the fluctuation angle when corresponding drift velocity is maximal, and the solid line represents the same when the drift velocity is much smaller than the maximum value.

quite randomly. But large fluctuations of the membrane along any random direction is not very efficient to accelerate chemotactic motions. There is an optimum membrane perimeter under certain conditions (for the production of barbed ends) which yields a maximal drift velocity. When the signal gradient becomes shallower or steeper than this particular ΔP_s induces an optimal combination of PIP3 accumulated membrane section and of filament barbed ends which both together produces a maximal or minimal drift velocity, respectively. I will discuss in more details the effect of this PIP3 accumulated membrane perimeter in next section.

From the simulations, one can estimate the membrane fluctuation in terms of the angle between the center of mass of the cell and a particular membrane bead. If for two consecutive time steps the value of angle is the same, then this indicates that the cell does not rotate and which implies that the cell membrane is unable to fluctuate. Fig.7.9 is the corresponding graph, where we show the fluctuation angle of cell when the drift velocity is maximum and minimum for corresponding three different signal gradients.

From our simulation result (fig.7.8) we can notice one interesting fact that when signal gradient is very steep the total number of branching phenomena is less than the total

number of ATP-barbed-end polymerization. But in case of very shallow signal gradients, the branching happens more in number than the corresponding ATP-barbed-end polymerization. This phenomena can be explained as follows. Earlier we have discussed how the fluctuations of membrane is related to signal gradients. In case of filament formation there is always a competition between branching and barbed end polymerization near the PIP3 accumulated membrane. ATP barbed end polymerization is possible when an ATP-G-actin is added at the barbed end of a filament which happens always near the PIP3 activated membrane. On the other hand, branching also happens near the signal activated membrane from where it gets the necessary chemical signal for branching. But the difference is that branched filaments can be formed at any position of a mother filament. We have already seen that when signal gradient is very steep, the membrane fluctuations are large. But when signal gradient is very shallow, the membrane fluctuations are small. Actually this membrane fluctuation is favorable for ATP barbed end polymerization which takes place in between signal activated membrane and the filament tip. When membrane can not fluctuate, then very often the filament tip with ATP-F-actin get stuck at the membrane and new G-actin can not get enough space to be added on to the filament barbed end. In this situation branching has an advantage and branched filaments can increase more than end polymerization. This is our explanation why the shallow signal gradient produce more branched filament than steeper signal gradient . So from the above observation it has been found that the drift velocity is a result of a force induced by polymerization filament barbed ends near the plasma membrane [160, 161], The maximum force which is able to push the cell with highest efficiency is generated by an optimum balancing between the production of PIP3 activated membrane and the remaining part of the membrane.

7.6 Cell velocity and branching:

Nucleation activity of the Arp2/3 complex has been extensively explored [162, 163, 57, 164, 165, 166, 65, 29] and it is now well established that the branching activity is an essential step in the dendritic nucleation model. However, there is no direct evidence that branching activity of the Arp2/3 complex is required for the extension of the lamellipod. So we are interested to see the effect of branching on the cell's drift velocity. We studied the cell velocity at different signal gradient ΔP_s in the absence of branching activity. Fig.7.10 shows the results.

From the result it is noticeable that without branching activity the cell cytoskeleton network is able to produce a protrusive force to the membrane but less efficiently. This result indicates the important fact that without branching, the cell is still able to move in a chemotactic way although little bit slowly. This prediction contradicts the experimental findings [167] in that side binding activity by Arp2/3 complex is essential for protrusion. Although this paper has mentioned that the generation of nucleation sites for actin polymerization, which is necessary [168, 169], but which is not sufficient for

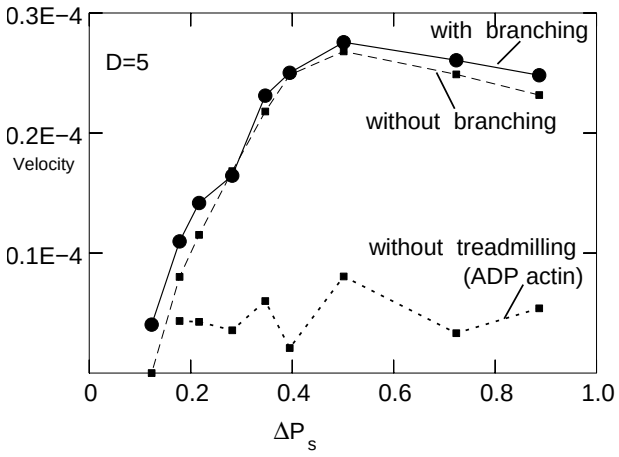

Figure 7.10: Plot of the drift velocity *versus* signal gradient ΔP_s for a mobile cell when P_s^{max} is constant. The solid line represents the velocity with branching, and the dashed line without branching. The dotted line is without treadmilling mechanism.

lamellipod extension, The latter observation agrees with our theoretical prediction. It is noticeable that when the signal gradient is less steep, then the difference between drift velocity with and without branching is larger than in the case of steep signal gradients. In section 7.5 we have discussed already that at shallower signal gradient the branching of filaments happens more than the corresponding barbed end polymerization. Also it has been discussed earlier that when PIP3 accumulated membrane perimeter is large, a big cluster of filament ends gets stuck at the activated membrane. As a result fluctuation of corresponding membrane periphery decreases. So actin monomers do not get enough space for barbed end polymerization and which leads to production of more branched filaments, because branched filament can be formed at any position of a mother filament. This implies that in the case of shallow gradients dendritic nucleation dominates over the barbed end polymerization. So the drift velocity for shallow signal gradients in branching inhibited cell becomes much slower compare to normal cell (branching present), on the other hand in case of steep signal gradients this difference is not significant. It is known that cell migration is initiated by plasma membrane protrusions, in the form of lamellipodia and filopodia. Another experimental result has demonstrated the dispensability of Arp2/3-complex for filopodia but not lamellipodia formation [170]. According to some biological suggestions [171], the force for protrusion could be generated locally at the leading edge, or by the cell body and transmitted to the leading edge by mechanical linkage or hydrostatic pressure. Experiments in amoeba clearly favor local force generation [172]. Mechanical linkage would require the cytoskeleton to be pushed into the leading edge. The evidence strongly favors generation of protrusive force directly at the leading edge. But by itself, the Arp2/3 complex weakly promotes the nucleation of new actin filaments [162]. So from all the biological suggestions and the experimental

results it is not possible to get a clear answer whether branching is indispensable for cell motility. Although undoubtedly it is clear that branching plays a very important role in cell motion. Our simulation result predicts that branching is more important when the gradient signal is shallow than when it is steep.

7.7 Cell velocity with saturating concentration of cAMP:

It is not very easy to experimentally construct the situation where a cell membrane is exposed to a saturating concentration of signals. In this case the theoretical model is very helpful to predict the nature of the response and the velocity of the cell. The pattern of PIP3 accumulation for a fixed section of the membrane with saturated concentration of signals differs from that seen previously [9]. In our studies the PIP3 accumulation on the membrane is inversely related to the membrane perimeter with signal activated receptors. But according to our simulation results, the PIP3 accumulates with almost maximum capacity on the signal-effected membrane of the cell. We measure the drift velocity of the chemotactic cell as a function of the PIP3 accumulated membrane perimeter (fig.7.11). When the membrane section, where PIP3 is accumulated, is very small (less than 10% of total membrane perimeter of cell) the production of ATP-barbed-end F-actin is small (see fig.7.11(c)). It is suggested by researchers that few barbed ends pushing the membrane are unable to overcome the membrane's resistance to movement and the cell moves at a very slow rate [173]. It should be noted here that in our model cell the velocity of cell depends on membrane fluctuation.
From fig.7.11(d) we can notice that the concentration of total F-actin is more than 50% of the total actin monomer concentration corresponding to lowest PIP3 accumulated membrane perimeter. So question comes naturally how F-actin comcentration become more than half of total actin concentration, when corresponding barbed end polymerization is very less ? According to our assumption, membrane bound PIP3 give signals to Arp2/3 associated branching phenomena and ATP associated barbed end polymerization only. Spontaneous nucleation and ADP associated polymerization does not get any signal from membrane synthesized PIP3. So this is the reason behind large filament concentration at lowest PIP3 accumulated membrane perimeter.

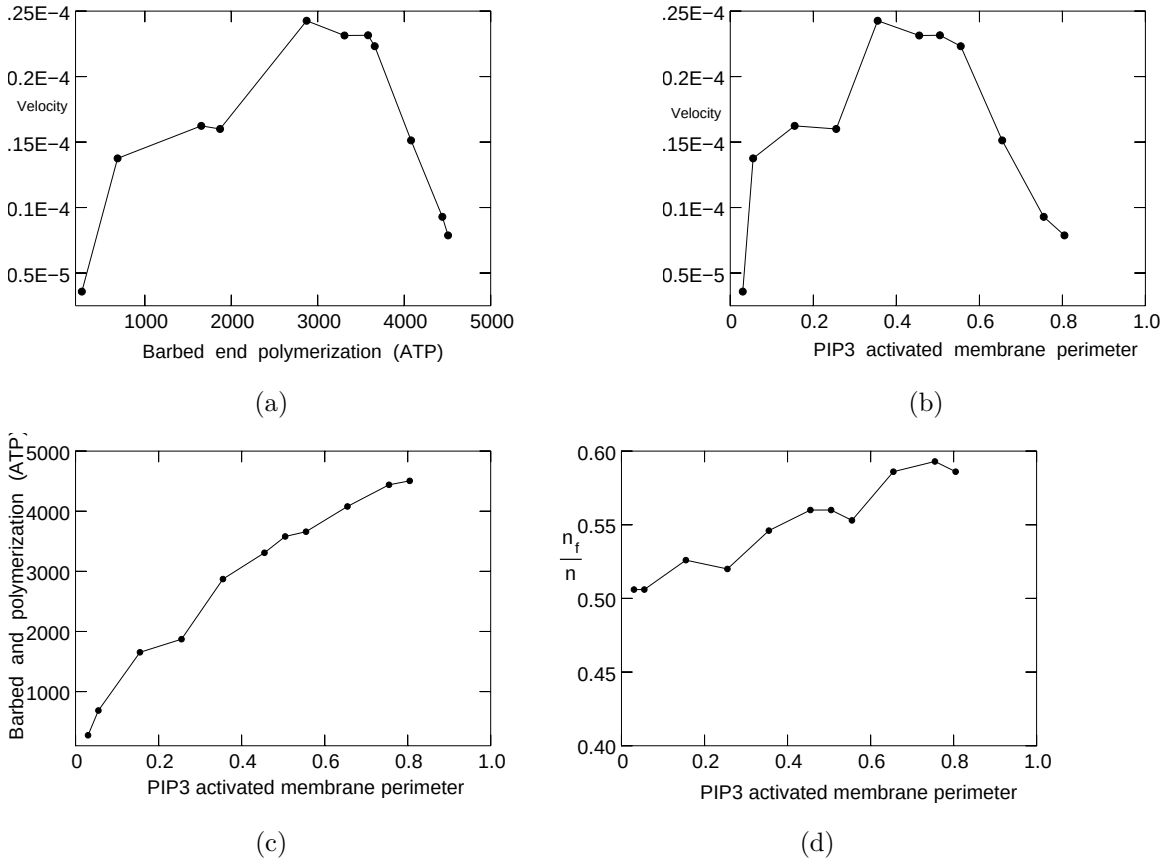

Figure 7.11: (a) Plot of drift velocity as function of the number of barbed end (ATP) polymerization for a moving cell exposed to a saturated dose of chemoattractant, while rest of the cell is not stimulated.
(b) Plot of drift velocity with respect to membrane perimeter covered by stimulant for a moving cell.
(c) Plot of number of filament barbed end (ATP) polymerization as function of membrane perimeter covered by stimulant for a moving cell.
(d) Plot of fraction of F-actin as function of membrane perimeter covered by stimulant for a moving cell.

These F-actins (other than ATP barbed end F-actin) contribute to the rise the concentration of total F-actin but this is not very effective for the protrusion of the leading edge of the cell. As the signal effected membrane area increases the production of ATP, barbed ends also increase and they produce more protrusive force on membrane, which leads to an increase of the drift velocity. When signal affected membrane perimeter reaches a certain optimum value the drift velocity becomes maximal. Further increment of signal along the membrane causes a decrease of the drift velocity. We have seen when the signal affected membrane perimeter become more than half of the total membrane perimeter, the drift velocity drops down very rapidly. Fig.7.11(a) and fig.7.11(b) shows the drift velocity as function of the area effected by signal and the ATP associated barbed end production, respectively. From fig.7.11(a) one can notice that even when barbed end production is maximal, the drift velocity is not maximal. Actually this result is similar to the observation seen in other theoretical model studies [155, 111]. Our simulation results imply that the maximum drift velocity is the result of optimum balancing between the barbed end filament, G-actin monomer and the PIP3 accumulated membrane perimeter. When the number of ATP barbed end filament and the activated membrane perimeter both are very small or very large it does not help the cell to move very rapidly towards the source. Although our result regrading drift velocity versus production of barbed end is similar to the other theoretical models [111, 155], the explanation and the origin of the maximum velocity is different. But both cases coincides in one point, namely that there exists an optimum concentration of barbed end of filament according to which the cell exhibits a maximum drift velocity.

7.8 Summary:

Directional sensing of a cell does not depend on cell polarization . But the protein network, which is responsible for directional sensing, requires signal from directional sensing response. According to our observation, cell's polarization ability depends more on the relative difference of PIP3 accumulation ${P_r}^{rel}$ of the cell than the absolute difference of PIP3 $\Delta \mathrm{P}_r$. Undoubtedly it should be noted that cell polarization also depends on actin dynamics.

This study is important, because we know there exists one signalling network responsible for directional sensing and it starts from extracellular signal and ends at the membrane bound PIP3. But it is believed that there is another regulatory network in between the PIP3 and the filament.

So studying the effect of varying gradient signal on these two networks (directional sensing and polarization) together will provide new insight regarding cell motility. Although our present model is quite trivial , but it can provide us important insight of polarized cell.

Our result agrees with previous model suggestion regarding the importance of barbed end filament production on cell motility and the existence of and optimum balancing in

between filament and the G-actin monomer for producing the maximum velocity. According to our observation the previous information does not give the complete picture of the parameters responsible for maximum cell velocity. There is another important parameter which also control the cell velocity and this parameter is the optimum balancing in between the membrane perimeter with accumulated PIP3 and filament barbed ends. Generally the filaments or more specifically the barbed end filaments are situated near the PIP3 accumulated membrane. When activated membrane perimeter is very small the barbed ends induced suppression in previously mentioned membrane is quite less and this leads the membrane fluctuation large extends. And when the case is reverse the barbed ends induced suppression produces restriction on membrane fluctuation. So for optimum membrane fluctuation, which can produces the maximum cell velocity is the result of a balancing.
Some other important prediction is also possible by our stochastic LEGI model. From the simulation results we can predict that branching dominates more over cell motion when the signal gradient is shallower than the steeper signal gradient.

8 Summary

The reported studies were an attempt to elucidate some aspects of two interacting regulatory protein networks which control the chemotactic locomotion of a cell. One of the networks, the directional sensing network, is responsible for the reception of external molecular signals to which the cell is exposed. This network also transforms the external signal into an internal amplified signal ('response'), which is used by the the second network, the polarization network, to tune and to guide the cellular motor which propells the cell using its polymerizing cytoskeleton.
Although many details about the molecular structure and interactions of regulatory proteins are known, such as Arp2/3 , cdc42, Ras, Rho, cofilin, gelsolin, profilin etc., their coordinated actions in a regulatory network are largely unknown.
Therefore, combining the LEGI model, proposed recently for the directional sensing network, with our polarization network model, which includes the particle-based polymerization of actin filaments, a stochastic cellular model has been developed and studied using Monte Carlo simulations in order to address various questions.

After a short introduction (chapter 1), the biological background of cell motility is described in chapter 2. In chapter 3 the numerical methods used during the studies are presented.

In chapter 4 the two dimensional stochastic lattice model for a cell comprising cell membrane and polymerizing actin filaments is described. The key features used are treadmilling actin filament and the regulatory protein Arp2/3 which induces side branching. The action of substrate adhesion, necessary for the cell's traction, is taken into account indirectly by immobilizing the actin filaments on the lattice. These ingredients form a minimal cell locomotion model from which static and dynamic properties can be calculated using Monte Carlo simulation. It is demonstrated that the antagonism of spontaneous nucleation and dendritic nucleation leads to the persistent random walk(PRW) of a motile cell. Spontaneous nucleation determines the direction of motion and dendritic nucleation enhances the speed of motion.

In chapter 5 a model for directional sensing mediated by a protein regulatory network is introduced. This network is responsible for transformation of weak external signal into a strongly amplified internal response. The control circuit of this regulatory network is based on local activation and global inhibition (LEGI) achieved by several interacting inhibitory and excitatory molecules, either diffusing in the cytoplasm or residing on the cell membrane. In this chapter, the case of a uniform distribution of signals, to

which the cell is exposed, is discussed. In response to such a signal, the cell is able to adapt which is considered as an inherent characteristic of motile cells. The analysis of simulation results reveals that the diffusion constant of the moving particles plays an important role in cell motility, since it influences the amplification and the adaptation of the response. Depending on the diffusion constant, the cell may adapt fully or partially, or even loses adaptation. Due to its complementary effect, it is very likely that there exist an optimal diffusion coefficient.

Chapter 6 deals with the situation when the cell (without filaments) is exposed to signals which are distributed with uniform gradient (infinite far source) or with non-uniform gradient (nearby point-like source). The efficiency in cell's directional sensing has been observed by changing the value of signal gradient. The ability of the cell to detect the direction of the external signal and to use the signalling network for amplification of chemical signal into internal response changes with change of signal's spatial localization along the membrane.
It was shown that, a) the amplification of the internal signal, i.e., the amount of activated PIP molecules (PIP3), and b) the spatial localization of PIP3 at a certain area of the membrane, which is crucial for directional guiding of the cell's movements, depend on the gradient,ΔP_s , and the maximum value,P_s^{max} , of the external signal. The response amplification, ΔP_r , exhibits a transition as function of the signal gradient ΔP_s . Furthermore, ΔP_r depends on the diffusion coefficients of the diffusing inhibitory and excitatory molecules.

Chapter 7 contains the results of my studies on the chemotaxis of the model cell. In this case, the model includes the second regulatory network, 'polarization', which is responsible for transmitting the internal response, PIP3, to the filamentous network of F-actins. This leads to directional sensing and polarization of the filaments. The cell's drift velocity has been studied as function of signal gradient, ΔP_s , depolymerization rate and the density of filaments. One of the most important results is that the maximum drift velocity is the result of an optimal balance between the density of filament ends near the leading edge of the membrane (barbed ends) and the localization of PIP3 at the membrane. The branching polymerization is the important driving force during chemotaxis. It has been observed that without branching, the movements of the cell become very slow.

A Dynamics of Membrane Movement

A.1 The Rouse model

The dynamics of lattice membrane is compaired to the polymer dynamics . The dynamics of polymer by the Brownian motion of the beads was first proposed by Rouse [174] and it was on the basis of the dynamics of dilute polymer solutions. In the Rouse model, the excluded volume interaction and the hydrodynamic interaction are disregarded. The polymers can be considered dynamically as independent from each other(free draining). The first attempt to study the free draining polymer model by mean of Monte Carlo simulations was performed by Verdier and Stockmayer [175]. For the normal random walk motion Verdiers results agree with prediction from Rouse-Zimm model. In their original work the relaxation time τ was defined as the time required for the smooth graph of r_n^2 (mean square end $-$to$-$end distance) against the number of Monte Carlo cycles to approach its final average value to within 1/e of the difference between the values of the original stretched-out configuration and the final equilibrium configuration. The equilibrium autocorelation function of the squared end $-$to$-$end distance was defined as

$$\phi_{rr}(t) = [< r_n^2(t_0) r_n^2(t_0 + t) - < r_n^2 >^2] / [< r_n^4 > - < r_n^2 >^2] \tag{A.1}$$

A general representation of the relaxation time τ is defined by

$$\tau_{rr} = \int_0^\infty dt \phi_{rr}(t) \tag{A.2}$$

This expression has been estimated by Monte Carlo simulations of the bead-rod model self interacting via a Lennard -Jones potential.
In Terms of number of beads , Rouse time or relaxation time τ is defined as

$$\tau_{rr} \propto n^(2\nu + 1) \tag{A.3}$$

Here n is representing the total number of beads.
And for ideal chain

$$\nu = 1/2 \& \tau_{rr} \propto n^2 \tag{A.4}$$

For our square lattice model we have studied the dynamics of membrane(without presence of any G-actin) and come to conclusion that in equilibrium state the lattice follows the Rouse Model.

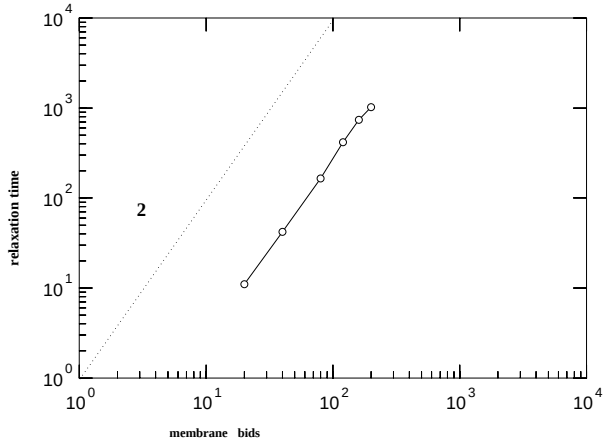

Figure A.1: Plot of relaxation time τ versus total number of membrane beads(N_m)

Relaxation time is proportional to square of number of membrane beads. Fig. A.1 is depicting the corresponding graph.
Due to free draining limit the diffusion coefficient D is inversely proportional to total no. of beads(N_m). So product of D and N_m is a constant and it gives a straight line when we plot it against N_m (see fig.A.2). And fig. A.3 is presenting the square of radius of gyration verses Monte Carlo time steps for different number of membrane beads.

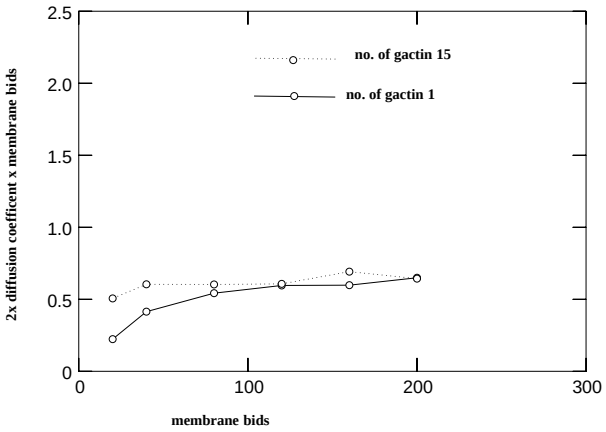

Figure A.2: Plot of product of diffusion coefficient and total number of beads versus total number of beads

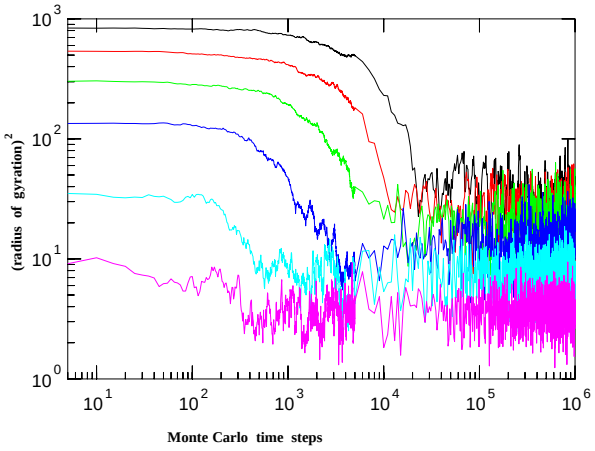

Figure A.3: Plot of square of radius of gyration verses Monte Carlo time steps for different number of membrane beads(from top to bottom different colours are representing different number of membrane respectively 200, 160, 120, 80, 60, 40 and 20)

B A proposal for probable candidates of LEGI mechanism in real cell

B.1 Introduction:

Cells are able to respond to chemoattractant gradient as shallow as a $2-5\%$ difference between front and rear of the cell by converting this shallow extracellular signal into a much steeper intracellular gradient [134] . The main important thing is to understand the mechanism by which cell can amplify a shallow extracellular gradient into a steep intracellular gradient and as a result the cell form a stable directional polarity. LEGI mechanism is one proposed model [9] for this conversion of shallow gradient to steep gradient. It is interresting to find out the probable candidates for the LEGI model in living cell. The most important part of the LEGI model is activity of binding sites of PI3K and PTEN. Because it is assumed that the binding site activation is the first place for asymmetry in chemotaxis.

B.2 Small GTPases:

Researchers are trying to find out the major components of chemotacting signal-transduction network downstream of the heterotrimeric G-proteins for past several years. The studies identified the involvement of small($20-35$ KDa) GTPases play important role at multiple stages of the chemotactic response [176]. Small GTPases behave as a monomeric entities. They function as a binary molecular switch, which interchange its state in between inactive GDP-bound and active GTP-bound. GEF(guanine-nucleotide-exchange factors) regulatory proteins catalyze the exchange of GTP for GDP and GAPs(GTPasa-activating proteins) regulatory proteins stimulate the slow intrinsic GTPase activity, promoting the formation of the inactive GDP-bound configuration. Fig. B.1 is representing a cartoon of GDP and GTP conversion. The 'Ras Superfamily' which is known name of the superfamily of small GTPases can be divided into five major subfamilies according to their sequence and functional similarities: Ras, Rho, Rab, Ran and Arf . The Ras and Rho subfamily are considered to be important components for signalling network responsible in the transduction of extra cellular stimuli [177] . Rho subfamily is further divided into three subgroups : Rho, Rac and Cdc42(Cell-division cycle 42).

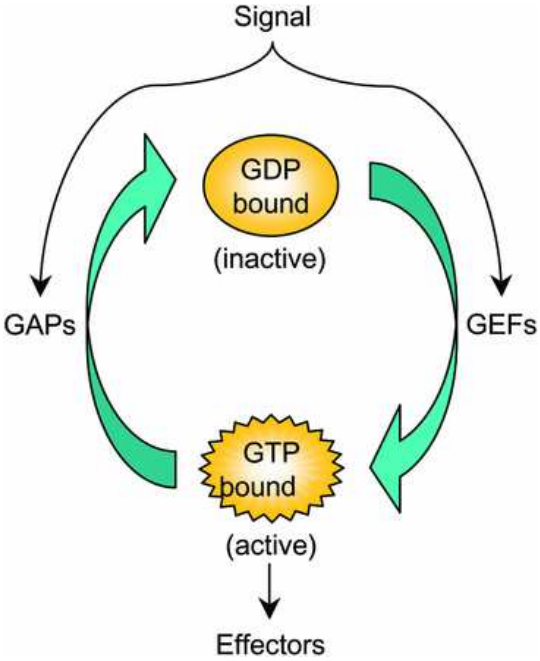

Figure B.1: The GTPase cycle [176].

B.3 Ras:

Research on Dictyostellium discoideum cell and mammalian leukocytes show that chemoattractant receptors and heterometric G protein subunit distribution is fairly uniform along the membrane [134]. G$\beta\gamma$ plays an important role to form the leading edge of cell. But it is found that G$\beta\gamma$ is not responsible for intracellular amplification of the chemoattractant gradient and localized activation of PI3K. And G-protein act persistently compair to PI3K whose activation is transient. So all the above observation indicate that a different component regulates the localization and activation of PI3K and this initial amplification step lies down-stream of G protein activation and up stream of generation of 3 phosphoinositide [178]. Ras has been assumed to be an activator of class I mammalian and Dictyostelium PI3K [179]. Ras protein is uniformly distributed along the cell membrane and Ras activation mainly takes place at the leading edge [127]. Experimental result shows in Dictyostelium Ras proteins : RasC and RasG rapidly and transiently activated in response to chemoattractant stimulation. This rapid activation and subsequent adaptation are consistent with cAMP-stimulated PI3K activity [127, 128]. Studies suggest that Ras activation occur independently to PI3K, but Ras-binding domain require for the activation of PI3K. So Ras might directly regulate PI3K activity [127, 128]. It has been found the directionality defect occur due to the inhibition of Ras signalling in Dictyostelium [127]. It is found that activated Ras bind to membrane bound PI3K

and form a complex which convert phosphatidyl inositol(4,5)biphosphate(PIP2) to phosphatidyl inositol(3,4,5)triphosphate(PIP3) [128, 77, 180]. All the experimental findings about Ras mechanism is similar to the PI3K binding site in LEGI model. PI3K binding site is evenly distributed around the membrane. Activation of BS_{PI3K} is independent of PI3K but the reverse is not true. So BS_{PI3K} may be a potential candidate for Ras.

B.4 Rho:

PTEN has been found to have an important role in the regulation of chemotaxis in Dictyostelium. Dictyostelium cell lack of PTEN shows weaker chemotaxis [11, 181]. Number of studies suggested that regulation of PTEN is very complex and involves multiple phosphorylation events, and in addition lipid and protein interactions that helps in PTEN activity and localization [182, 183]. Recently it is found out that Rho GTPases regulate the localization and activation of PTEN in chemotactic cell [184]. The first investigation which suggested that Rho GTPasea are responsible for regulation of PTEN , showed that the Cdc42 signalling is required at the leading edge for the exclusion of PTEN [185]. Alternatively other studies suggest that PTEN is regulated by RhoA, and its downstream effector ROCK (p160-Rho-associated coil-containing protein kinase) acts as a link in between two [176]. In a chemoattractant- induced cell binding of RhoGEF Lsc/p115 to Gα12/13 activate RhoA [176]. It is assumed that the mechanism which activate RhoA , also activate ROCK and after then ROCK, PTEN and activated RhoA form a complex in vivo. Experiments show inhibition of ROCK affect nutrophil polarity and motility [186, 187, 188]. Fig.B.2 representing a model for directional sensing [176]. So all the experimental evidences above strongly suggest that the Rho likely plays the role of PTEN binding site. And fig. B.3 is representing the present LEGI model.

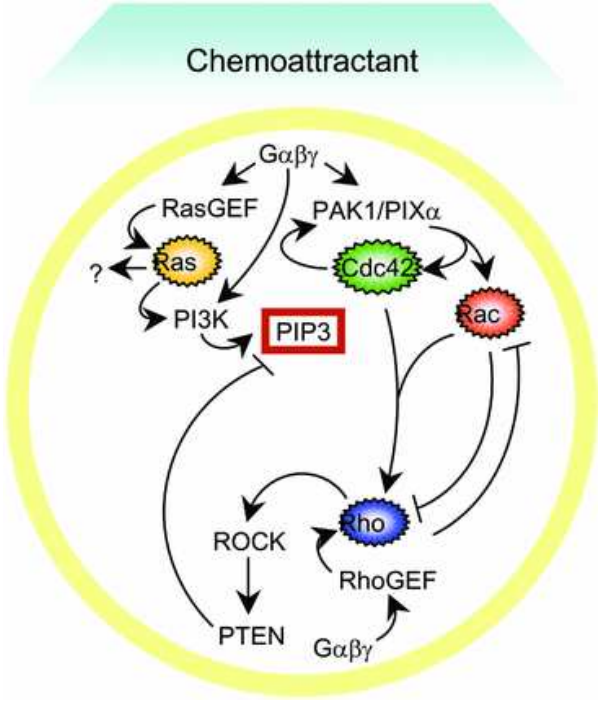

Figure B.2: Model of directional sensing [176].

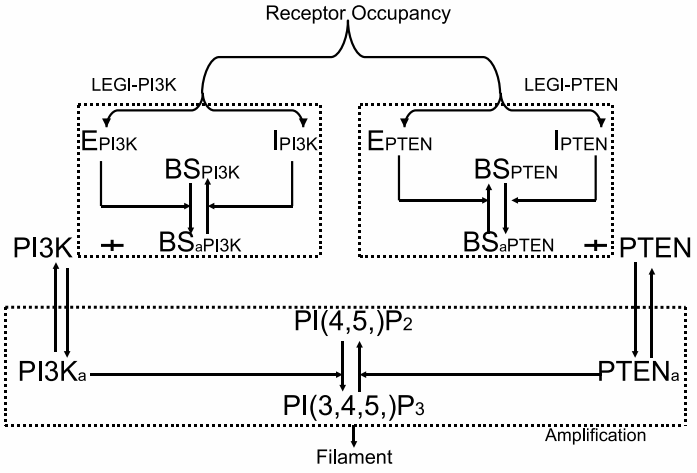

Figure B.3: LEGI model.

C Short definition

$\mathbf{BS}^a_{PI3K}$: Active binding site of PI3K.

$\mathbf{BS}_{PI3K}$: Binding site of PI3K is immobile and is located at the membrane. Binding site of PI3K become active by the active Exciter of PI3K at the same position of membrane. And The conversion of active BS_{PI3K} to inactive BS_{PI3K} happens when a I^a_{PI3K} binds with it.

$\mathbf{BS}^a_{PTEN}$: Active binding site of PTEN.

$\mathbf{BS}_{PTEN}$: Immobile binding site of PTEN is situated at the membrane . Active PTEN inhibitor binds with inactive binding site of PTEN and the binding site become active. And the E^a_{PTEN} converts the active binding site to inactive state.

$\mathbf{E}^a_{PI3K}$: Active exciter of PI3K.

$\mathbf{E}_{PI3K}$: Exciter of PI3K resides on the membrane and become activated by signal activated receptor.

$\mathbf{E}_{PTEN}$: Exciter of PTEN also situated on the membrane and become activated by signal activated receptor.

$\mathbf{E}^a_{PTEN}$: Active exciter of PTEN.

$\mathbf{I}_{PI3K}$: Inhibitor of PI3K randomly diffuses throughout the cytosol of the cell . and they become active by binding with signal activated receptor.

$\mathbf{I}^a_{PI3K}$: Active inhibitor of PI3K.

$\mathbf{I}_{PTEN}$: It is inhibitor of PTEN which diffuse randomly inside the cell and reaches active state form inactive state by binding with signal activated receptor.

$\mathbf{I}^a_{PTEN}$: Active inhibitor of PTEN.

N_m : This represents the total number of membrane beads and this number is 200. The middle point of nm (=100) represents the closest point from the source to the cell and the furthest points are represented by membrane bead 1 and 200.

PIP2 : Phosphatidylinositol (3,4)-bisphosphate (PtdIns(3,4)P2) is an important second messenger of cell membranes.

$\Delta PIP3$: The difference between the highest and the lowest concentration of PIP3 at the front and at the back of the cell respectively and it is also represented as $PIP3^{max} -$

$PIP3^{min}$.

ΔP_s : The difference between the highest and the lowest signal concentration of a gradient signal and is also represented as $P_s^{max} - P_s^{min}$.

PIP3 : Phosphatidylinositol (3,4,5)-trisphosphate (PtdIns(3,4,5)P3) commonly abbreviated to PIP3. PIP3 is generated at plasma membrane by activation of PI3K.

$\langle PIP3\rangle_0$: The average concentration of response (PIP3(nm)) with respect to time (Monte Carlo steps) in case of a uniform homogeneous signal exposed cell is called the global amplified PIP3 or $\langle PIP3\rangle_0$.

$\langle PIP3\rangle$: The average concentration of response (PIP3(nm)) with respect to time (Monte Carlo steps) in case of gradient signal exposed cell is called response intensity.

PIP3^{max}: The front part of the cell contains highest response concentration and this is denoted as PIP3^{max}. Along the membrane beads, the middle number bead (=100) is presented as the most front part of the cell and corresponding response concentration is considered as the maximum responce concentration.

PIP3^{min}: The lowest response concentration at the most rear part of the cell is represented as PIP3^{min}. Along the membrane beads, two extreme membrane beads (=1, 200) are presented as the most rear part of the cell.

$\mathbf{P}_s^{max}$: Among the membrane beads the the closest point from the source to cell is considered as the most front part of the cell and the signal concentration to the corresponding bead is considered as the highest signal concentration P_s^{max}. The position of this highest signal concentration is in the middle (membrane bead number=100) of the total signal gradient and for this reason it is also called the **signal gradient midpoint**.

$\mathbf{P}_s^{min}$: The extreme opposite point of most front part of the cell is considered the most back part of the cell. Along the membrane beads, two membrane beads (=1, 200) are called the most back part of the cell. The signal concentration to the corresponding membrane beads are represented as P_s^{min}.

PTEN : A major tumor-suppressor gene and help to dephosphorylation of $PI(3,4,5)P_3$ to $PI(4,5)P_2$.

$\langle P_s\rangle$: The average accumulation of signal concentration $P_s(nm)$ with respect to time (Monte Carlo steps) is called the signal intensity.

Receptor occupancy : The fraction of activated receptors in a cluster of receptors which locates in a membrane bead .

Signal gradient midpoint : Midpoint concentration is the highest concentration of a gradient signal and it is situated at the middle of the whole gradient signal. It is formulated as P_s^{max}.

Bibliography

[1] B.Alberts, D. Bray, J. Lewis, M. Raff, K. Roberts, , and J. Watson. Molecular biology of the cell. *Garland Publishing. New York.*, 2001.

[2] D.Bray. Cell movements: From molecules to motility. *(Garland, New York)*, 2001.

[3] H. Lodish, A. Berk, S. L. Zipursky, P. Matsudaira, D. Baltimore, and J. Darnell. Molecular cell biology. *(W H Freeman Co)*, 1995).

[4] T.P. Stossel. On the crawling of animal cells. *Science.*, 260:1086–1094, 1993.

[5] T.Stossel. The machinery of cell crawling. *Sci Am.*, 271:54–63, 1994.

[6] J.Condeelis. Are all pseudopods created equal? *Cell Motil. Cytoskeleton.*, 22:1–6, 1992.

[7] J.Condeelis. Life at the leading edge: the formation of cell protrusions. *Annu Rev Cell Biol.*, 9:411–444, 1993.

[8] L. P.Cramer, T. J.Mitchison, and J. A. Theriot. Actin-dependent motile forces and cell motility. *Curr. Opin. Cell Biol.*, 6:82–86, 1994.

[9] L.Ma, L.Yang, P.N.Devreotes, and P.A.Iglesias. Two complementary, local excitation, global inhibition mechanisms acting in parallel can explain the chemoattractant-induced regulation of pi(3,4,5)p3 response in dictyostelium cells. *Biophys J.*, 86:3764–3774, 2004.

[10] J. Adler and W.W. Tso. Decision-making in bacteria: Chemotactic response of escherichia coli to conflicting stimuli. *Science.*, 184:1292–1294, 1974.

[11] P.Devreotes and C. Janetopoulos. Eukaryotic chemotaxis: distinctions between directional sensing and polarization. *J. Biol. Chem*, 278:20445–20448, 2003.

[12] H.Meinhardt. Orientation of chemotactic cells and growth cones: models and mechanisms. *J. Cell Sci.*, 112:2867–2874, 1999.

[13] R.Sambeth and A. Baumgaertner. Autocatalytic polymerization generates persistent random walk of crawling cells. *Phys. Rev. Lett.*, 86:5196–5199, 2001.

[14] R.Sambeth and A. Baumgaertner. Locomotion of a two dimensional keratocyte model. *J.Biol.Systems.*, 9:201–219, 2001.

[15] U. Alon, L. Camarena, M. G. Surette, B. A. Arcas, Y. Liu, S. Leibler, and J. B. Stock. Response regulator output in bacterial chemotaxis. *EMBO J.*, 17:4238–4248, 1998.

[16] D.Bray. Signaling complexes: biophysical constraints on intracellular communication. *Ann.Rev.Biophys.Biolmol.Struct.*, 27:59–75, 1998.

[17] L.H.Hartwell, J. J.Hopfield, S. Leibler, and A. W. Murray. From molecular to modular biology. *Nature.*, 402:C47–c52, 1999.

[18] RA. Firtel and CY.Chung. The molecular genetics of chemotaxis: sensing and responding to chemoattractant gradients. *Bioessays.*, 22:603–615, 2000.

[19] O.D.Weiner. Regulation of cell polarity during eukaryotic chemotaxis: the chemotactic compass. *Curr.Opin.Cell Biol.*, 14:196–202, 2002.

[20] U.Alon, MG. Surette, N.Barkai, and S. Leibler. Robustness in bacterial chemotaxis. *Nature.*, 397:168–171, 1999.

[21] S.J. Singer and A.Kupfer. The directed migration of eukaryotic cells. *Ann. Rev. Cell Biol.*, 2:337–365, 1986.

[22] JV. Small, K. Rottner, I. Kaverina, and KI. Anderson. Assembling an actin cytoskeleton for cell attachment and movement. *Biochim Biophys Acta.*, 1404:271–81, 1998.

[23] T. M. Svitkina, A. B. Verkhovsky, K. M. McQuade, and G. G. Borisy. Analysis of the actin-myosin ii system in fish epidermal keratocytes: Mechanism of cell body translocation. *J. Cell Biol.*, 139:397–415, 1997.

[24] J.Reiter. Monte carlo study of diffusion of an ideal ring polymer in a network of obstacles on a cubic and a square lattice. *J. Chem. Phys.*, 95:1290–1294, 1991.

[25] SM. Rafelski and JA. Theriot. Crawling toward a unified model of cell mobility: spatial and temporal regulation of actin dynamics. *Annu Rev Biochem.*, 73:209–239, 2004.

[26] H. E. Huxley. Electron microscope studies on the structure of natural and synthetic protein filaments from striated muscle. *J. Mol. Biol.*, 7:281–308, 1963.

[27] MO. Steinmetz, D. Stoffler, A. Hoenger, A. Bremer, and U. Aebi. Actin: from cell biology to atomic detail. *J Struct Biol.*, 119:295–320, 1997.

[28] Audesirk, Teresa, and Gerald. *Biology(Prentice Hall)*, 1999.

[29] L. Blanchoin, T.D. Pollard, and R.D. Mullins. Interactions of adf/cofilin, arp2/3 complex, capping protein and profilin in remodeling of branched actin filament networks. *Curr Biol .*, 10:1273–1282, 2000.

[30] M.F.Carlier. Control of actin dynamics. *Curr. Opin. Cell Biol.*, 10:45–51, 1998.

[31] P. W. Atkins. Physical chemistry. *Oxford University Press*, 1994.

[32] F. Oosawa and S. Asakura. Thermodynamics of the polymerization of protein. *Academic Press*, 1975.

[33] D.Didry, M.-F. Carlier, and D.Pantaloni. Synergy between actin depolymerizing factor/cofilin and profilin in increasing actin filament turnover. *J. Biol. Chem.*, 273:25602–25611, 1998.

[34] T.D. Pollard. Rate constants for the reactions of atp- and adp-actin with the ends of actin filaments. *J.Cell.Biol.*, 103:2747–54, 1986.

[35] A.Wegner. Head to tail polymerization of actin. *J. Mol. Biol.*, 108:139–150, 1976.

[36] Y.L. Wang. Exchange of actin subunits at the leading edge of living fibroblasts: Possible role of treadmilling. *J. Cell Biol.*, 101:597–602, 1985.

[37] J. V. Small, M. Herzog, and K. Anderson. Actin filament organization in the fish keratocyte lamellipodium. *J. Cell Biol.*, 129:1275–1286, 1995.

[38] J.A. Theriot and T.J. Mitchison. Actin microfilament dynamics in locomoting cells. *Nature*, 352:126–131, 1991.

[39] M.F. Carlier, C. Jean, K. J. Rieger, M. Lenfant, and D. Pantaloni. Modulation of the interaction between g-actin and thymosin beta 4 by the atp/adp ratio: possible implication in the regulation of actin dynamics. *Proc. Natl. Acad. Sci.*, 90:5034–5038, 1993.

[40] A. Weber, V. T. Nachmias, C. R. Pennise, M. Pring, and D. Safer. Interaction of thymosin beta 4 with muscle and platelet actin: implications for actin sequestration in resting platelets. *Biochemistry*, 31:6179–6185, 1992.

[41] E. Hannappel and F. Wartenberg. Actin-sequestering ability of thymosin beta 4, thymosin beta 4 fragments, and thymosin beta 4-like peptides as assessed by the dnase i inhibition assay. *Biol. Chem. Hoppe-Seyler.*, 374:117–122, 1993.

[42] D. Heintz, A. Reichert, M. Mihelic, W. Voelter, and H. Faulstich. Use of bimanyl actin derivative (tmb-actin) for studying complexation of beta -thymosins. inhibition of actin polymerization by thymosin beta. *FEBS Lett.*, 329:9–12, 1993.

[43] F.X. Yu, S.C. Lin, M. Morrison-Bogorad, M. A. L. Atkinson, and H. L. Yin. Thymosin beta 10 and thymosin beta 4 are both actin monomer sequestering proteins. *J. Biol. Chem.*, 268:502–509, 1993.

[44] C. Jean, K. Rieger, L. Blanchoin, M.F. Carlier, M. Lenfant, and D. Pantaloni. Interaction of g-actin with thymosin beta 4 and its variants thymosin beta 9 and thymosin beta 9met. *J. Muscle Res. Cell Motil.*, 15:278–286, 1994.

[45] T. Huff, D. Zerzawy, and E. Hannappel. Interactions of beta-thymosins, thymosin beta 4-sulfoxide, and n-terminally truncated thymosin beta 4 with actin studied by equilibrium centrifugation, chemical cross-linking and viscometry. *Eur. J. Biochem.*, 230:650–657, 1995.

[46] A. Reichert, D. Heintz, W. Voelter, M. Mihelic, and H. Faulstich. Polymerization of actin from the thymosin beta 4 complex initiated by the addition of actin nuclei, nuclei stabilizing agents or myosin s1. *FEBS Lett.*, 347:247–250, 1994.

[47] P.J. Goldschmidt-Clermont, M. I. Furman, D. Safer D. Wachsstock, V. T. Nachmias, and T. D. Pollard. The control of actin nucleotide exchange by thymosin beta 4 and profilin: a potential regulatory mechanism for actin polymerization in cells. *Mol. Biol. Cell*, 3:1015–1024, 1992.

[48] V. K. Vinson, E. M. De La Cruz, H. N. Higgs, and T. D. Pollard. Interactions of acanthamoeba profilin with actin and nucleotides bound to actin. *Biochemistry*, 37:10871–10880, 1998.

[49] M.F. Carlier, D. Didry, I. Erk, J. Lepault, M. L. Van Troys, J. Vandekerckhove, I. Perelroizen, H. Yin, Y. Doi, and D. Pantaloni. Tbeta 4 is not a simple g-actin sequestering protein and interacts with f-actin at high concentrations. *J. Biol. Chem.*, 271:9231–9239, 1996.

[50] A. Reichert, D. Heintz, H. Echner, W. Voelter, and H. Faulstich. The ternary complex of dnase i, actin, and thymosin beta 4. *FEBS Lett.*, 387:132–136, 1996.

[51] E. Ballweber, E. Hannappel, T. Huff, and H. G. Mannherz. Mapping the binding site of thymosin beta 4 on actin by competition with g-actin binding proteins indicates negative co-operativity between binding sites located on opposite subdomains of actin. *Biochem. J.*, 327:787–793, 1997.

[52] D. Safer, T. R. Sosnick, and M. Elzinga. Thymosin beta 4 binds actin in an extended conformation and contacts both the barbed and pointed ends. *Biochemistry*, 36:5806–5816, 1997.

[53] M. De La Cruz Enrique, E. Michael Ostap, Rodney A. Brundage, K. S. Reddy, H. Lee Sweeney, and D. Safer. Thymosin-beta 4 changes the conformation and dynamics of actin monomers. *Biophys. J.*, 78:2516–2527, 2000.

[54] M.Fechheimer and SH. Zigmond. Focusing on unpolymerized actin. *J. Cell Biol.*, 123:173–181, 1993.

[55] R. Hopmann and K. G. Mille. A balance of capping protein and profilin functions is required to regulate actin polymerization in drosophila bristle. *Mol. Biol. Cell.*, 14:118–128, 2003.

[56] L.M.Machesky, S. J.Atkinson, C. Ampe, J. Vandekerckhove, and T. D. Pollard. Purification of a cortical complex containing two unconventional actins from acanthamoeba by affinity chromatography on profilin-agarose. *J. Cell Biol.*, 127:107–115, 1994.

[57] D. Pantaloni, R. Boujemaa, D. Didry, P. Gounon, and M.F. Carlier. The arp2/3 complex branches filament barbed ends: functional antagonism with capping proteins. *Nat. Cell Biol.*, 2:385–391, 2000.

[58] M.J.Dayel, E.A. Holleran, and R.D.Mullins. Arp2/3 complex requires hydrolyzable atp for nucleation of new actin filaments. *Proc. Natl Acad. Sci. USA*, 98:14871–14876, 2001.

[59] C.Le Clainche, D. Didry, M. F. Carlier, and D. Pantaloni. Activation of arp2/3 complex by wiskott2̆013aldrich syndrome protein is linked to enhanced binding of atp to arp2. *J. Biol. Chem.*, 276:46689–46692, 2001.

[60] E. D.Goley, S. E. Rodenbusch, A. C.Martin, and M. D.Welch. Critical conformational changes in the arp2/3 complex are induced by nucleotide and nucleation promoting factor. *Mol. Cell.*, 16:269–279, 2004.

[61] A. C. Martin, X. Xu, I. Rouiller, M. Kaksonen, Y. Sun, L. Belmont, N. Volkmann, D. Hanein, M. Welch, and D. G. Drubin. Effects of arp2 and arp3 nucleotide-binding pocket mutations on arp2/3 complex function. *J. Cell Biol.*, 168:315–328, 2005.

[62] M. J.Dayel and R. D.Mullins. Activation of arp2/3 complex: addition of the first subunit of the new filament by a wasp protein triggers rapid atp hydrolysis on arp2. *PLoS Biol.*, 2:476–485, 2004.

[63] A. C.Martin, M. D.Welch, and D. G. Drubin. Arp2/3 atp hydrolysis-catalyzed branch dissociation is critical for endocytic force generation. *Nature Cell Biol.*, 8:826–833, 2006.

[64] C.Le Clainche, D. Pantaloni, and M. F. Carlier. Atp hydrolysis on actin-related protein 2/3 complex causes debranching of dendritic actin arrays. *Proc. Natl. Acad. Sci.USA*, 100:6337–6342, 2003.

[65] K.J. Amann and T.D. Pollard. The arp2/3 complex nucleates actin filament branches from the side of pre-existing filaments. *Nature Cell Biol.*, 3:306–310, 2001.

[66] K.J. Amann and T.D. Pollard. Direct real-time observation of actin filament branching mediated by arp2/3 complex using total internal reflection fluorescence microscopy. *Proc. Natl. Acad. Sci. USA*, 98:15009–15013, 2001.

[67] I.Fujiwara, S. Suetsugu, S. Uemura, T. Takenawa, and S.Ishiwata. Visualization and force measurement of branching by arp2/3 complex and n-wasp in actin filament. *Biochem. Biophys. Res. Commun.*, 293:1550–1555, 2002.

[68] I.Ichetovkin, W.Grant, and J.Condeelis. Cofilin produces newly polymerized actin filaments that are preferred for dendritic nucleation by the arp2/3 complex. *Curr. Biol.*, 12:79–84, 2002.

[69] L. Bankir, M. Ahloulay, P. N. Devreotes, and C. A. Parent x. Extracellular camp inhibits proximal reabsorption: are plasma membrane camp receptors involved? *Am. J. Physiol. Renal. Physiol.*, 282:376–392, 2002.

[70] G.Servant, O. D.Weiner, E. R. Neptune, J. W.Sedat, and H. R.Bourne. Dynamics of a chemoattractant receptor in living neutrophils during chemotaxis. *Mol. Biol. Cell.*, 10:1163 –1178, 1999.

[71] Z.Xiao, N.Zhang, D. B.Murphy, and P. N.Devreotes. Dynamic distribution of chemoattractant receptors in living cells during chemotaxis and persistent stimulation. *J. Cell Biol.*, 139:365 –374, 1997.

[72] T.Jin, N.Zhang, Y. Long, C. A.Parent, and P. N.Devreotes. Localization of the g protein betagamma complex in living cells during chemotaxis. *Science*, 287:1034 –1036, 2000.

[73] S. Cockcroft. Biology of phosphoinositides. *(Oxford UP)*, 2000.

[74] S. Funamotoa, K. Milana, R. Meilia, and R. A. Firtela. Role of phosphatidylinositol 3' kinase and a downstream pleckstrin homology domain containing protein in controlling chemotaxis in dictyostelium. *J. Cell Biol.*, 153:795–810, 2001.

[75] CA.Parent, BJ. Blacklock, WM.Froehlich, DB. Murphy, and PN.Devreotes. G protein signaling events are activated at the leading edge of chemotactic cells. *Cell*, 95:81–91, 1998.

[76] JM.Haugh, F. Codazzi, M.Teruel, and T. Meyer. Spatial sensing in fibroblasts mediated by 3' phosphoinositides. *J. Cell Biol.*, 151:1269–1280, 2000.

[77] Y. E. Huang, M. Iijima1, C. A. Parent, S. Funamoto, R. A. Firtel, and P. Devreotes. Receptor mediated regulation of pi3ks confines pi(3,4,5)p3 to the leading edge of chemotaxing cells. *Mol. Biol. Cell*, 14:1913–1322, 2003.

[78] M. Iijima and P. Devreotes. Tumor suppressor pten mediates sensing of chemoattractant gradients. *Cell*, 109:599–610, 2002.

[79] R.Meili, C. Ellsworth, S.Lee, TB.Reddy, H. Ma, and RA.Firtel. Chemoattractant-mediated transient activation and membrane localization of akt/pkb is required for efficient chemotaxis to camp in dictyostelium. *EMBO J.*, 15:2092–2105, 1999.

[80] R.Insall, A. Kuspa, P. J. Lilly, G. Shaulsky, L. R. Levin, W. F. Loomis, and P. Devreotes. Crac, a cytosolic protein containing a pleckstrin homology domain, is required for receptor and g protein-mediated activation of adenylyl cyclase in dictyostelium. *J. Cell Biol.*, 126:1537–1545, 1994.

[81] P.J.Lilly and P. N.Devreotes. Identification of crac, a cytosolic regulator required for guanine nucleotide stimulation of adenylyl cyclase in dictyostelium. *J. Biol. Chem.*, 269:14123–14129, 1994.

[82] P. J.Lilly and P. N.Devreotes. Chemoattractant and gtpgammas-mediated stimulation of adenylyl cyclase in dictyostelium requires translocation of crac to membranes. *J. Cell Biol.*, 129:1659–1665, 1995.

[83] B.Wang, G. Shaulsky, and A.Kuspa. Multiple developmental roles for crac, a cytosolic regulator of adenylyl cyclase. *Dev. Biol.*, 208:1–13, 1999.

[84] G.Servant, O. D.Weiner, P. Herzmark, T. Balla, J. W. Sedat, and H. R.Bourne. Polarization of chemoattractant receptor signaling during neutrophil chemotaxis. *Science*, 287:1037–1040, 2000.

[85] M. Dinauer, TL. Steck, and P. Devreotes. Cyclic 3', 5'-amp relay in dictyostelium discoideum. iv. recovery of the camp signaling response after adaptation to camp. *J. Cell Biol.*, 86:545–553, 2001.

[86] A. R. Asthagiri and D. A. Lauffenburger. A computational study of feedback effects on signal dynamics in a mitogen-activated protein kinase (mapk) pathway model. *Biotechnol. Prog.*, 17:227 –239, 2001.

[87] N. Barkai and S. Leibler. Signaling pathways controlling cell polarity and. chemotaxis. *Nature*, 387:913–917, 1997.

[88] D. Koshland, A. Goldbeter, and J. Stock. Amplification and adaptation in regulatory and sensory systems. *Science*, 217:220–225, 1982.

[89] R. A. Normann and I. Perlman. Background and bleaching adaptation in luminosity type horizontal cells in the isolated turtle retina. *J. Physiol.*, 421:321–341, 1990.

[90] SH. Zigmond and SJ. Sullivan. Sensory adaptation of leukocytes to chemotactic peptides. *J. Cell Biol.*, 82:517–527, 1979.

[91] J. Lee, A. Ishihara, J. A. Theriot, and K. Jacobson. Principles of locomotion for simple-shaped cells. *Nature*, 362:167–171, 1993.

[92] JM. Lackie and J. Dow. The dictionary of cell molecular biology. *(Academic Press, London)*, 1999.

[93] F.Richelme, AM.Benoliel, and P. Bongrand. The leukocyte actin cytoskeleton. *Bull. Inst. Pasteur*, 94:257–284, 1996.

[94] O. D. Weiner, G. Servant, M. D. Welch, T. J. Mitchison, J. W. Sedat, and H. R. Bourne. Spatial control of actin polymerization during neutrophil chemotaxis. *Nature Cell Biol.*, 1:75–81, 1999.

[95] L. Grebecka, P.Pomorski, A.Grebecka, and L. Lopatowska. Adhesion-dependent f-actin pattern in amoeba proteus as a. common feature of amoebae and the metazoan motile cells. *Cell Biol. Int.*, 21:565–573, 1997.

[96] L. Grebecka, P.Pomorski, and L. Lopatowska. Adhesion to the substratum improves the motility ofamoeba proteus in the absence of a cell nucleus. *Protoplasma.*, 197:174–181, 1997.

[97] KJ.Tomchik and PN. Devreotes. Adenosine 3',5'-monophosphate waves in dictyostelium discoideum: a demonstration by isotope dilution–fluorography. *Science*, 212:443–446, 1981.

[98] Spatial control of actin filament assembly: lessons from Listeria. Mc. beckerle. *Cell*, 95:741–748, 1998.

[99] S. Dramsi and P. Cossart. Intracellular pathogens and the actin cytoskeleton. *Annu. Rev. Cell Dev. Biol.*, 14:137–166, 1998.

[100] A.van. Oudenaarden and J.A. Theriot. Cooperative symmetrie-breaking by actin polymerization in a model for cell motility. *Nature Cell Biol.*, 1:493–499, 1999.

[101] H. C. Berg. E. coli in motion. *Springer-Verlag, NY*, 2003.

[102] Z. Brzezniak and T. Zastawniak. Basic stochastic processes: A course through exercises. *Springer-Verlag*, 1998.

[103] W. S. Brainerd, C. H. Goldberg, and J. C. Adams. Programmer's guide to fortran 90. *Springer*, 1995.

[104] W. E. Mayo and M. Cwiakala. Schaum's outline of theory and problems of programming with fortran 77. *McGraw-Hill*, 1995.

[105] N. Metropolis, A. W. Rosenbluth, M. N. Rosenbluth, and A. H. Teller. Equation of state calculations by fast computing machines. *J. Chem. Phys.*, 21:1087–1092, 1953.

[106] K. Binder. Applications of monte carlo methods to statistical physics. *Rep. Prog. Phys.*, 60:487–559, 1997.

[107] K. P. N. Murthy. Monte carlo: Basics. *Indian Society for Radiation Physics*, 2001.

[108] A.Baumgaertner. Simulation of polymer models in applications of the monte carlo method in statistical physics. *Springer*, 1984.

[109] K. Binder and W. Paul. Monte carlo simulations of polymer dynamics: Recent advances. *J. Polym.Sci.*, 35:1–31, 1997.

[110] H. P. Deutsch and K. Binder. Interdiffusion and self-diffusion in polymer mixtures: A monte carlo study. *J. Chem. Phys.*, 94,:2294–2304, 1990.

[111] S.V.M.Satyanarayana and A.Baumgaertner. Shape and motility of a model cell : a computational study. *J.Chem.Phys.*, 121:4255–4265, 2004.

[112] F.Oosawa. Physical chemistry of actin: Past, present and future. *Biophys. Chem.*, 47:101–111, 1993.

[113] C. Egile, I. Rouiller, XP. Xu, N. Volkmann, R. Li, and D. Hanein. Mechanism of filament nucleation and branch stability revealed by the structure of the arp2/3 complex at actin branch junctions. *PLoS Biol.*, 3:1902–1909, 2005.

[114] B.Alberts. Essential cell biology. *(New York: Garland)*, 1998.

[115] D. J.Webb, J. T.Parsons, and A. F.Horwitz. Adhesion assembly, disassembly and turnover in migrating cells - over and over and over again. *Nat. Cell Biol.*, 4:97–100, 2002.

[116] K. A.DeMali and K.Burridge. Coupling membrane protrusion and cell adhesion. *J. Cell Sci.*, 116:2389–2397, 2003.

[117] D. A.Lauffenburger and A. F. Horwitz. Cell migration: a physically integrated molecular process. *Cell*, 84:359–369, 1996.

[118] D. Shreiber, V.Barocas, and R. Tranquillo. Temporal variations in cell migration and traction during fibroblast-mediated gel compaction. *Biophys J.*, 84:4102–4114, 2003.

[119] D.Pantaloni, R. Boujemaa, D. Didry, P.Gounon, and M.F.Carlier. The arp2/3 complex branches filament barbed ends: functional antagonism with capping proteins. *Nat. Cell Biol.*, 2:385–391, 2000.

[120] B. Nandy and A.B. Competing polymerization of actin skeleton explains relation between network polarity and cell movements. *J.Phys.:Cond.Mat.*, 17:S1871–S1879, 2005.

[121] P. R. Fisher, R. Merkl, and G. Gerisch. Quantitative analysis of cell motility and chemotaxis in dictyostelium discoideum by using an image processing system and a novel chemotaxis chamber providing stationary chemical gradients. *J. Cell Biol.*, 108:973–984, 1989.

[122] A.Levchenko and P. Iglesias. Models of eukaryotic gradient sensing: application to chemotaxis of amoebae and neutrophils. biophys j 82: 50-63. *Biophys. J.*, 82:50–63, 2002.

[123] W. J.Rappel, P. J. Thomas, H. Levine, and W. F. Loomis. Establishing direction during chemotaxis in eukaryotic cells. *Biophys. J.*, 83:1361–1367, 2002.

[124] A.Narang, K. K. Subramanian, and D. A. Lauffenburger. A mathematical model for chemoattractant gradient sensing based on receptor-regulated membrane phospholipid signaling dynamics. *Ann. Biomed. Eng.*, 29:677–691, 2001.

[125] C.Janetopoulos, L. Ma, P. N. Devreotes, , and P. A. Iglesias. Chemoattractant-induced phosphatidylinositol 3,4,5-trisphosphate accumulation is spatially amplified and adapts, independent of the actin cytoskeleton. *Proc. Natl. Acad. Sci. USA*, 101:8951–8956, 2004.

[126] M. Iijima, Y. E. Huang, H. R. Luo, F. Vazquez, and P. N. Devreotes. Novel mechanism of pten regulation by its phosphatidylinositol 4,5-bisphosphate binding motif is critical for chemotaxis. *J. Biol. Chem.*, 279:16606–16613, 2004.

[127] A. T.Sasaki, C. Chun, and K.Takeda.and R. A. Firtel. Localized ras signalling at the leading edge regulates pi3k, cell polarity, and directional cell movement. *J. Cell Biol.*, 167:505–518, 2004.

[128] S.Funamoto, R.Meili, S. Lee, L. Parry, and R. A Firtel. Spatial and temporal regulation of 3-phosphoinositides by pi 3-kinase and pten mediates chemotaxis. *Cell*, 109:611–623, 2002.

[129] L.Chen, C. Janetopoulos, Y. E. Huang, M. Iijima, J. Borleis, and P. N. Devreotes. Two phases of actin polymerization display different dependencies on pi(3,4,5)p3 accumulation and have unique roles during chemotaxis. *Mol. Biol. Cell.*, 14:5028–5037, 2003.

[130] M.Iijima, YE. Huang, and P. Devreotes. Temporal and spatial regulation of chemotaxis. *Dev. Cell*, 3:469–478, 2002.

[131] C. Arrieumerlou and T. Meyer. A local coupling model and compass parameter for eukaryotic chemotaxis. *Dev. Cell*, 8:215–227, 2005.

[132] M. Postma, J. Roelofs, H. Loovers, A. Visser, and PV. Haastert. Sensitization of dictyostelium chemotaxis by phosphoinositide-3-kinase-mediated self-organizing signalling patches. *J. Cell. Sci.*, 117:2925–2935, 2004.

[133] M. Onsum and C. V. Rao. A mathematical model for neutrophil gradient sensing and polarization. *PLoS Comput. Biol.*, 3:436–450, 2007.

[134] C. Parent and P.N. Devreotes. A cells sense of direction. *Science*, 284:765–770, 1999.

[135] S. H.Zigmond. Ability of polymorphonuclear leukocytes to orient in gradients of chemotactic factors. *J. Cell Biol.*, 75:606–616, 1977.

[136] M.Postma and P. J. Van Haastert. A diffusion-translocation model for gradient sensing by chemotactic cells. *Biophys. J.*, 81:1314–1323, 2001.

[137] L.Ma. Feedback control in the chemotactic signaling pathway of dictyostelium discoideum. *Phd Thesis*, 2004.

[138] PJ. Van Haastert. Sensory adaptation of dictyostelium discoideum cells to chemotactic signals. *J. Cell Biol.*, 96:1559–1565, 1983.

[139] H.Aizawa, K. Sutoh, S. Tsubuki, S. Kawashima, A. Ishii, and I. Yahara. Identification, characterization, and intracellular distribution of cofilin in dictyostelium discoideum. *J. Biol. Chem.*, 270:10923–10932, 1995.

[140] P.A.Clow and J.G. McNally. In vivo observations of myosin ii dynamics support a role in rear retraction. *Mol. Biol. Cell*, 10:1309–1323, 1999.

[141] G.Gerisch, R. Albrecht, E. De Hostos, E. Wallraff, C.Heizer, M. Kreitmeier, and A. Muller-Taubenberger. Actin-associated proteins in motility and chemotaxis of dictyostelium cells. *Symp. Soc. Exp. Biol.*, 47:297–315, 1993.

[142] M. Mishima and E. Nishida. Coronin localizes to leading edges and is involved in cell spreading and lamellipodium extension in vertebrate cells. *J. Cell Sci.*, 112:2833–2842, 1999.

[143] I.Weber, R. Neujahr, A. Du, J. Kohler, J. Faix, and G.Gerisch. Two-step positioning of a cleavage furrow by cortexillin and myosin ii. *Curr. Biol.*, 10:501–506, 2000.

[144] P.N.Devreotes and S.H Zigmond. Chemotaxis in eukaryotic cells - a focus on leukocytes and dictyostelium. *Annu. Rev. Cell Biol.*, 4:649–686, 1988.

[145] V.Niggli. A membrane-permeant ester of phosphatidylinositol 3,4, 5-trisphosphate (pip(3)) is an activator of human neutrophil migration. *FEBS Lett.*, 473:217–221, 2000.

[146] O.D. Weiner, P.O. Neilsen, G.D. Prestwich, M.W.Kirschner, L.C.Cantley, and H.R. Bourne. A ptdinsp3- and rho gtpase-mediated positive feedback loop regulates neutrophil polarity. *Nat. Cell Biol.*, 4:509–513, 2002.

[147] S.H.Zigmond. Chemotaxis by polymorphonuclear leukocytes. *J. Cell Biol.*, 77:269–287, 1978.

[148] G.Gerisch. Cyclic amp and other signals controlling cell development and differentiation in dictyostelium. *Annu. Rev. Biochem.*, 56:853–879, 1987.

[149] T.Hayashi and R. Rosenbluth. Studies on actin. ii. polymerization and the bound nucleotide. *Biol. Bull.*, 119:290, 1960.

[150] D. Selmeczi, S. Mosler, P. H. Hagedorn, N. B. Larsen, and H. Flyvbjerg. Cell motility as persistent random motion: Theories from experiments. *Biophys. J.*, 89:912–931, 2005.

[151] R.Sambeth. Theoretical studies of biological cell motility. *Phd Thesis*, 2001.

[152] A. Samadani, J. Mettetal, and A. V. Oudenaarden. Cellular asymmetry and individuality in directional sensing. *Proc. Natl. Acad. Sci. U S A.*, 103:11549–11554, 2006.

[153] J. Condeelis, A. Hall, A. Bresnick, V. Warren, R. Hock, H. Bennett, and S. Ogihara. Actin polymerization and pseudopod extension during amoeboid chemotaxis. *Cell Motil Cytoskeleton.*, 10:77–90, 1988.

[154] E. Lee, K. Pang, and D.Knecht. The regulation of actin polymerization and cross-linking in dictyostelium. *Biochim. Biophys. Acta.*, 1525:217–227, 2001.

[155] A.Mogilner and G. Oster. Regulation of actin dynamics in rapidly moving cells: A quantitative analysis. *Biophys. J.*, 83:1237–1258, 2002.

[156] P.Vallotton, S. L. Gupton, C. M. Waterman-Storer, and G. Danuser. Simultaneous mapping of f-actin flow and turnover in migrating cells by quantitative fluorescent speckle microscopy. *Proc. Natl. Acad. Sci.USA.*, 101:9660–9665, 2004.

[157] TD. Pollard, L. Blanchoin, and RD. Mullins. Molecular mechanisms controlling actin filament dynamics in nonmuscle cells. *Nature*, 404:1007–1011, 2000.

[158] ED. Korn, MF. Carlier, and D. Pantaloni. Actin polymerization and atp hydrolysis. *Science*, 238:638–644, 1987.

[159] J. L. McGrath, E. A. Osborn, Y. S. Tardy, C. F. Dewey Jr., and J. H. Hartwig. Regulation of the actin cycle in vivo by actin filament severing. *PNAS.*, 97:6532–6537, 2000.

[160] H. Miyata and H. Hotani. Morphological changes in liposomes caused by polymerization of encapsulated actin and spontaneous formation of actin bundles. *Proc. Natl. Acad. Sci. USA.*, 89:11547–11551, 1992.

[161] TD. Pollard and GG. Borisy. Cellular motility driven by assembly and disassembly of actin filaments. *Cell*, 21:453–465, 2003.

[162] R.D. Mullins, J.A. Heuser, and T.D. Pollard. The interaction of arp2/3 complex with actin: nucleation, high affinity pointed end capping, and formation of branching networks of filaments. *Proc. Natl. Acad. Sci. USA.*, 95:6181–6186, 1998.

[163] L. Blanchoin, K.J. Amann, H.N. Higgs, J.B. Marchand, D.A. Kaiser, and T.D. Pollard. Direct observation of dendritic actin filament networks nucleated by arp2/3 complex and wasp/scar proteins. *Nature*, 404:1007–1011, 2000.

[164] R.D. Mullins. How wasp-family proteins and the arp2/3 complex convert intracellular signals into cytoskeletal structures. *Curr. Opin. Cell Biol.*, 12:91–96, 2000.

[165] R.D. Mullins and T.D. Pollard. Structure and function of the arp2/3 complex. *Curr. Opin. Struct. Biol.*, 9:244–249, 1999.

[166] M.D. Welch. The world according to arp: regulation of actin nucleation by the arp2/3 complex. *Trends Cell Biol.*, 9:423–427, 1999.

[167] M. Bailly, I. Ichetovkin, W. Grant, N. Zebda, L. Machesky, J. Segall, and J. Condeelis. The f-actin side binding activity of the arp2/3 complex is essential for actin nucleation and lamellipod extension. *Current Biology*, 11:620–625, 2001.

[168] A.Y. Chan, S. Raft, M. Bailly, J.B. Wyckoff, J.E. Segall, and J.S. Condeelis. Egf stimulates an increase in actin nucleation and filament number at the leading edge of the lamellipod in mammary adenocarcinoma cells. *J. Cell Sci.*, 111:199–211, 1998.

[169] A.Y. Chan, M. Bailly, N. Zebda, J.E. Segall, and J.S. Condeelis. Role of cofilin in epidermal growth factor-stimulated actin polymerization and lamellipod protrusion. *J. Cell Biol.*, 148:531–542, 2000).

[170] A. Steffen, J. Faix, G. P. Resch, J. Linkner, J. Wehland, J. V. Small, K. Rottner, and T. E.B. Stradal. Filopodia formation in the absence of functional wave- and arp2/3-complexes. *Mol. Biol. Cell*, 17:2581–2591, 2006.

[171] T. J. Mitchison and L. P. Cramer. Actin-based cell motility and cell locomotion. *Cell*, 84:371–379, 1996.

[172] A. Grebecki. Membrane and cytoskeleton flow in motile cells with emphasis on the contribution of free-living amoebae. *Int. Rev. Cyt.*, 148:37–80, 1994.

[173] A. T. Dawes, G. B. Ermentrout, E. N. Cytrynbaum, and L. Edelstein-Keshet. Actin filament branching and protrusion velocity in a simple 1d model of a motile cell. *J. Theor. Biol.*, 242:265–279, 2006.

[174] P. E.Rouse. A theory of the linear viscoelastic properties of dilute solutions of. coiling polymers. *J. chem. Phys.*, 21:1272–1280, 1953.

[175] P. H. Verdier and W. H. Stockmayer. Monte carlo calculations on the dynamics of polymers in dilute solution. *J. Chem. Phys*, 36:227–235, 1962.

[176] P. G. Charest and R. A. Firtel. Big roles for small gtpases in the control of directed cell movement. *Biochem. J.*, 401:377–390, 2007.

[177] K.Wennerberg, K. L. Rossman, and C. J Der. The ras superfamily at a glance. *J. Cell Sci.*, 118:843–846, 2005.

[178] S.Merlot and R. Firtel. Leading the way: Directional sensing through phosphatidylinositol 3-kinase and other signaling pathways. *J. Cell Sci.*, 116:3471–3478, 2003.

[179] P.G.Charest and R.A. Firtel. Feedback signaling controls leading-edge formation during chemotaxis. *Curr. Opin. Genet. Devel.*, 16:339–347, 2006.

[180] S. Suire, A. M. Condliffe, G. J. Ferguson, C. D. Ellson, K. Davidson H. Guillou, H. Welch, J. Coadwell, M. Turner, E. R. Chilvers, P. T. Hawkins, and L. Stephens. Gbetagammas and the ras binding domain of p110gamma are both important regulators of pi(3)kgamma signalling in neutrophils. *Nat. Cell Biol.*, 8:1303–1309, 2006.

[181] F. I.Comer and C. A. Parent. Pi 3-kinases and pten: how opposites chemoattract. *Cell*, 109:541–544, 2002.

[182] A.Gericke, M. Munson, and A. H. Ross. Regulation of the pten phosphatase. *Gene*, 374:1–9, 2006.

[183] F.Vazquez and P. Devreotes. Regulation of pten function as a pip3 gatekeeper through membrane interaction. *Cell Cycle*, 5:1523–1527, 2006).

[184] Z.Li, X. Dong, Z. Wang, W Liu, N.Deng, Y.Ding, L.Tang, T.Hla, R.Zeng, L.Li., and D.Wu. Regulation of pten by rho small gtpases. *Nat. Cell Biol.*, 7:399–404, 2005.

[185] Z.Li, M. Hannigan, Z.Mo, B.Liu, W.Lu, Y. Wu, A.V. Smrcka, G. Wu, L. Li, and M. Liu. Directional sensing requires gbg-mediated pak1 and pixa-dependent activation of cdc42. *Cell*, 114:215–227, 2003.

[186] J.Xu, F. Wang F, A. Van Keymeulen, P. Herzmark, A. Straight, K. Kelly, Y. Takuwa, N.Sugimoto, T. Mitchison, and HR. Bourne. Divergent signals and cytoskeletal assemblies regulate self-organizing polarity in neutrophils. *Cell*, 114:201–214, 2003.

[187] K.Fujisawa, A. Fujita, T. Ishizaki andY. Saito, and S. Narumiya. Identification of the rho-binding domain of p160rock, a rho-associated coiled-coil containing protein kinase. *J. Biol. Chem.*, 271:23022–23028, 1996.

[188] V.Niggli. Rho-kinase in human neutrophils: a role in signalling for myosin light chain phosphorylation and cell migration. *FEBS Lett.*, 445:69–72, 1999.

List of Tables

List of Figures

Acknowledgments

I would like to thank all friends and colleagues for their generous help during my research in Germany.

First of all I would like to thank my research adviser Prof. Dr. Artur Baumgaertner for his great support of my work and many helpful discussions and suggestions. Then I would like to thank Dr. S.V.M. Satyanarayana for his introductory help regarding Monte Carlo Simulation and on other simulation related problems. Many thanks to Dr. Jean-Fang Gwan for generous help in my nonacademic and academic life both. Thanks to Dr. Sergei Grudinin for helpfull discussions and informations. I would like to thank Mr. Willi Homberg of ZAM and all the people in IFF from whom I got different technical and non technical helps .

And finally special thanks to my parents. Without their constant support it was impossible for me to achieve anything.